3-2020

Development and Characterization of a Filter-Based Bioaerosol Sampler Capable of Integration into Small Unmanned Aerial Systems

Stephanie A. Ohms

DEVELOPMENT AND CHARACTERIZATION OF A FILTER-BASED BIOAEROSOL SAMPLER CAPABLE OF INTEGRATION INTO SMALL UNMANNED AERIAL SYSTEMS

THESIS

Stephanie A. Ohms, 1st Lieutenant, USAF

AFIT-ENV-MS-20-M-230

DEPARTMENT OF THE AIR FORCE
AIR UNIVERSITY

AIR FORCE INSTITUTE OF TECHNOLOGY

Wright-Patterson Air Force Base, Ohio

AFIT-ENV-MS-20-M-230

DEVELOPMENT AND CHARACTERIZATION OF A FILTER-BASED BIOAEROSOL SAMPLER CAPABLE OF INTEGRATION INTO SMALL UNMANNED AERIAL SYSTEMS

THESIS

Presented to the Faculty

Department of Systems Engineering and Management

Graduate School of Engineering and Management

Air Force Institute of Technology

Air University

Air Education and Training Command

In Partial Fulfillment of the Requirements for the

Degree of Master of Science in Industrial Hygiene

Stephanie A. Ohms, BS

1st Lieutenant, USAF

March 2020

DISTRIBUTION STATEMENT A.
APPROVED FOR PUBLIC RELEASE; DISTRIBUTION UNLIMITED.

AFIT-ENV-MS-20-M-230

DEVELOPMENT AND CHARACTERIZATION OF A FILTER-BASED BIOAEROSOL SAMPLER CAPABLE OF INTEGRATION INTO SMALL UNMANNED AERIAL SYSTEMS

Stephanie A. Ohms, BS

1st Lieutenant, USAF

Committee Membership:

Dr. Jeremy Slagley, PhD
Chair

Col. Robert Eninger
Member

Lt Col. Casey Cooper
Member

AFIT-ENV-MS-20-M-230

Abstract

In developing functional SUAS, performance characteristics that indicate system capability should be developed prior to initiating initial system design. Key performance parameters should be developed involving all system elements (including vehicle body, operator, ground station, sensor, and algorithm or processing module). A bioaerosol sampler designed specifically for the use in SUAS was characterized based on designated performance measures to determine overall effectiveness compared to traditional bioaerosol samplers. For a system with a goal of accurately identifying and quantifying areas of airborne biological contamination or surveying background levels for longitudinal studies, performance parameters such as weight of the vehicle with payload and sampler specific parameters will be quantitatively evaluated. These sampler-specific parameters include operational noise levels, power demand compared to performance, and sampling fraction. These were evaluated in a series of lab-based tests to determine if the developed model of bioaerosol sampler could be deployed for use in military environments. Overall, it was found that the developed EOS inlet oversampled for the background concentrations compared to the modeled performance for the inlet, and oversampled compared to the closed face cassette filter. This may be due to ground effects acting on the system—as the bottom placement for the sampler performed worse than expected based on previous research in comparison to the sampler closer to the rotors.

Acknowledgments

I would like to express my sincere appreciation to my faculty advisors, Col Robert Eninger and Dr. Jeremy Slagley for their guidance and support throughout the course of this thesis. Their insight, inspiration, and experience were invaluable to this effort. I would also like to thank the ENV faculty members Lt Col. Casey Cooper and Dr. David Jacques, and the AFIT ANT Lab staff, for providing me with materials, and extensive knowledge in subject matter that was foreign to me a little over a year ago.

Thank you to family and friends for their unwavering support and encouragement throughout this process. I could not succeed without their love and patience. Additionally, I thank Ms. Ariel Parker, Ms. Megan Steele, and UES affiliates for the support and latitude provided to me in this endeavor. I am grateful to have had the opportunity to have worked with you, and within your facilities.

Stephanie A. Ohms

Table of Contents **Page**

List of Figures **Page**

List of Tables Page

List of Symbols Used

$Q = VA_s = air\ flow\ rate\ in\ the\ sampler$

$\Delta p = pressure\ drop\ across\ a\ filter$

$A = A_1A_2 = overall\ aspiration\ efficiency\ for\ the\ sampler$

$\beta = aerodynamic\ bluntness$

$\delta = inlet\ diameter\ of\ a\ blunt\ body\ sampler$

$d_{AE} = aerodynamic\ diameter\ of\ a\ particle$

$D = diameter\ of\ blunt\ body\ sampler\ (width)$

$\eta = viscosity\left(1.81\ x\ 10^{-5}\left(\frac{kg}{m*s}\right)\right)$

$\phi_A = \frac{r^2}{R} = sampling\ ratio\ of\ axisymmetric\ flow$

$\rho_p = particle\ density, as\ this\ time\ assumed\ to\ be\ 1000\ kg/m^3$

$r = \frac{\delta}{D} = ratio\ of\ sample\ inlet\ diameter\ to\ the\ blunt\ body\ diameter$

$R = \frac{U}{U_s} = ratio\ of\ free\ stream\ velocity\ to\ sampling\ air\ velocity$

$St = Stoke's\ number$

$U = free\ stream\ velocity$

$U_s = sampling\ velocity$

$V_H = fan\ velocity\ at\ highest\ theoretical\ setting$

$V_M = fan\ velocity\ at\ medium\ theoretical\ setting$

$V_L = fan\ velocity\ at\ lowest\ theoretical\ setting$

DEVELOPMENT AND CHARACTERIZATION OF A BIOAEROSOL SAMPLER CAPABLE OF INTEGRATION INTO SMALL UNMANNED AERIAL SYSTEMS (SUAS)

I. Introduction

Background

Unmanned Aircraft Systems (UAS) and Unmanned Aerial Vehicles (UAVs) have been used since their inception for support of military endeavors. SUAS technology presents many environmental sampling advantages. These range from removing danger to humans during the sampling task, to improving amount and types of data that can be collected. This is all possible via combinations of imaging, current direct reading instruments, and the potential for computer integration of multiple sample collection types (Eninger and Johnson, 2015). Previous research has been conducted to investigate the potential for bioaerosol sampling from similar platforms. Many of the SUAS platforms used were based on fixed-wing aircraft, which are ideal for long-range operations; however, in order to gather a representative sample of a specific area a multi-rotor aircraft is more ideal. Though limited by lower endurance, multi-rotors are ideal for Chemical, Biological, Radiological, and Nuclear (CBRN) agent operations, and ability to rapidly sample hazardous areas is currently being investigated across the entire CBRN spectrum.

Though each of the CBRN agents come with their own sampling and detection challenges, biologicals (and bioaerosols particularly) carry with them multiple challenges when being sampled from a multi-rotor platform. One of the foremost challenges using this platform is the presence of rotor-wash from the multi-rotor itself impacting the flow of particles around the vehicle. Bioaerosols also hold the challenge of determining

whether viable aerosols can or should be collected. Many factors involved in sampling, including sample time, sample media, and environment where the sample is taken can influence the viability of a biological sample. In most cases, it is less costly and more effective to sample for non-viable bioaerosols or those that retain viability for long periods of time in adverse conditions, like bacterial spores, than viable bioaerosols. Finally, bioaerosols do not have a standard collection methodology or exposure limits and can be difficult to quantify outside of laboratory methods like quantitative Polymerase Chain Reactions (qPCR) or dilution plating.

Problem Statement

SUAS platforms have become wildly popular due to their potential application in a broad variety of fields in environmental and industrial surveillance of indoor and outdoor contaminants. However, this new technology presents a unique set of challenges to those who would conduct it. Previous research has suggested that the impacts of wind speed, turbulence from SUAS rotors, and sampler orientation may bias aerosol sampling results. Additionally, aerosol sampling has revealed that particle inertial effects and environmental factors, like wind speed, and sampler orientation all have an impact on the particle size distributions that can be collected (Chavez, 2017). This research investigates a new sampler design for bioaerosols—particularly spores around one micron in diameter—while minimizing bias due to environmental impacts and classifying what bias remains in the system. The focus of this research was the development and classification of a new filter-based bioaerosol sampling system; the methods used, assumptions made to

answer the research questions, and the implications of the research are discussed further below.

Research Objectives/Questions/Hypotheses

The objective of this research was to contribute to the understanding of bioaerosol sampling using multi-rotor SUAS as a sampling platform. Development of a SUAS-based bioaerosol sampler and characterizing its performance through the initial system design phase was achieved—though further characterization is necessary in the later design phases.

Investigative Questions

A new inlet and centrifugal fan-based collection system was developed and optimal configurations for bioaerosol particle collection on a multi-rotor SUAS were investigated. The objectives for this research were accomplished by exploring the following three specific aims:

Specific Aim 1: Design a bioaerosol sampler based on mission requirements of flight time, maneuverability, and sample capture ability. Aspiration efficiencies across several inlet types will be modeled to determine the optimal configuration for a inclusion on SUAS.

Specific Aim 2: Assess design to minimize aspiration bias and increase other performance factors. Key considerations for assessment include the effects of wind speed, turbulence, orientation, and sampler flow rate on particle aspiration. Future modification recommendations will be made.

Specific Aim 3: Determine the size selectivity bias for the UAS airframe and aerosol sampler in forward flight. Characterize particle size sampling bias for flight in a calm air environment.

Methodology

Mission parameters were developed by performing a review of literature to determine the needs of the military and other interested parties. These mission parameters were then used as the foundation of the preliminary design of a modular SUAS and its corresponding bioaerosol sampler. After Technical Performance Measures and blueprints for the design were made, the appropriate bioaerosol sampler was designed based on filter and sampler performance models.

The efficiency models for sampler performance also served as a baseline for expected performance of the sampler in laboratory conditions—inside an exposure chamber. Two types of aerosol (Ultrafine ISO Test Dust and Medium ISO Test Dust) were generated for separate gravimetric and particle count tests in order to assess the sampler's performance. Trials of this test were run in still air and with significant air turbulence—to simulate sampling while the SUAS is on the ground vs the effects of sampling in-flight.

Assumptions/Limitations

Multiple assumptions were made in the modeling portion of this research. These are discussed in more depth in Chapter III. Some examples of these assumptions include: the background velocity of the air within the chamber during sampling, the validity of the equations used to model the aspiration efficiency of the inlet, and some performance

factors for the SUAS. Additionally, though there are some losses in total particulate from aerosols sticking to the sides of a close-faced cassette (CFC) that have been examined in previous research, they were discovered to be minimal (<5%). These losses were also not demonstrated to be dependent on sampler orientation. Ultimately, it was assumed in this research that particles sticking to the inlet sides were a negligible loss of mass for the CFC and the designed EOS sampler (Cook et al., 2015).

Though cellulose nitrate membrane filters are known to sometimes have an affinity for quickly reabsorbing water, desiccators and a mass balance were used on site immediately after sample collection. Triplicate measurements throughout the pilot study and spot-checks, yielded a standard deviation of 4.89E-04 mg per filter. This was deemed acceptable and assumed to remain constant throughout the experiments. During the sampling itself, paired samples were taken—meaning that two samplers (either CFC and EOS, or two EOSs in variable locations)—were run at the same time in the same quadrant of the aerosol chamber for the trials. For this to be done, it was assumed that the interference of the other sampler body had minimal effect on the results of the other sampler. During chamber characterization, it was found that the quadrants of the chamber had an even test aerosol distribution, so a pair of samplers within the confines of the quadrant, but with low profiles, should theoretically have no impact on the performance of the other sampler (M. Steele, personal interview, Oct 01, 2019).

Perhaps the largest limitation of the study is the proximity of the SUAS to the floor of the exposure chamber. The mounting mechanism to hold the SUAS in place with no control systems for the system being operational, kept the feet of the SUAS approximately two inches off the chamber bottom. This decision was made due to time

constraints and ease of obtaining materials, though the ground effect meant that air that was pushed downward to create thrust was recirculated directly into the turbulence surrounding the SUAS. This phenomenon likely occurred under the sampling conditions of the chamber, therefore the results must be viewed with a critical eye (Light, 1993). Additionally, due to the significant impact of bias that the proximity of the SUAS to the floor of the exposure chamber might introduce to the sampling, it is recommended to conduct further experimentation where the impacts of ground effects are either investigated themselves or are eliminated to the extent possible. The environmental factors (temperature, humidity, etc.) were also a limitation in the study, as the entirety of the experiment took place in the course of one month where conditions were relatively similar. These factors may have an impact on sampler performance, which warrants further investigation in the future with differing environmental factors.

Implications

This research aimed to develop a cost effective and efficient means of collecting bioaerosol samples from a SUAS platform, which would directly impact the environmental, health and safety industries. Also, emergency responders and DoD operations may benefit from the continued development and implementation of bioaerosol sampling that this research warrants. In fields where health risk analyses are performed, specifically Air Force Bioenvironmental Engineering and related health organizations in the sister services, this research has the potential to limit health risks to personnel responding to biological incidents. The SUAS technology itself may benefit emergency responders by directly curtailing response time—as the SUAS takes less time

than evaluating personnel for entry and ensuring personal protective equipment is appropriately assigned and worn. Additionally, bioaerosol SUAS will empower health risk agencies to perform longitudinal studies that will assist in identifying background levels of endemic bacteria and fungi. One such effort was proposed by the Department of Homeland Security (DHS) in 2014. This was called BioWatch, but this program was ultimately abandoned due to monetary and technological constraints at the time. This research will contribute to the understanding of bioaerosol sampling and paves the way for further investigation and improvements on a cost-effective sampling platform for universal use.

Preview

Chapter II reviews the basic techniques of bioaerosol sampling, the relevance of such sampling, and how such techniques might be incorporated into a fully designed SUAS. Chapter III covers the basic aerosol sampling principles and assumptions used to model for an inlet to use in conjunction with a centrifugal fan, ultimately the EOS design used throughout the experiment. This chapter also highlights systems engineering design concepts and introduces the specific metrics to be used in evaluating the designed inlet and system. Chapter IV highlights the experimental methods used for determining the sampling efficiencies of the selected aerosol samplers on and off UAS, their performance relative to each other, and how other technical performance measures were evaluated. Chapter V summarizes the results and provides an analysis of the data and its relevance.

II. Literature Review

Chapter Overview

The purpose of this chapter is to detail relevant literature and the potential for contributions to the existing body from this work. The scope of this chapter includes literature relevant to the design of SUAS for aerosol sampling, filter-based methods for bioaerosol sampling, and studies relevant to the development of test methodology to evaluate the designed bioaerosol sampler.

Description

Small Unmanned Aerial Systems (SUAS) is a rapidly growing field, where flexibility and ease of user interface are promoting their use in many diverse fields. One aspect of SUAS that is currently being investigated is their potential to be used in military emergency response contingencies—specifically in the recognition, detection, and quantification of Chemical, Biological, Radiological, or Nuclear (CBRN) agents. A key consideration in developing SUAS for this use is the need to minimize cost of instruments and maintenance needs to improve short-term functionality and allow for the quickly changing field of SUAS (Eninger and Johnson, 2015). Chapter II reviews the basic techniques of bioaerosol sampling in general, current UAS incorporation efforts, and modern UAS design considerations.

The Need for Bioaerosol Sampling

Biological microorganisms are ubiquitous in both indoor and outdoor environments. Bioaerosols specifically refer to living microorganisms or their byproducts that are suspended in the air; these include bacteria, viruses, fungal spores, pollen, and

algae (Després et al., 2012). Studying the typical distribution of biologicals in the environment and their impacts on human health has been a topic of growing interest in the past decade. Previous studies, from the early 2000's to the present, have investigated environments as diverse as microbial exposures in public transportation to bioaerosols present in homes after a hurricane.

A large portion of these studies were longitudinal in nature, aimed at identifying typical distributions of bioaerosols in their native environments. The difficulties with accomplishing longitudinal surveys for biologicals stems, in part, from the fact that there is no standard protocol for accomplishing such studies, nor are there set limits for exposure that levels can be compared to. Despite these challenges, bioaerosols have been successfully sampled in a variety of environments via impinger, cascade impaction, and even via low flow sampling pumps with Teflon filters. Design of a Bioaerosol SUAS will make emergency response biological sampling and longitudinal surveys faster and easier to accomplish in diverse environments—where humans may not safely perform surveillance (Fornace et al., 2014; Leber).

SUAS bioaerosol sampling could assist with monitoring the spread of potentially dangerous bioaerosols across diverse environments. A study from 2005, by Ji-Hyun Lee and Wan-Kuen Jo, examined the impacts of temperature on bioaerosols in public transportation. Sampling was performed inside and outside of public transportation during the winter and summer to determine the prevalence of fungi and bacteria in these environments and timeframes. Sampling was accomplished via cascade impaction onto agar plates—which introduced some variance in genus of fungi or bacteria identified, though total counts trended similarly. Bacterial concentrations were significantly higher

for public buses than for the passenger cars in the summer months, and the opposite was found for total fungal concentrations; outdoor sampling corroborated this trend. In the winter months the difference between buses and personal vehicles was minimized, though fungal spores were higher in concentration in all environments during the winter. This trend makes sense as bacteria thrive in warm environments, while fungi favor moist conditions and have lower preference for temperature. Though the sampling conducted relied on viable sampling, this technique is uncommon, as the variability in target bioaerosol growth associated with different agars means extra cost for sampling when the target is unknown, there are many targets, or the bioaerosol is difficult to isolate (Lee and Wan-Kuen, 2005). This study is still valuable in its examination of transportation having similar bioaerosol concentrations as built environments—if a target bioaerosol is introduced to an environment and identified as being present quickly, it can be transported to new locales by vehicle where individuals have the potential for significant exposures. The trends in type of bioaerosol as they relate to weather are also important to consider when planning a longitudinal bioaerosol sampling event, as better resolution of quantity of bacteria might need to be conducted in summer.

Another example of where SUAS bioaerosol sample could have been used is the post-hurricane response from Hurricane Katrina. In the hurricane's wake mold and fungal spores, and their associated endotoxins were investigated by Chew, et al (2006) to determine how to best direct remediation efforts and to monitor exposures during the clean-up. Particle counts were taken which aimed at classifying the fungal spores but may have captured other aerosolized particles as well. In this study, BioCell impaction cassettes were used in concert with a high flow sampling pump (15 L/min) positioned at

the worker's breathing zone. An optical particle counter was used to monitor real-time data for the aerosolized spores over 1 min averaging times. Though this technique allows separation into 15 size ranges, it is not selective for bioaerosols alone (or the spores of interest). 2.0 micron pore Teflon filters were used with AirCheck 2000 pumps at a lower flow rate to collect spores for PCR. Though the specific manufacturer could not be found, studies quote Teflon filters with the same pore size and sampling rate to have a minimum collection efficiency of around 99% (Soo, et al., 2016). This technique is the most realistic and repeatable of those mentioned in the study. The cultured plates were used to count colony forming units (CFUs) to estimate airborne concentration. Aliquots of these samples were run in PCR to identify 23 different species/types of fungi that were of concern to the researchers, while quantification was accomplished via culturing viable samples and microscopy (Chew et al., 2006). Though the research was completed successfully, the danger associated with researchers entering hurricane damaged properties could have been avoided via use of SUAS.

A longitudinal study, done by a research team led by J. Qian, on classroom occupancy and bioaerosol emission rates identified human beings as a significant contributor of bioaerosol exposures. The size range and identification of these bioaerosols indicated that microbes from the skin, hair, mouth, and nostrils are all major contributors to the airborne microbiota of indoor environments. Researchers investigated the size of the particles as well as type, using uncoated polycarbonate track-etched filters in a multi-stage impactor at 28.3 L/min. The filters were then weighed and qPCR was performed on the samples to determine the amount of bacterial DNA present and to approximate concentration of bioaerosols in the classroom air. Ultimately, the study found that

genome concentrations increase 12-2700 times for bacteria when the classroom was occupied vs sampling performed when it was vacant (Qian, et al., 2012). Though humans are a relevant factor in the microbiomes of indoor environments, outdoors our contribution is smaller. The input that the human microbiome may have on our environments and subsequent samples is still an important factor to consider, as matrix interference from native microbes could occur when investigating the presence of a target bioaerosol. Still, the sampling techniques used here are relevant to developing methods for sample collection with UAS.

Bioaerosol Sampling Technologies

Many factors impact the type of bioaerosol sample that can be collected. These factors include temperature, pressure, and humidity where samples are taken; type of sample collection media; and cost allowed for the sampling, among others. In 2001, Zheng and Reponen performed research investigating parameters such as optimal temperature and humidity for collecting bioaerosols. In their study a Button Inhalable Aerosol Sampler and the 37-mm cassette sampled under relative humidities (RH) of 30 and 85, and variable time intervals for three different bioaerosol types—bacterial spores, fungal spores, and bacterial vegetative cells. The viability of spores decreased with sampling time, up until 30 minutes—at which point the effectiveness at culture for some species flatlined until eight or more hours. Overall bacterial spores were most effectively collected and cultured at moderate relative humidities (between 30 to 80 percent). This concluded that the bio-efficiency of filter samplers not only depends on the microbial species, but also on the sampling time and relative humidity (Zheng, et al., 2001). Other

research on optimal temperature and humidity for collecting bioaerosols corroborated these findings (Yuanping, 2019).

Several types of sampling that are common for bioaerosols are impaction, impinging, and filtration. The first two techniques are sometimes used in attempt to isolate viable bioaerosols, via collecting the aerosols on or in a growth medium—impaction and impinging respectively. For example, the XMX/2L-MIL is an impinging technology that draws a high flow bioaerosol sample that is then trapped in a liquid medium, usually water or a Phosphate Buffer Saline (PBS) solution, which can be analyzed via culture or PCR. Drawbacks of this technology in general, are the high noise output and power demand, as well as relying on glass parts that are easily breakable, and having substantial weight that limits maneuverability (Enderby, 2012). These drawbacks translate into severe limitations for the integration of similar impinging technologies into airborne sampling platforms.

Impaction was previously discussed in the "Need for Bioaerosol Sampling" section and has proven especially useful for size selective sampling events. Inertial impaction technologies operate via the aerosol being sucked through a nozzle and directed toward the impaction plate. When the airstream meets the plate, the flow is deflected at two 90° angles, and particles with the right inertia break off from the flow streams and impact the plate. The smaller particles in the airstream either exit the sampler or continue onto a different impaction plate setup (Hinds, 1999, p. 122-123). Limitations of this technology for bioaerosol sampling in general include the cost of the individual components needed. Additionally, if agar is needed in the impaction plates, the selectivity of the agar might significantly skew results (Juozaitis et al., 1994).

Though impaction is one of the most common technologies used to sample for bioaerosols, filtration can also be used. Filtration is regarded as one of the most effective and simplest air purification methods for biological agents, used in a variety of industrial and home environments. Technologies ranging from HEPA filters (Hurley et al., 2019) to currently developing metal microfiber enhanced filters (Dehghan et al., 2020) have been investigated for air purification; however, this simple technology can easily be applied to sample collection as well. In addition to the previously mentioned examples, where filtration was sometimes used in conjunction with other sampling techniques, scientists have investigated using filters in all their forms to examine bacteria in the air. One example of this was a study where researchers investigated if biologicals or their genetic components could be identified and then quantified from car filters. To study this, birch pollen was released in car cabins, where air flow was verified with real time methods. The car's air filter was then removed and any bioaerosols that were trapped in the filter were extracted for analysis. Even this most basic form of filtration sampling did yield measurable results (Hurley et al., 2019). Overall, low and high-flow filtration samples coupled with a quantitative technique appears to be one of the most accepted forms of sampling for bioaerosols. This is likely due to the relatively low cost-point of collecting and analyzing non-viable filter-based samples.

Bioaerosol Sampling and the Department of Defense

In addition to longitudinal microbiome studies, biologicals are of interest to the Department of Defense (DoD), homeland security, and emergency management teams across the United States due to the potential for hostile parties to use biowarfare agents (BWAs). For this purpose, a low-cost and maintenance system is ideal—in order to

operate in garrison and deployed setting—factors which will both weigh heavily on design optimization (O'Hanlon, 2018).

Despite growing interest in longitudinal studies on microbiomes and how they impact the humans around them, little progress has been made in the realm of sampling techniques or legislation on how to classify or control potential hazards espoused from microbiota. 29 CFR 1910.1030 covers workers who are exposed to bloodborne pathogens, which applies to settings where human tissues are manipulated, and other workers are covered from microbial harm via the general duty clause, but little other guidance exists. Organizations like the National Institutes of Health (NIH) and the Centers for Disease Control and Prevention (CDC), help classify biological agents via risk groups. Under this framework, there are four different risk classifications for biologicals, which correspond with the outcomes of disease in those infected (Carroll and Foster, 2011).

The same general principles for determining hazard level for individual bacteriological samples can be extended to determining risk of a population from biowarfare agents or invasive microbiota in their environment. Developing a system to monitor bioaerosols in the air is consistent with the vision and previous efforts of the DHS Office of Health Affairs (OHA) to produce autonomous systems to perform bioaerosol sampling as a part of their program BioWatch. Though their efforts to procure a fully autonomous system were unsuccessful and put on hold as of 2014 due to high cost, the OHA still emphasizes the value of developing procedures and equipment for monitoring typical environmental microbiota via longitudinal studies, as well as expedient biowarfare agent samplers (Brinsfield and Brothers, 2018).

Minimizing the cost of bioaerosol sampling events would require careful consideration on which bioaerosol sampling method is used, as well as what other components are used in the system. For example, commercial off-the-shelf components would cost less than custom Unmanned Aerial Vehicle (UAV) frame parts used for integrated bioaerosol sampling. The next few sections of literature review examine alternative methods of collecting bioaerosol samples as part of a SUAS, as well as theoretical components of such a system that would theoretically improve the performance of a SUAS in conducting bioaerosol sampling.

SUAS and Bioaerosol Sampling

Though bioaerosol sampling is not uncommon, the theoretical integration of this form of sampling into SUAS has gained traction in the latter half of the past decade. Impinging is a common bioaerosol sampling method, but often requires larger infrastructure than a SUAS could support. One research team investigated adapting impinging into smaller form for use on surface and air based UAS. They successfully collected samples over various bodies of water; however, their impinger demonstrated bias toward increasing collected concentration with increasing particle diameter—a fact not conducive to collecting bacterial spores (Powers et al., 2018). In addition to this bias, the sampler was still relatively heavy for airborne use. Due to these weight constraints (and others like power demand and cost), using a SUAS platform with bioaerosol sampling has resulted in some creative efforts—generally using impaction as a more adaptable collection technique. For instance, a group of researchers based in France used a fixed wing SUAS with a petri-plate and impaction plate attached perpendicular to the airstream. In this manner, it acted as a rudimentary form of impaction, and background

environmental samples for multiple locations (in France and the US) were analyzed for types of bacteria present, and an estimate of concentration (in CFU/m^3) was made. The researchers identified 21 genera of bacteria and fungi from the samples. Though the research was successful, the limitations of this method are cost of different agar types necessary to isolate targeted forms of bacteria or fungi, the time and cost of culture, and environmental impacts on the viability of the organisms collected (Jimenez-Sanchez et al., 2018).

Another example of the adaptation of impaction bioaerosol sampling into SUAS was created in 2019 by a team in Germany. Instead of using a fixed-wing model, this team used a multirotor set-up. A common issue with these platforms is the turbulence created by the rotors while generating lift. This means that isokinetic sampling conditions near the SUAS are near impossible to achieve. In order to work around this, the German team designed an inlet that reached 30 cm above the rotors on the SUAS, the particles were carried to the impaction plate where the concentration (#/m^3) was later determined via microscopy. The sampling results determined that the collected particle concentrations were accurate to the recorded background concentrations (Crazzolara et al., 2019). The major limitation of this design is the inlet itself—being 30 cm above the rotor blades means that the spaces the SUAS could occupy are very limited. For open areas covering long distances, fixed wing SUAS are favorable, while in urban or variable environments where obstacles may be encountered a lower SUAS profile would hold the advantage.

Configuration of sensors to avoid rotor wash impacts, as well as other flight pattern characteristics that impact sensor capabilities, is a major consideration for more

than just bioaerosol sampling. One study, by Aurrel et al., 2017, incorporated CO, particulate matter (PM), and perchlorate sensors (among others) on the front of a hex-rotor system. Even with the rather unconventional placement of sensors, the PM results collected from the hex-rotor were not statistically different from those gathered from traditional ground stations. The ability of rotary wing aircraft to hover does in theory minimize impacts of the rotor wash when collecting samples from an airborne plume (Aurell et al., 2017; Bates et al., 2013).

In addition to isokinetic sampling efforts, other studies have been done with particulate sampling in general in order to isolate the best position for any type of aerosol sampler. Using multiple different particulate sampler types, including one designed omnidirectional sampler, the sampling efficiencies were tested for top and bottom placements on a hex-rotor SUAS with mounting in variable orientations (upward, downward, and horizontal). The researcher determined that positioning the samplers underneath the SUAS (farther away from the rotors) was the optimal placement for particulate aerosol samplers. Horizontal orientations of the inlets resulted in a negative sampling bias compared to the upright and downward positions. Results also suggested that a combination of both the UAS turbulence and low wind speed produced a negative sampling bias in all the tested inlets (Chavez, 2017).

SUAS Design Considerations

Though many options for bioaerosol sampling with SUAS have been examined, there are several design considerations that impact this set-up as opposed to traditional bioaerosol sampling. Decontamination is one such consideration in developing operationally capable SUAS. One idea is generating data that can be retrieved remotely,

which is useful if the SUAS cannot be retrieved and would empower faster decisions based on real-time data. However, in the case of a biological sampler, generating data in real-time is not likely and the aim should be at collecting stable samples to analyze at a laboratory off-site. In this case, biological sampling devices and electrical systems must be able to withstand traditional decontamination measures of soap and water rinse, ideally via being mostly enclosed in the SUAS body. Optimal SUAS body configurations with the biological sensors will also be explored to minimize potential for damage to system components, as well as optimizing flight ability of the SUAS. It is of great importance for analyzing the field samples that are collected that the samples be able to be sealed to the environment after collection (Fitch et al., 2003).

Filtration with integration into SUAS has a set of benefits that are worth discussing on their own. As previously mentioned, most filtration systems are lightweight in comparison to impinger or impaction technologies. In addition to the versatility afforded by using different filters in the sampling train to target different sizes of bioaerosol, the collected samples on filters can serve multiple analytical purposes. Filtration has also been integrated into SUAS designs for radiological sampling. For instance, a research team in Finland investigated a filtration and gamma detection system for radiological particles, that could also theoretically be used to gather bioaerosols for PCR on the same filter (Pöllänen et al., 2009). In contrast to impingers or impactors, whose target for collection is limited to bioaerosols, the ability to collect multiple types of data for analysis makes this a desirable technology for emergency responses (Powers et al., 2018; Smith et al., 2015). Ultimately, the simple and cost-effective technology

performs as well or better for identification of biological agents in multivariant SUAS missions.

Beyond specific instrumentation to detect or quantify CBRN agents, the ability to image potential sources in an unfamiliar environment is important to ensuring that using SUAS in lieu of emergency responders on the ground, is not limiting the critical thinking necessary to adequately evaluate and respond to risk. To enhance the user interface of remote CBRN detection systems, augmented or "virtual" reality programming is one of the avenues being explored. Research has been conducted on the potential for integrating such technology into a ground-based radiation reconnaissance robot. It was found that for ground-based systems, projecting the camera image into a virtual reality would be feasible, though lag times were significant for emergency response scenarios (Lazna, 2018). Virtual reality technology is already heavily used in the civilian sector. Student researchers at MIT have even begun work on a virtual reality training environment for their autonomous drones—with the goal of their autonomous system being able to beat human driven SUAS on race courses designed to test speed and agility, so adapting this technology to military operations should be feasible (Chu, 2018). Also, SUAS can easily be set up to perform sampling events for a large area autonomously. This feature allows for larger data sets to be collected for an area without placing a significant demand on the human operators in the system (Schmale et al., 2008).

Though not studied in reference to aerosol sampling, ground effects also should be given some consideration in a constrained sampling environment. When taking off or hovering near the ground, the downward thrust of the rotors under the body of the aircraft causes air to be recirculated in a manner that creates a pocket of air which enhances

helicopter and fixed-wing aircraft performance by adding more lift into the system than is present in normal conditions. This creates a recirculation of air which may skew sampling concentration results in a positive direction (Eberhart, 2017). Electric Ducted Fan (EDF) based propulsion has been examined in a variety of studies for its ability to minimize rotor wash effects on sampling (Yoon et al., 2016). Current design considerations for the SUAS also include the possible necessity that the EDF may need to be balanced to maintain stable flight, the large power draw necessary to maintain endurance, and minimizing payload weight.

Summary

In this section, the results of some previous bioaerosol sampling and SUAS integration efforts were reviewed. Along with the history of SUAS bioaerosol sampling efforts, this chapter included SUAS design considerations. The relevance of bioaerosol sampling as an important aspect to consider for longitudinal environmental exposure assessments, as well as for potential use in the DoD in emergency response scenarios was also briefly discussed.

III. Sampler Design Process and Modeling

Chapter Overview

The purpose of this chapter is to establish which mission requirements were used as a basis for the sampler design, as well as metrics that were established to determine if the sampler would perform to desired specifications within a SUAS. This includes a brief overview of systems engineering concepts that were used in development of this SUAS bioaerosol sampler and some recommendations on further testing that should be performed prior to accepting such a sampler as operationally capable. The other purpose

of this chapter is to detail the calculations that were used to develop the inlet design for the EOS. The chapter starts with a review of the system engineering concepts, then dives into the sampler performance metric of aspiration efficiency and guiding principles in centrifugal fans. These concepts were used to guide the design of the sampler inlet. Calculations for various flight regimes and flow rates are then detailed, before concluding on which inlet size and style was chosen for the EOS sampler.

Defining Mission Requirements

In order to determine the appropriate configuration of SUAS and bioaerosol sampler properties needed, the mission requirements were first developed.

Mission Requirements:

Mission requirements include a vehicle capable of executing a 30-minute survey mission, including flight time to site and back to decontamination line. The system should also be capable of collecting non-viable bioaerosol sample to determine concentration and identity of bioaerosols present. Finally, the system should also be modular; built with commercial off-the-shelf components, and is transportable and operable in variable environments.

Mission requirements are generally set by the customer; however, in this case the technology is being developed in anticipation of future customer needs. These requirements are based on professional judgement of the designer and from a mission set defined by the Department of Energy (DOE) for a similar multirotor SUAS to be used in CBRN detection (D. Jacques, personal interview, Jan 23, 2019).

The mission requirements as described by this customer can be referenced in

Appendix 2. DOE Guidance for Radiological SUAS

Customer Needs

Detecting and locating the existence of CBRNE material in an urban environment

Tactically deployable and operable

Capable of semi-autonomous operation with human-in-the-loop control

Appendix 3. 12V DC Fugetek Fan Manufacturer's Data

DC BLOWER

75x75x30mm(2.95"x2.95"x1.18")

General Specification:

- Frame:Plastic 94V-0
- Impeller:Plastic 94V-0
- Lead wire:UL Type
  (+):Red (-):Black
- Operation Temperature:-10℃~ 70℃

Motor Protection:

- Impedance Protected
- Reverse Polarity Protected

Specifications(Normal) S=Sleeve bearing B=One ball bearing D=Two ball bearing

Model No.	Bearing System	Rated Voltage (VDC)	Speed Type	Rated Current (A)	Rated Speed (RPM)	Air Flow (CFM)	Air Pressure (mmAg)	Noise Level (dBA)	Weight (g)
HT□C07530	S/D	12	H	0.30	3500	12.02	16.81	42.0	85
			M	0.16	3000	9.40	9.30	38.0	
			L	0.12	2500	7.81	5.96	33.0	
		24	H	0.16	3500	12.02	16.81	42.0	
			M	0.12	3000	9.40	9.30	38.0	
			L	0.10	2500	7.81	5.96	33.0	

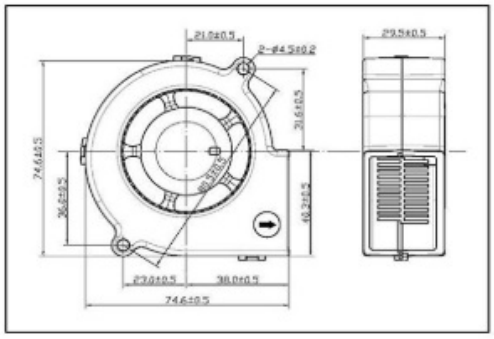

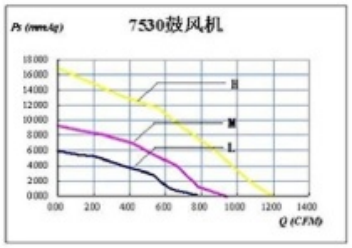

◎ All reading are typical values at rated voltage.
◎ Specifications are subjected to change without prior notice.

Retrieved from: https://www.amazon.com/Fugetek-Brushless-HT-07530D12-75x75x30mm-Computer/dp/B00B2ARV22

. It was decided that a non-viable sample would be targeted for collection, since many BWAs generate spores; and because the concept of operations relies on a centrifugal fan and filter—both of which may dry out and kill biological cells themselves due to the nature of their operation.

Defining Measures of Effectiveness and Performance Measures

Measures of Effectiveness (MOEs) are quantifiable metrics that can be applied to the scope of the mission, in order to determine its success or failure (Sproles, 2000). The MOEs in Table 1 are the numeric extensions of the Mission Requirements previously defined.

Table 1. Identified Measures of Effectiveness and their Descriptions

MOE identifier	Description
Tactical Deployability	The number of people required to operate the system. HMMWV transportable; launch and operation ≤ 4 people.
Identification of BWAs	Capability of capturing 100% of particles 0.5 to 1 microns in diameter present in the sampled environment.

Key Performance Parameters are those characteristics that are fundamental to system operation. If these standards are not met, the performance of the mission would be fundamentally changed, and may cause a project to be terminated (Roedler et al., 2005).

Table 2. Identified Key Performance Parameters

Subsystem	KPP Identifier	Description
Air Vehicle	Navigation	The Air Vehicle shall be capable of waypoint navigation
Air Vehicle	Telemetry: Send	The Air Vehicle shall always be capable of transmitting telemetry to Ground Control Station during the mission.
Ground Station	Telemetry: Receive	The Ground Station shall always be capable of receiving telemetry from the Air Vehicle during the mission.
System	System Transportability	Modular system capable of small team transport and operation. Capable of safe retrieval of sample without adding contamination.
Payload	Quantification of Biologicals	Capability of captured sample to quantify the true concentration of bioaerosols in the environment or accurately identify bioaerosols present, to a 95% confidence interval.

Technical Performance Measures (TPMs) were defined next. TPMs are metrics that can be applied to each major subsystem, and aid in the definition of mission "success". They also serve as checkpoints to the designer to determine whether the system is on-track to meeting the mission requirements during the design process (Roedler et al., 2005). The first two TPMs identified were weight and endurance. These are specific to the UAV itself, and both were derived from DOE guidance for an SUAS capable of radiological detection in an urban environment; the start-time was also derived from the DOE build (see Appendix 2. DOE Guidance for Radiological SUAS

Customer Needs

Detecting and locating the existence of CBRNE material in an urban environment

Tactically deployable and operable

Capable of semi-autonomous operation with human-in-the-loop control

Appendix 3. 12V DC Fugetek Fan Manufacturer's Data

DC BLOWER

75x75x30mm(2.95"x2.95"x1.18")

General Specification:

- Frame:Plastic 94V-0
- Impeller:Plastic 94V-0
- Lead wire:UL Type
  (+):Red (-):Black
- Operation Temperature:-10℃~ 70℃

Motor Protection:

- Impedance Protected
- Reverse Polarity Protected

Specifications(Normal) S=Sleeve bearing B=One ball bearing D=Two ball bearing

Model No.	Bearing System	Rated Voltage (VDC)	Speed Type	Rated Current (A)	Rated Speed (RPM)	Air Flow (CFM)	Air Pressure (mmAg)	Noise Level (dBA)	Weight (g)
HT□C07530	S/D	12	H	0.30	3500	12.02	16.81	42.0	85
			M	0.16	3000	9.40	9.30	38.0	
			L	0.12	2500	7.81	5.96	33.0	
		24	H	0.16	3500	12.02	16.81	42.0	
			M	0.12	3000	9.40	9.30	38.0	
			L	0.10	2500	7.81	5.96	33.0	

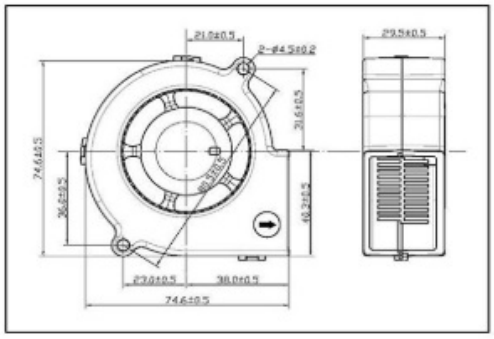

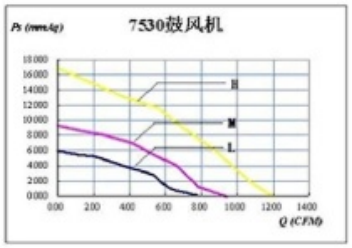

◎ All reading are typical values at rated voltage.
◎ Specifications are subjected to change without prior notice.

Retrieved from: https://www.amazon.com/Fugetek-Brushless-HT-07530D12-75x75x30mm-Computer/dp/B00B2ARV22

). Next, the bioaerosol specific TPMs were chosen. The sound level measurement was set at 60 dBA because this is the sound level of a normal conversation, and well below hazardous levels (Risojević et al., 2018). The sampler bias—how different the sampled value is from the actual concentration value, and in what direction the difference lies—was set at ±25%.

Table 3. Identified Technical Performance Measures

System Element	Parameter	Target
UAV Frame, Battery, Propulsion	Weight	20 lbs
	Endurance	30 min
Operator	Time for start-up and system interface	30 min
Payload—EOS Bioaerosol Sampler	Sound Level Measurement	60 dBA
	Bioaerosol Sampling Bias	±25%

This value was chosen based on the percent error established by National Institute for Occupational Safety and Health (NIOSH) and the Occupational Safety and Health Administration for the evaluation of sampling methods for airborne contaminants in 1974. Though these experiments were for direct reading instruments primarily used for airborne chemical detection, biological agents do not have a similar guidepost for detection—likely because the exposure to biologicals does not follow typical exposure curves (NIOSH, 2012). Though not designated as a TPM, minimizing cost was also

considered throughout the design process. Keeping systems minimal from a technical perspective, served to limit both weight of components and cost of the designed technology.

Once the design requirements for the mission, and their corresponding TPMs were decided on, the components for the build were considered. The rest of this chapter discusses the modeling done to select the appropriate filter and sampler body type for sampling.

Fundamental Inlet Design Concepts

Forward curved centrifugal or "squirrel cage" fans are a very versatile technology, commonly used in industrial facilities across the world, or even cooling computers for at home use. Their range of sizes and unique design make them ideal for this broad spectrum of uses, and an ideal candidate for adaptation into new technologies. As seen in Figure 1, air is drawn into the centrifugal fan from the inlet at the top of the fan. As the blades (lining the impeller like a pinwheel) spin, they create a high static pressure (SP) along the outside edge and along the sides at the outlet—represented by red in the diagram—and low SP at the center—represented by the green.

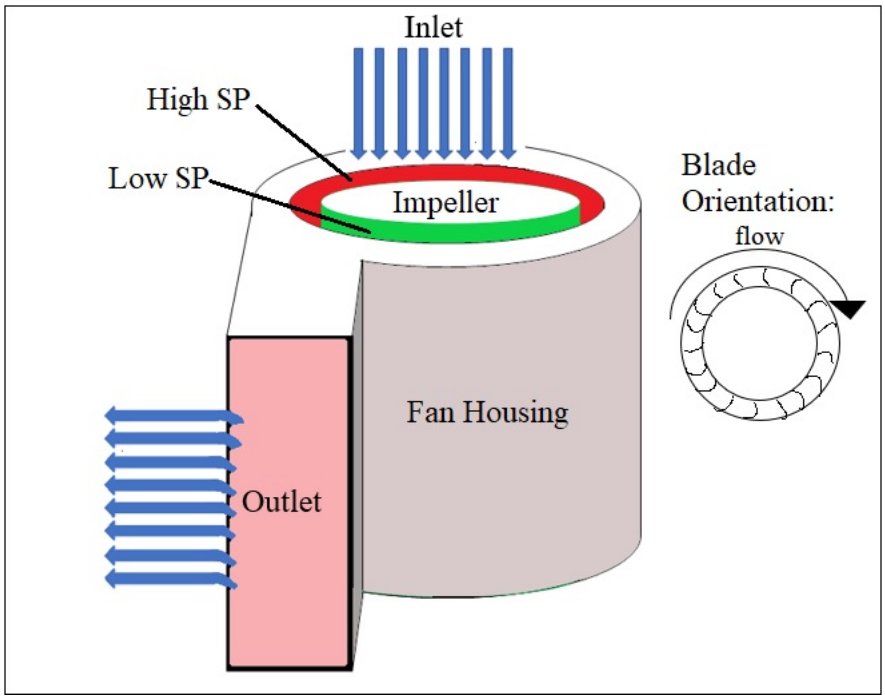

Figure 1. Static Pressure and Relative Flow in Squirrel Cage Fan

The orientation of the blades in the direction of the flow of air results in the air being thrust forward (ACGIH, 2019). This equates to very high velocity pressure entering the spinning blades, allowing for a very high air flow rate (Q), for relatively little power draw and minimal weight compared to other aerosol samplers of the same Q (Kind and Tobin, 1989). In the development of the EOS sampler model, a Fugetek 12V DC Brushless Fan (Houston, Texas) was used—the low cost per fan ($10 each) also providing an attractive addition to a disposable system. This fan theoretically allowed for variable Qs of 12.02 cfm, 9.40 cfm, or 5.96 cfm and an inlet diameter of 46 mm was used as the squirrel cage model—the flow values were adjusted based on actual measurements, as seen in the Revised Modeling Results section of this chapter. Different sizes of filter and blunt sampler body were considered based on these metrics. Blunt samplers—those that do not have long or tapered inlets typically needed to create isokinetic sampling conditions—

were chosen over isokinetic samplers (Paik et al., 2018). This is due to their common use in Industrial Hygiene and due to the consideration that the sampling conditions near UAS in flight are highly turbulent, making effective isokinetic sampling impractical.

Bioaerosol sampling presents a challenge for filtration sampling, as one must consider the tradeoffs between sampling flow rate and capability of capturing identifiable cells or—more likely—their spores (Reponen, et al. 2011). This is in addition to the challenge of adequately capturing samples of small aerosols in turbulent conditions, which exist in the area surrounding a multirotor SUAS as it generates thrust to hover. Isokinetic sampling is the ideal flow regime for aerosol sampling and relies on laminar flow being achieved at the face of the sampler and would result in an efficiency approaching 100% for any given particle size; however it is nearly impossible to create this in real-world conditions as factors such as sampler position, air flow, and others will all impact the flow regime. This difficulty of obtaining isokinetic sampling conditions is exacerbated by the incorporation of sampling into UAS platforms, where Bernoulli's principles for maintaining flight will impact the flow dynamics of an aerosol sampler. This is especially true of operations occurring in outdoor environments, as different wind speeds will create even more turbulence than would have existed in laboratory conditions; in addition to the turbulence of rotor wash. For design purposes, three variable velocities, representing ideal conditions were used—testing with higher speeds would cause the sampling efficiencies to decrease (Hinds, 1999, p. 206-230).

In developing air sampling strategies based in filtration, aspiration efficiency is a prime metric for determining sampler performance. Aspiration efficiency is a measure of how many particles in the free stream enter the inlet of the sampler—essentially a

measure of how isokinetic a sampler is (Paik et al., 2002). Blunt samplers are common in the field of Industrial Hygiene and for filter-based bioaerosol sampling. Some common types are the multi-stage close-faced cassette sampler, the Institute of Occupational Medicine sampler (IOM) which is a variant of semi open-faced sampler, and open-faced cassette samplers. In some cases, the advantages of open-faced filters are clear—such as in highly saturated environments, where the spread of contaminant on a close-faced filter would bias toward the inlet (Beulieu, 1980). However, since the sampling environment cannot be known, both types of filters are investigated for their efficiency over a range sampling conditions.

For a blunt sampler, there are two primary flow regimes as seen in

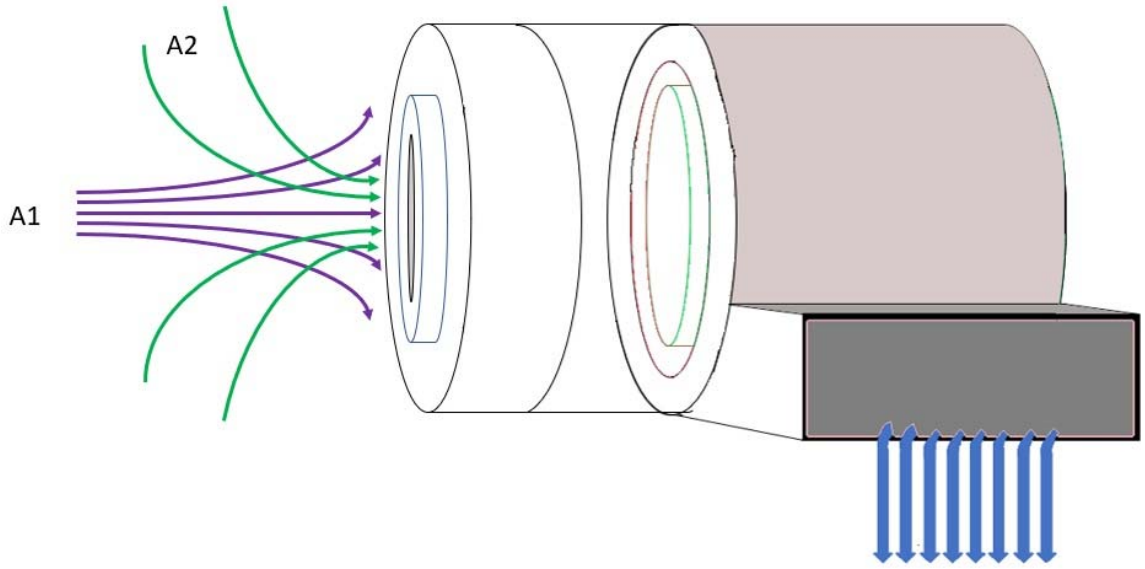

Figure 2. The first (A_1) is the effect of the blunt body itself on the flow stream. That is, the streams will diverge from their original path to go around the blunt object; this is represented by the violet streamlines in Figure 2. The second regime (A_2) is where the

suction of the sampler influences the divergence and pulls the streams back toward each other and in the inlet; indicated by the green streamlines in Figure 2.

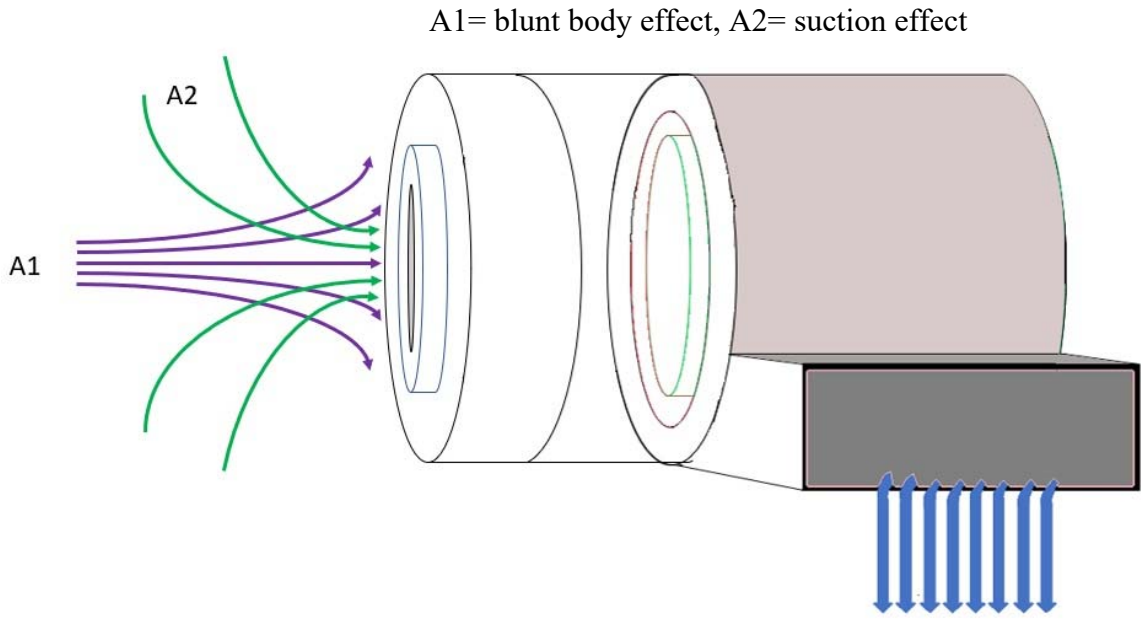

Figure 2. Flow Regimes for a Theoretical Blunt Sampler

The overall efficiency of the sampler is the product of the efficiencies from A_1 and A_2 (Vincent, 2007). These calculations, and others manipulated in the Methods section are from Vincent's *Aerosol Sampling* and Hind's *Aerosol Technology*.

Calculations

Aspiration efficiency is a function of the Stoke's number, the sampler inlet diameter, and the ratio of air velocities. Table 1 shows the values of the parameters explored in this simulation. The closed face cassette (CFC) and IOM were modelled with respect to sampling velocity (U_S), free stream velocity (U), aerodynamic diameter (d_{AE}), and inlet diameter (δ).

Table 4. Investigated Parameters for Bioaerosol Sampler Design

Parameter	Value
U_S	1.7, 2.7, 3.4, 5, 8 m/s
U	0.1, 0.5, 1.0, 5.4 m/s
δ	IOM: 0.015, 0.030 m CFC: 0.010, 0.009 m
d_{AE}	0.5, 1, 2, 3, 4, 5, 10, 15, 20, 30, 40, 50 µm

First, the respective U_S values were calculated given the Q and diameter of the Fugetek fan mentioned above. Using Equation 1, and the Fugetek operational characteristics, the U_S values were calculated to be 3.4 m/s, 2.7 m/s, and 1.7 m/s for the high, medium, and low Q's. Also investigated were very high sampling velocities of 5 and 8 m/s. Most of the free stream velocities investigated, assumed relatively still air that will be present in the aerosol chamber during testing or conditions for sampling off a UAS that has landed (Zaripov, 2014). Also investigated was the theoretical velocity contributed by downdraft from a UAS in hover. A_S in Equation 1 is the area of the sampler inlet, and was calculated from the listed δ values in Table 4.

Equation 1 $\boldsymbol{Q = U_S A_S}$

The values for U_S were also used with Equation 2, to calculate the pressure drop (Δp) across several theoretical types of commercially available filters. The type of filters used and their calculated pressure drops at the designated velocities are in Table 5 in the Results. In Equation 2, η is the viscosity of air, and f(α) which is a function of the filter's porosity (α), usually given by the manufacturer.

Equation 2 $\boldsymbol{\Delta p = \frac{\eta t U_s f(\alpha)}{{d_f}^2}}$ where $\boldsymbol{f(\alpha) = 64\alpha^{1.5}(1 + 56\alpha^3)}$ for $\boldsymbol{0.006 < \alpha < 0.3}$

Membrane based filters with pores are commonly used for bioaerosol sampling, however the d_f in Equation 2 represents the diameter of fibers in a filter. Where pore sizes were published by the manufacturer, these were estimated to be the same as the effective fiber diameter with the same sampling characteristics (Hinds, 1999, p. 182-204). This relationship has been observed in some other studies, though characteristics like porosity and d_f are often measured indirectly, and even when modeled accurately modern filter treatments and variability of individual filters may impact results (Matsumotok et al., 2004).

Next, the Stokes number was calculated for a variety of particle sizes using Equation 3. The majority of bioaerosols exist below 10 µm in size, but they may be carried through the air in larger droplets of water or even on solid particulate matter. Since bioaerosols come in a vast array of sizes, the spectrum ranges from 0.5 to 50 µm. Biological collection efficiency applies to viable biological samples, so was not included in these simulations, as spores are the primary target of this sampling. The Cunningham slip correction factor (C_c)—found in Appendix A-11 in Hinds—was included for particles whose aerodynamic diameter was less than 2 microns, for the rest of the trials this was disregarded.

Equation 3 $$\boldsymbol{St = \frac{d_{ae}^2 * \rho_p * U * C_c}{18 * \eta * \delta}}$$

From these values, the first aspiration efficiency, A_1 was calculated using Equations 4-6. In these equations *St* represents the Stoke's number, β is the aerodynamic bluntness of the sampler, *r* is the ratio of sample inlet diameter to the blunt body

diameter, and ϕ_A is the sampling ratio of axisymmetric flow. G_1 is a constant determined empirically to be 0.25 (Paik et al., 2002).

Equation 4 $$St_1 = St\left(\frac{r}{\phi_A^{\frac{1}{3}}}\right)$$

Equation 5 $$\beta_1 = 1 - \left(\frac{1}{1+G_1 St_1}\right)$$

Equation 6 $$A_1 = 1 + \beta_1(\phi_A^{-\frac{1}{3}} - 1)$$

After A_1 was calculated, A_2—pertaining to the effect of the suction from the inlet—was calculated. The St values initially calculated were used to calculate the value of St_2.

Equation 7 $$St_2 = St\phi_A^{\frac{1}{3}}$$

Equation 8 $$\beta_2 = 1 - \left(\frac{1}{1+G_2 St_2}\right)$$

Like G_1, G_2 is an empirically determined constant. In this case, the best fit was achieved when G_2 was 6. Though these values were determined for the d_{AE} range of less than 12 µm, Chung and Ogden measured aspiration efficiencies of up to 60 µm. They observed good agreement with the values for both G_1 and G_2 that were calculated in the lower d_{AE} range to what was observed in the higher d_{AE} range (Chung and Ogden, 1986).

Equation 9 $$A_2 = 1 + \beta_2\left(\left(\frac{r}{\phi_A^{\frac{1}{3}}}\right)^2 - 1\right)$$

Finally, both efficiencies were multiplied together to give the final aspiration efficiency for the sampler under the given simulation conditions (Equation 10).

Equation 10 $$A = A_1 A_2$$

These equations were derived for blunt body samplers both free-standing and fixed to a person. Though attachment to a SUAS, especially while operational, would create significant differences in flow dynamics near the sampler compared to the initial scenarios the model was made for, other models specifically for SUAS application have not been developed and tested. Though conditions may be different than what were used to develop the equations, they were assumed to be accurate enough to base an initial design off of.

Final simulations also involved calculating the velocity induced by the multirotor blades in hover—presumably when sampling would take place. This was calculated using Equation 11 and Figure 3.4 in Reg Austin's *Unmanned Aircraft Systems: UAVS Design, Development and Deployment*. In the below equation, k_n is a correction factor, here assumed to be 1.1 for a moderate performance SUAS (the typical range being 1.05 to 1.2). The disc-loading in N/m^2 (p) was derived from the airspeed assumption and Figure 3.4 from the referenced text; in this case $p = 60\frac{N}{m^2}$. Density in the equation is the density of air where the flight is maintained, in this case assumed to be 1.225 kg/m^3.

Equation 11 $$v_i = k_n\left(\frac{p}{2\rho}\right)^{1/2}$$

The assumption was made that the SUAS would fly at a maximum height of 20 ft at 10 m/s; this was based on the mission profile that biological sampling would require and performance of standard SUAS models (Austin, 2010, p. 30).

Initial Model Results

In some cases, the solidity of the filters was not available and so these filter porosity values were estimated given the general relationship between pore size and filter solidity (Hinds, 1999, p. 202). Given the general range of solidities and pore sizes that membrane filters do not exceed, and data from other manufacturers, the relationship is depicted below in Figure 3. Ultimately, the two highest performing filters were those whose filter porosities were listed by the manufacturer. The relationship between pore size and solidity also has not been studied in depth outside of the assertation in Hinds that the relationship exists, so more research would be required before accepting this model as accurate.

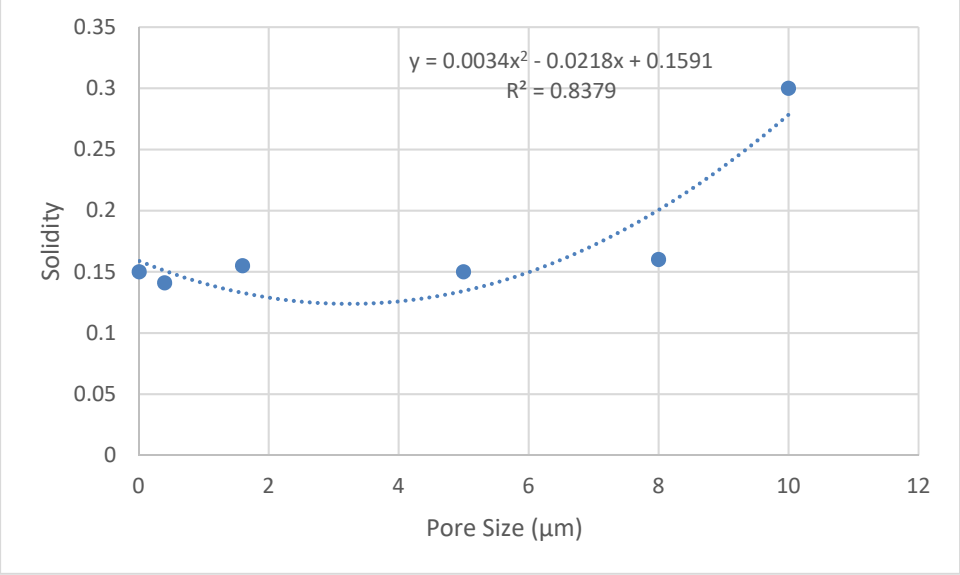

Figure 3. Modeled Pore Size vs Solidity in Membrane Filters

The results of the pressure drop calculations are documented in Table 5. After examining a variety of filters, the lowest pressure drop occurred in a filter with a 5 µm pore size, a thickness of 5.75E-05 m, and a 47 mm filter diameter. The second best performing filters were 8 µm in pore size; it should be noted that both of these types of filters had their pore sizes published by the manufacturer, so their pressure drops can be assumed to have a higher degree of accuracy than other filters, whose porosities were derived. The filter diameter is as important as the pressure drop in this case, because this dimension drives part of the design of a blunt sampler overall.

Table 5. Pressure Drop (Pa) Over Filters of Varying Pore Size and Thickness

Pore Size	0.4 µm	1.6 µm	2 µm	5 µm	8 µm	11 µm	20 µm
t (m)	0.000025	2.60E-04	4.60E-05	5.75E-05	0.000135	0.00018	0.000215
$\Delta p\ V_H$ (Pa)	43263.97	25100.00	2360.00	628.52	656.58	2429.18	877.71
$\Delta p\ V_M$ (Pa)	33833.72	19600.00	1850.00	491.52	513.47	1899.69	686.36
$\Delta p\ V_L$ (Pa)	21452.02	12400.00	1170.00	311.64	325.56	1204.49	435.20

Given this new data, the parameters from Table 1 were manipulated until the desired overall efficiency was obtained. For this simulation, this means the lower aerodynamic diameters were at 100% efficiency—especially the one to two µm diameters characteristic of bacterial spores. Table 2 represents one scenario, where the lowest possible sampling velocity was used—due to the lower resultant pressure drop—and the ambient air was modeled at velocities from 0.1 m/s to 1 m/s; essentially, still air.

Table 6. Efficiencies Associated with a Sampling Velocity (U_s) of 1.7 m/s

	CFC			IOM		
U:	**0.1 m/s**	**0.5 m/s**	**1 m/s**	**0.1 m/s**	**0.5 m/s**	**1 m/s**
0.5 µm	99.99%	100.00%	100.00%	99.98%	99.97%	99.97%
1 µm	99.98%	99.99%	99.99%	99.94%	99.90%	99.88%
2 µm	99.93%	99.96%	99.98%	99.79%	99.64%	99.55%
3 µm	99.85%	99.92%	99.95%	99.57%	99.26%	99.07%
4 µm	99.74%	99.31%	99.03%	99.23%	93.78%	85.67%
5 µm	99.59%	98.93%	98.49%	98.81%	90.61%	79.28%
10 µm	98.37%	95.88%	94.30%	95.39%	70.71%	48.93%
15 µm	96.41%	91.27%	88.29%	90.20%	51.79%	29.90%
20 µm	93.81%	85.63%	81.42%	83.82%	37.71%	19.40%
30 µm	87.12%	73.34%	68.02%	69.74%	21.28%	9.73%
40 µm	79.28%	61.94%	57.25%	56.51%	13.27%	5.78%
50 µm	71.18%	52.57%	49.40%	45.46%	8.99%	3.83%

The inlet diameter for the CFC was 10 mm and the diameter for the IOM was 20 mm. Per the table, the efficiencies were at or near 100% across all ambient air conditions for particles with low aerodynamic diameters—those lower than 4 µm. The most drastic change occurs for particles larger than 30 µm when sampled at 1 m/s. In this category, the CFC performs much better than the modeled IOM.

In the next scenario, the inlet diameters were changed to 9 mm for the CFC and 30 mm for the IOM. The difference in diameter of the CFC in these conditions did not significantly impact the performance. The only category where aspiration efficiency improved was the wind speed of 0.5 m/s, and even this increase was only approximately 1% for each aerodynamic diameter. Other scenarios run with the CFC with an inlet diameter smaller than 9 mm, decreased theoretical sampler performance in all conditions. The IOM performance did change from 20 to 30 mm. Efficiencies were boosted

dramatically across the higher end of the spectrum, with diameters of 10 microns and under all at or approaching 99% efficiency.

Table 7. Modified Efficiencies Associated with a Sampling Velocity of 1.7 m/s

	CFC			IOM			Open Faced Cassette		
U:	**0.1 m/s**	**0.5 m/s**	**1 m/s**	**0.1 m/s**	**0.5 m/s**	**1 m/s**	**0.1 m/s**	**0.5 m/s**	**1 m/s**
0.5 µm	99.99%	100%	100.00%	99.99%	100%	99.98%	100%	100%	100%
1 µm	99.98%	100%	99.99%	99.97%	100%	99.94%	100%	100%	100%
2 µm	99.93%	100%	99.98%	99.90%	100%	99.77%	100%	100%	100%
3 µm	99.85%	100%	99.95%	99.78%	100%	99.53%	100%	100%	100%
4 µm	99.74%	99%	99.03%	99.62%	97%	92.19%	100%	100%	100%
5 µm	99.59%	99%	98.49%	99.40%	95%	88.31%	100%	100%	100%
10 µm	98.37%	96%	94.30%	97.64%	83%	65.43%	99%	98%	99%
15 µm	96.41%	91%	88.29%	94.85%	68%	45.78%	98%	96%	97%
20 µm	93.81%	86%	81.42%	91.21%	55%	32.31%	97%	94%	95%
30 µm	87.12%	73%	68.02%	82.22%	35%	17.71%	93%	88%	91%
40 µm	79.28%	62%	57.25%	72.32%	23%	10.99%	88%	82%	87%
50 µm	71.18%	53%	49.40%	62.69%	17%	7.49%	83%	76%	83%

Many studies have been done that found the IOM is more efficient with larger particle sizes, however the relative efficiencies of these sampling types are generally comparable at lower particle sizes (Harper and Muller, 2002). This appears to be substantiated by the models for sampling efficiencies for particles under five microns. This is especially true when considering appropriately sized inlet diameters for each respective sampler. Also tested in the second round of modeling was an open-faced cassette. Overall, this performed best out of all the samplers at the lowest sampling velocity in relatively still air. This performance is also supported by literature dating back to the 1980's and through the present (Beaulieu et al., 1980).

The next phase in modeling involved using the calculated hover velocity expected in small sized hexacopters. Under these assumptions, the calculated velocity was 5.4

m/s—this only models the downward velocity of the rotors created in hover mode and does not account for forward flight. Since the flight pattern assumes the samples are taken in hover, forward flight was not modeled at this stage of development. For the hover simulation, the CFC was compared to the open-faced cassette, as these were the best performing samplers from earlier trials. Table 8, below, holds the results of this simulation. At the lowest sampling velocities, the sampling efficiency improved to 100% for all particle sizes for both the CFC and open-faced cassette. Only at the highest sampling velocities did sampling performance decrease.

Table 8. Modeling Effects of Rotor-Wash on Sampling Efficiency

	CFC					Open Faced				
U_s:	**1.7 m/s**	**2.7 m/s**	**3.4 m/s**	**5 m/s**	**8 m/s**	**1.7 m/s**	**2.7 m/s**	**3.4 m/s**	**5 m/s**	**8 m/s**
0.5 µm	100%	100%	100%	100%	100%	100%	100%	100%	100%	100%
1 µm	100%	100%	100%	100%	100%	100%	100%	100%	100%	100%
2 µm	100%	100%	100%	100%	100%	100%	100%	100%	100%	100%
3 µm	100%	100%	100%	100%	100%	100%	100%	100%	100%	100%
4 µm	100%	100%	100%	100%	100%	100%	100%	100%	100%	100%
5 µm	100%	100%	100%	100%	100%	100%	100%	100%	100%	100%
10 µm	100%	100%	100%	100%	100%	100%	100%	100%	100%	100%
15 µm	100%	100%	100%	100%	99%	101%	100%	100%	100%	100%
20 µm	101%	100%	100%	99%	99%	101%	101%	100%	100%	100%
30 µm	101%	100%	99%	98%	97%	103%	102%	101%	100%	99%
40 µm	102%	100%	99%	97%	95%	105%	103%	102%	100%	98%
50 µm	104%	100%	99%	96%	93%	107%	104%	103%	100%	98%

Modeling Discussion

The high performance of the samplers when modeled for a rotor-wash environment is interesting, as even in similar conditions, real-world sampler classification demonstrates that these types of samplers often have a negative sampling bias when used with UAS. The overall trend of decreased sampler performance with increased sampler

speed for particles larger than 10 microns, matches literature (Chavez, 2017). However, the efficiencies being over 100% for several trials of larger particles does indicate that these calculations have a positive bias. This simulation does not account for the unique variations in air flow that are created with rotor wash, only the air speed itself—so in reality the efficiencies would be expected to decrease in real-world conditions. Additionally, the assumption that the UAS is only taking samples while in hover does not account for the possibility that a UAS can draw samples during forward flight—a flight pattern which increases the overall efficiency of the aircraft—or the possibility of variable winds creating velocity vectors in the x- and z-axis, in addition to the y-axis hover profile.

Initial Modeling Conclusions

Through running a variety of empirical models for different sampler types, the optimal perceived configuration for a SUAS-based bioaerosol sampler is an open-faced cassette. This is supported by some evidence in the literature where open-faced cassettes out-performed CFCs in high-saturation environments and were used as successfully as CFCs and IOMs sampling particulates with small aerodynamic diameters. These reasons, among others make open faced cassettes a catch-all for sampling unknown environments in the field of Industrial Hygiene and make this configuration optimal for serving as the basis for a new type of bioaerosol sampler.

Revised Modeling Results

As discovered in the initial performance measurements taken from the EOS, the sampler could not achieve a high flow rate—this conclusion is discussed in Chapter V.

Analysis and Results. Since the sampler could not achieve a high flow for sampling, the U_s had to be adjusted to 0.09 m/s for the EOS across all background velocities. Though the calculated rotor wash velocity was 5.4 m/s, since the sampler flow rate decreased significantly, the feasibility of drawing a representative sample in hover is less likely. To account for this, the modeled background velocity was increased to 21.0 m/s—adding forward flight velocity and accounting for some rotor wash and ground effects that would be present in the chamber. Table 9 contains the adjusted values for the lower sampling velocity with the forward flight assumption in place.

Table 9. Adjusted Modeling for EOS (w/ Rotor-Wash) on Sampling Efficiency

U (m/s):	21.0	5.4	1.0	0.5
0.5 µm	100%	100%	100%	100%
0.7 µm	100%	100%	100%	100%
1 µm	100%	100%	100%	100%
5 µm	91%	94%	97%	97%
12 µm	65%	74%	33%	56%
30 µm	24%	32%	8%	17%

The modeled aspiration efficiency for forward flight, is compared to the actual efficiencies gathered from Optical Particle Count (OPC) sampling done in the Results.

IV. Methodology

Chapter Overview

The purpose of this chapter is to detail the quantitative testing that will be done to verify that the sampler can perform the mission developed in Chapter II, and to what level the sampler performance deviated from the target TPMs. Testing to be performed also included a qualitative look at flow characteristics in the chamber while the SUAS was operational, and a qualitative analysis of proposed system components aside from the

payload that would serve as a modular and functional biological sampling system for emergency response and environmental health personnel.

Small Unmanned Aerial System

The SUAS used in this research was built by the AFIT ANT Center. In order to fit inside the Multi-Use Research for Particulate Hazards and Exposure Environment (MURPHEE) chamber, an X-8 quadcopter frame, from the 3D-Robotics (3DR) Do-It-Yourself Quad Kit, capable of fitting four to eight motors was used. This frame was stripped down to only four 3DR 880 kV brushless motors and 20 Amp 3DR electronic speed controllers (ESC) (Berkeley, CA), as the frame could not maintain flight within the chamber. 11x4.7SFP APC propellers (Woodland, CA) were used in this build. In lieu of batteries, which would require charging between each test, a variable DC power supply the Volteq model HY30100EX—a 30V and 100A source (San Jose, CA), was used for the duration of testing.

Equipment

The MURPHEE chamber was used for this research as it was well-characterized for laminar flow potential. The results of the characterization study indicated that Section 7 of the chamber had uniform flow conditions, so that section was used for trials where the rotors were not used. In order to accommodate the power source when the rotors were on, the tests were done just inside the door section of the chamber, as the cords on the power source could not reach Section 7. Though the section of MURPHEE by the door is not laminar or uniform flow, the movement of the rotors created well-mixed conditions which were verified via a smoke test prior to sampling.

Various test aerosols were considered for this research, including Polystyrene latex (PSL) spheres, Arizona Road Dust (ARD), a 0.2 g/mL sucrose solution, and *Bacillus globigii* (BG) spores. Since the average aerodynamic diameter of anthrax spores is between 1-2 µm, monodisperse aerosols within this range were primarily considered. BG spores have a median aerodynamic diameter of 1.42 µm (Edmonds, et al. 2016). For this reason, they are commonly used as a surrogate for *Bacillus anthracis*, and are nonhazardous as a biosafety level 1 organism. These were also considered but abandoned due to time constraints. Figure 4 demonstrates a common range of bioaerosol sizes; almost all bacteria and their spores fall under 12 microns in diameter (Jacobson and Morris, 1976). However, studies done by Davies and Noble in 1962, revealed that skin particles that commonly carry bacteria fall around the 12-micron size range. For these reasons, this size range was included in the data collection. While most of the analysis was concerned with particles under two microns, particles less than 1 micron were still included, in order to verify if the sampler might theoretically be used to collect viruses or smaller bacteria spores in the future. For continuity of observing the behavior of the sampler with large particles, a bin up to 30 microns was also included during the OPC data collection and analysis. Figure 4 was reproduced from data published by Davies and Noble (1962), Carrera, et al. (2007), and Hinds (1999).

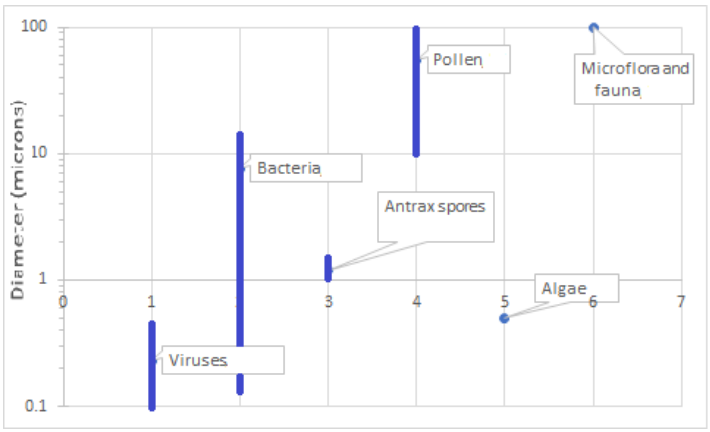

Figure 4. Particle Sizes for Common Bioaerosols

Monodisperse PSL test aerosols of 1, 2, and 12 µm aerodynamic diameter were also considered, but ultimately rejected. This was because though monodisperse aerosols of an established size offer highly accurate results, these aerosols are often expensive and require extensive testing—involving many test repetitions (John and Kreisberg, 1999). Though the sucrose solution and ARD were both used successfully in previous experiments, ultimately ARD was favored over sucrose due to the easier nature of cleanup and the well-characterized distribution associated with ARD when compared to sucrose (Chavez, 2017). Polydisperse ARD ISO Ultrafine, which has a nominal aerodynamic diameter between 0.5 to 22 µm (CMD of 4.32 µm, density of 0.9 g/cm^3), was generated and introduced into the test chamber via a Rotating Brush Generator (RBG 1000) from Palas (Karlsruhe, DE) in order to conduct initial characterization. Polydisperse ISO Medium test dust (shape factor of 1; CMD of 13.81 µm, density of 2.5 g/cm^3) was used in the final test, to investigate size selectivity of the EOS (Fletcher and Bright, 2000).

Two GilAir Plus air sampling pumps (Sensidyne IH Instruments, Muelheim, DE)—numbers 029 and 057—were used with the CFC and calibrated against the primary

standard TSI 4100 (TSI; Shoreview, MN), throughout the experiment. The same primary standard was also used in conjunction with a 3D printed calibration adapter (depicted in orange in Figure 5) to determine the average flow rates of the EOS. An OPC (Particles Plus model 8506-30; Stoughton, MA) was used at in attempt to verify the particle size selectivity of the EOS.

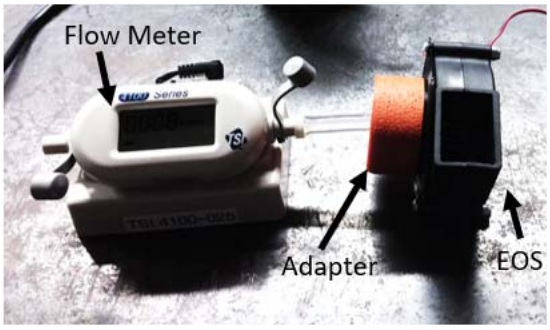

Figure 5. Calibration Train Set-Up for EOS

Gravimetric analysis was used to determine how the EOS performs in different orientations and flight regimes. Gravimetric analysis is a primary method of concentration measurement for total and respirable dusts, per NIOSH Methods 0500 and 0600; however, this form of analysis is not often used with cellulose nitrate membrane filters or biological sampling, due to the affinity of the filters for quickly regaining moisture when in the open environment. Desiccators and a mass balance were used on site immediately after sample collection; therefore, these impacts were assumed to be minimal.

Sound level measurements were also taken to ensure that the potential for extraneous noise from the system is kept to a minimum. To accomplish these, a Larson Davis SLM 831 from Depew, NY (S/N 1188) was pre- and post-calibrated against a

060043 Acoustic Calibrator (Larson Davis, Depew, NY) and several measurements were taken at the source.

Procedures

After initial production of the bioaerosol sampler was completed, the first step was to test the conditions around the door where the non-stationary tests were run. This was accomplished via a smoke generator being enclosed in the first third of MURPHEE and generating smoke as the fan (set at 16 Hz or 0.2 m/s) pulled air through the chamber to the test location. This location is marked by the unlabeled red line in Figure 6. The rotors of the UAS were then turned on, as the trial was filmed, in order to verify approximate flow conditions for testing. All other tests that were done are summarized in Table 10.

Table 10. Summary of Methods Used in EOS Sampler Characterization

Method Description	Purpose/Aims	General Equipment Used
Gravimetric analysis of EOS vs CFC performance	Compare developed sampler to standard sampler in ambient conditions for characterization purposes. Analyzed via ANOVA, paired t-tests, and descriptive statistics.	MURPHEE, Ring stand, aerosol generator, Ultrafine ARD, EOS, CFC, desiccator, mass balance
	Compare performance of samplers in different environmental conditions (temperature, pressure, and humidity). Analyzed via regression models.	Same as above, with Kestrel 5700 (Kestrel Meters; Boothwyn, PA)
Gravimetric analysis of EOS in top vs bottom position of UAV while in various flight regimes.	Isolate the ideal placement of the EOS sampler in various flight regimes, based on sample variance and comparison of means. Analyzed via paired t-tests, Student t-tests, and Kruskal Wallis.	MURPHEE, SUAS, aerosol generator, EOS, Ultrafine ARD, desiccator, mass balance
Gravimetric analysis of EOS in top vs bottom position of UAV in 10° hover.	Determine if the flight angle while in hover impacts sampler performance when compared to level hover (0°). Analyzed via descriptive statistics and Student t-tests.	MURPHEE, SUAS, aerosol generator, EOS, Ultrafine ARD, desiccator, mass balance
Gravimetric analysis of EOS in top vs bottom position of UAV in hover at various pulse rates.	Determine if rotor speed while in hover impacts sampler performance. High, medium, and low speeds were investigated. Analyzed via descriptive statistics and Student t-tests.	MURPHEE, SUAS, aerosol generator, EOS, Ultrafine ARD, desiccator, mass balance
OPC analysis of EOS in top vs bottom position of UAV in forward flight.	Determine the size selectivity bias for the UAS airframe and aerosol sampler in forward flight. Percent differences between each sampling position and background particle count concentration were examined. Analyzed via 95% confidence interval on the percent differences and comparison between modeled and actual aspiration efficiencies.	MURPHEE, SUAS, aerosol generator, EOS, Medium ARD, OPC
Flow rate analysis of variable voltages and currents on EOS performance.	Determine whether the voltage or current available to the system impacts the sampler performance of EOS while not sampling ARD. Analyzed via calculating LPM from calibration train setup with variable V and I (Figure 5).	EOS, Primary standard calibrator, variable DC power source, calibration adapter
Weight, power, and endurance metric evaluation.	Determine if weight, power, and endurance metrics are feasible in the current system setup. Analyzed by estimating subsystem parts weight and power demand, and calculating endurance using standard SUAS systems engineering equations.	EOS, SUAS, mass scale, endurance and power spreadsheets
Sound Level Measurement for EOS	Determine if sound levels for EOS sampler are hazardous noise or nuisance noise.	EOS, Sound Level Meter

Next, the performance of the sampler's aspiration efficiency in relatively still air was compared to another common bioaerosol sampler, in this case the 37 mm CFC. This

was approximated with the sampler running while a polydisperse aerosol was generated inside of the characterized aerosol chamber. Twelve paired samples were taken with the EOS and a traditional CFC while ISO Ultrafine test dust was introduced via a port beneath the MURPHEE. The paired samples were taken in Section 7 of the MURPHEE, labeled accordingly in Figure 6 below. The number of samples taken for this and each subsequent test were calculated based off data from pilot studies to reach a 95% confidence level in the data. This was determined using Equation 12 below, where t is the Student t-value, s_s^2 is the sampling variance, r is the acceptable relative standard deviation, and x is the average of the test results.

Equation 12. $$n = \frac{t^2 s_s^2}{r^2 x^2}$$

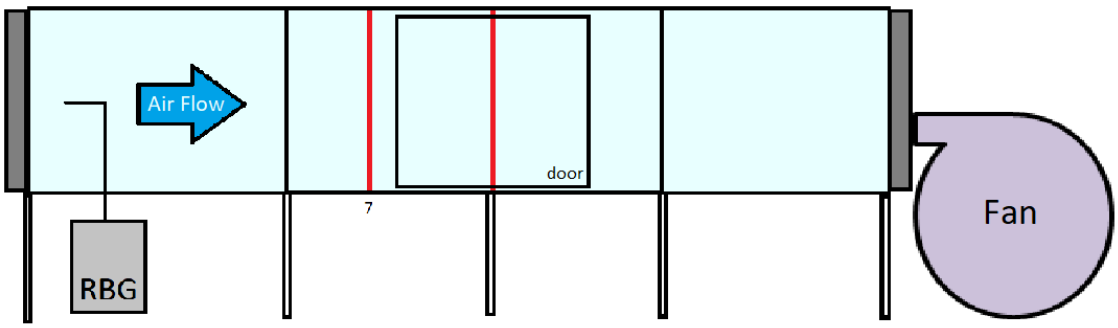

Figure 6. Overall Setup of MURPHEE

Prior to initiating the collection of aerosol samples, the sample filters were desiccated for 24 hours in the laboratory. These were then immediately weighed three times on a microbalance scale. These steps were done in order eliminate mass added to the filters by moisture in the environment and minimize bias from precise pre-sampling weight measurements (

Table 11 in Results). After sample collection, the desiccation process was

Test Day	Order	CFC Weight (mg)	EOS Weight (mg)	CFC Volume (m3)	EOS Volume (m3)	CFC Concentration (mg/m3)	EOS Concentration (mg/m3)	Difference	Ratio
1	1	1.98 ± 0.001	1.00 ± 9E-04	0.117	0.040	16.9	25.3	8.4	1.50
1	2	1.60 ± 5E-07	0.790 ± 6E-04	0.106	0.041	15.1	19.1	4.0	1.26
1	3	0.965 ± 5E-08	0.693 ± 6E-04	0.110	0.039	8.74	17.7	9.0	2.03
1	4	0.997 ± 5E-06	0.906 ± 3E-04	0.114	0.059	8.79	15.2	6.4	1.73
2	5	1.00 ± 5E-08	0.758 ± 7E-04	0.103	0.039	9.73	19.2	9.5	1.97
2	6	0.550 ± 0.001	0.799 ± 5E-04	0.102	0.040	5.39	20.2	14.8	3.75
2	7	0.721 ± 5E-09	0.468± 5E-04	0.104	0.040	6.93	11.8	4.9	1.70
3	8	0.480 ± 5E-04	0.486± 4E-04	0.098	0.043	4.91	11.3	6.4	2.30
3	9	1.36 ± 0.001	0.846 ± 8E-04	0.106	0.043	12.8	19.9	7.1	1.55

repeated. Since the variance between measurements was no greater than 0.001 and had a coefficient of variance below one for all samples; after this initial study, samples were only measured once, except for one random spot-check per each study. Each pump associated with the traditional sampling methods was calibrated in accordance with NIOSH guidance.

Following filter weighing and instrument calibration, each sampling train was assembled within the aerosol exposure chamber in accordance with Figure 7. Undepicted

in this figure are the air flow arrows, which in this case are moving toward the viewer (the cross section looks from the back of MURPHEE where the fan is located, to the front). In this initial pilot study, each sample inlet was oriented downward, as this is the traditional placement of samplers on a human body and decreases the amount of interference from aerosol settling onto the filters. The order in which each sample was taken was randomized via the Excel random number generator, to minimize bias from order in which samples were taken.

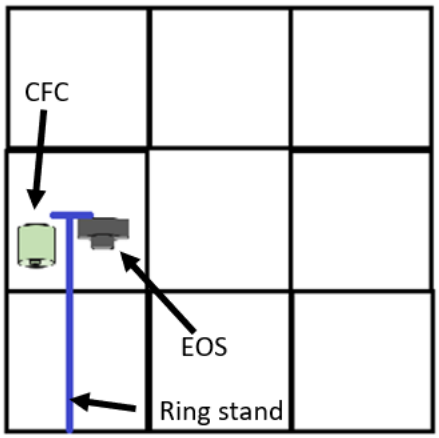

Figure 7. Aerosol Chamber CFC vs EOS Test Set-Up

Aerosols were generated within the chamber by injecting 50 mm (approximately 11.9 g) of dust from the aerosol particle generator through an inlet on the side of the exposure chamber at 2.5 bar. The amount to introduce was based on previous sampling done during characterization of the chamber—full chamber characterization pending publication in 2020. Using NIOSH Methods for the sampling was considered, but biologicals have no such corresponding metric for sampling, and the corresponding amounts allowed previous researchers to accurately perform gravimetric analysis (Titus et al., 2019). This was then circulated via the fan moving air at 0.2 m/s (39.37 ft/min)—a

speed associated with ambient air conditions. Each trial was run for approximately 50 minutes with an average flow rate of 1 LPM for each sampler. These were all running concurrently with the aerosol generator. Sampling occurred over three separate days, with one field blank from each sampler collected per day. Since environmental factors like humidity, temperature, and pressure have the potential to impact sampler performance, these were tracked as well. After sample collection, the filters were placed into the desiccator for 24 hours once again and final weights, done in triplicate only for the initial study, were recorded. A statistically significant sample size for the 95th percentile was calculated for each collected data set via Equation 12. For all statistical tests performed in this research, the statistical significance level (α) of 0.05 was used. This is a common α value for pilot studies in the field of Industrial Hygiene.

During the second test, the sampler's performance while mounted on the UAV while resting on the ground was investigated. This was done in order to approximate the effects that the vehicle body might have on the sampler versus the samplers hanging free from a ring-stand. Since no power was needed, these tests were also performed in Section 7, albeit closer to the center of the chamber due to limitations of the dimensions of the UAV. The difference in orientation—top mounting vs bottom mounting—for the sampler was also examined during this test. Other than mounting position on the vehicle, all other test procedures were repeated from the initial test of EOS vs CFC.

The third test involved examining a UAS in the hover flight regime. In order to conduct any tests without achieving actual flight in the chamber, a platform was built to hold the vehicle, attached to the chamber floor via industrial strength suction cups. Since forward flight was the primary flight regime to be investigated, this platform was built

with a 10° angle—simulating a common tilt of a UAS moving forward (D. Thacker, personal interview, Aug 26, 2019). This presented a limitation for testing the hover flight performance and had to be compensated for. In order to ascertain if this angle had an impact on the sampling of the EOS, two sets of hover data were taken. The first was with the rotors spinning but the fan kept at 16 Hz with the 10° angle kept intact, and the second was with the lower end of the platform raised up on weights that were high enough to keep the platform level (0°). The higher end still relied on the suction cups to ensure the UAS did not take off—it is also important to note that during the non-stationary tests, the suction cups were re-wetted between each trial. The rotors were spun at three different pulse rates by the servo tester during the first trial, to observe if the speed of the blades had an impact on the concentrations sampled. The amount of dust added into the chamber, sampling time, and sampling rates were kept consistent with the earlier tests.

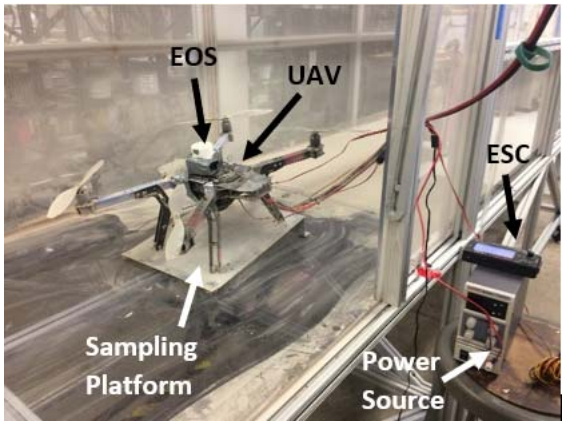

Figure 8. Unadjusted Hover and Forward Flight Set-Up

Next, the forward flight regime was investigated. Since the sampler as developed was not capable of high flow air sampling, this flight regime is of the utmost importance.

For this test, the fan was set at 60 Hz (simulating 16 m/s flight) while the rotors were operating at their highest frequency, to simulate the forward flight of the UAS. As with the hover tests, the amount of dust added into the chamber, sampling time, and sampling rates were kept consistent with all previous tests. After gathering an initial statistically significant sample, another test was run with the Medium ISO test dust with the OPC positioned at the opening of the EOS sampler via connection tubing. This occurred for the sampling with the EOS in the top and bottom sampling positions, Figure 9 demonstrates the position of the tubing at the inlet while the EOS is in the top position. The OPC itself was outside the chamber for ease of monitoring and is not shown in the figure.

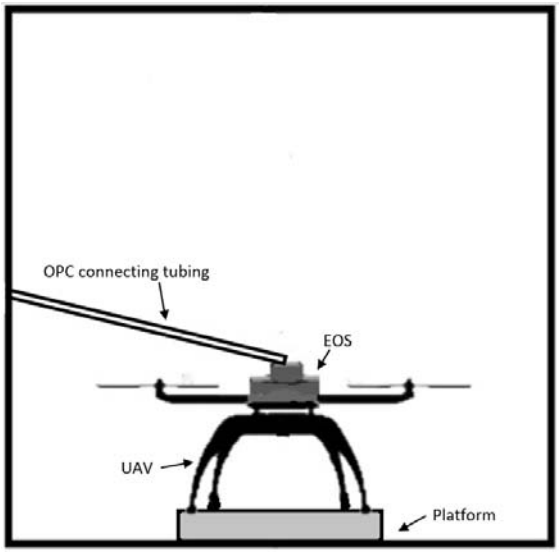

Figure 9. OPC Positioning Relative to EOS

Additionally, a sound level meter was used to gauge the sound outputs from the EOS sampler, and a variable voltage power source was used on the EOS to determine how voltage and current available to the system impacted the sampler's performance. These measurements were aimed at addressing the TPMs outlined in Chapter III. The

sound level measurements were taken in triplicate at the source in a quiet environment—background measurements were also taken and the difference between the two measurements was taken as the result. To investigate the impact of varying voltages and currents available to the system, the EOS was attached to the Eventek Power Supply with the primary standard in-line to measure the flow rates at each voltage.

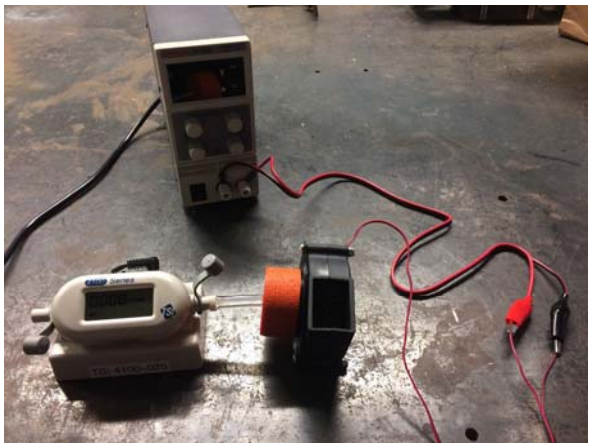

Figure 10. Set-Up for Voltage and Current Analysis

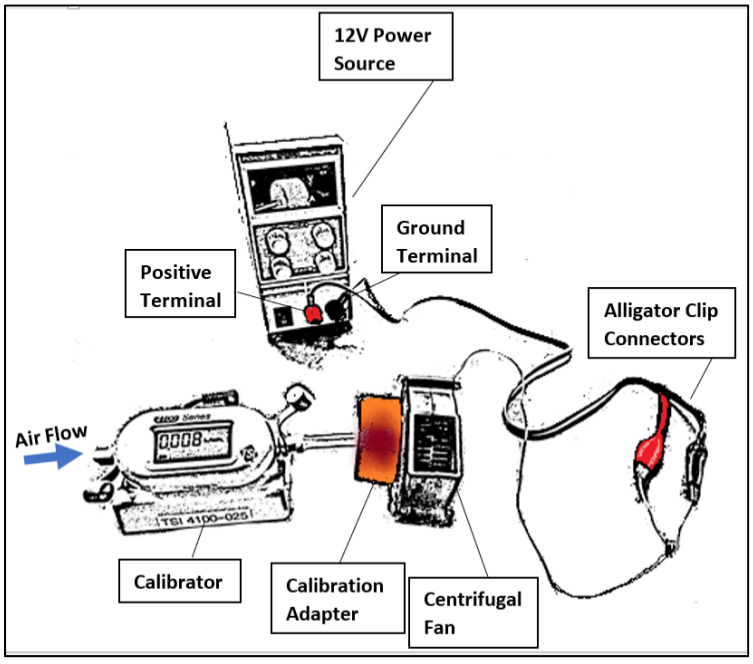

Figure 11. Set-Up for Voltage and Current Analysis Labeled

The limiting factor for power draw was the current being pulled by the EOS. Since this value was 0.1 Amps, the lowest voltage set was the 11V that corresponded to this value. The other two voltages tested were 12V and 11.5V. This test was done to determine if operating on a battery—where voltage decreases over time—would impact the performance of the sampler.

Summary

This chapter covered the methods and equipment that were used to determine the best sampling position and sampling efficiency (among other performance factors) of the developed EOS. Gravimetric analysis, sound level measurements, optical particle counting, and other techniques were used to these ends. The analysis and discussion of the data collected is addressed in Chapter V.

V. Analysis and Results

Chapter Overview

This chapter revisits the assumptions made in the design process as well as the assumptions encountered during the testing of the EOS's performance. The chapter also covers the gravimetric analysis for the EOS vs the CFC, and for the top positioning vs the bottom positioning of the samplers. Additionally, the usefulness of the particle counters used to compare sampling efficiency was addressed. Finally, the metrics that were developed to evaluate the system performance (outlined in Chapter III) were revisited and assessed here.

Results of MURPHEE Chamber Flow Dynamics

Prior to gravimetric samples being taken, the chamber verification is demonstrated in the video below. The chamber appears to be well-mixed while the rotors on the SUAS are turned on. This verifies the chamber assumptions, made in the methods section.

video-1571878916.
mp4

Figure 12. MURPHEE Flow Visualization

Figure 13. MURPHEE Flow Visualization without Rotors On

Figure 14. MURPHEE Flow Visualization with Rotors On

Results of Gravimetric Analysis for EOS

Table 11 records the summary of sample weights and concentrations as averages

Test Day	Order	CFC Weight (mg)	EOS Weight (mg)	CFC Volume (m^3)	EOS Volume (m^3)	CFC Concentration (mg/m^3)	EOS Concentration (mg/m^3)	Difference	Ratio
1	1	1.98 ± 0.001	1.00 ± 9E-04	0.117	0.040	16.9	25.3	8.4	1.50
1	2	1.60 ± 5E-07	0.790 ± 6E-04	0.106	0.041	15.1	19.1	4.0	1.26
1	3	0.965 ± 5E-08	0.693 ± 6E-04	0.110	0.039	8.74	17.7	9.0	2.03
1	4	0.997 ± 5E-06	0.906 ± 3E-04	0.114	0.059	8.79	15.2	6.4	1.73
2	5	1.00 ± 5E-08	0.758 ± 7E-04	0.103	0.039	9.73	19.2	9.5	1.97
2	6	0.550 ± 0.001	0.799 ± 5E-04	0.102	0.040	5.39	20.2	14.8	3.75
2	7	0.721 ± 5E-09	0.468± 5E-04	0.104	0.040	6.93	11.8	4.9	1.70
3	8	0.480 ± 5E-04	0.486± 4E-04	0.098	0.043	4.91	11.3	6.4	2.30
3	9	1.36 ± 0.001	0.846 ± 8E-04	0.106	0.043	12.8	19.9	7.1	1.55

for the first test, with their standard deviations. The samplers were paired within the chamber, because both samplers fit withing one square division of Section 7, where flow

was uniform. Location and interference of the other sampler body were assumed to have minimal effect. This allowed the data to be analyzed via a paired t-test when possible, and ANOVA, student t-tests, and Kruskal Wallis when necessary.

Table 11. CFC vs EOS Filter Weights and Concentration

Test Day	Order	CFC Weight (mg)	EOS Weight (mg)	CFC Volume (m^3)	EOS Volume (m^3)	CFC Concentration (mg/m^3)	EOS Concentration (mg/m^3)	Difference	Ratio
1	1	1.98 ± 0.001	1.00 ± 9E-04	0.117	0.040	16.9	25.3	8.4	1.50
1	2	1.60 ± 5E-07	0.790 ± 6E-04	0.106	0.041	15.1	19.1	4.0	1.26
1	3	0.965 ± 5E-08	0.693 ± 6E-04	0.110	0.039	8.74	17.7	9.0	2.03
1	4	0.997 ± 5E-06	0.906 ± 3E-04	0.114	0.059	8.79	15.2	6.4	1.73
2	5	1.00 ± 5E-08	0.758 ± 7E-04	0.103	0.039	9.73	19.2	9.5	1.97
2	6	0.550 ± 0.001	0.799 ± 5E-04	0.102	0.040	5.39	20.2	14.8	3.75
2	7	0.721 ± 5E-09	0.468± 5E-04	0.104	0.040	6.93	11.8	4.9	1.70
3	8	0.480 ± 5E-04	0.486± 4E-04	0.098	0.043	4.91	11.3	6.4	2.30
3	9	1.36 ± 0.001	0.846 ± 8E-04	0.106	0.043	12.8	19.9	7.1	1.55

As the data was collected it was compiled into control charts for each individual sampler (and later each position for the samplers) as seen in

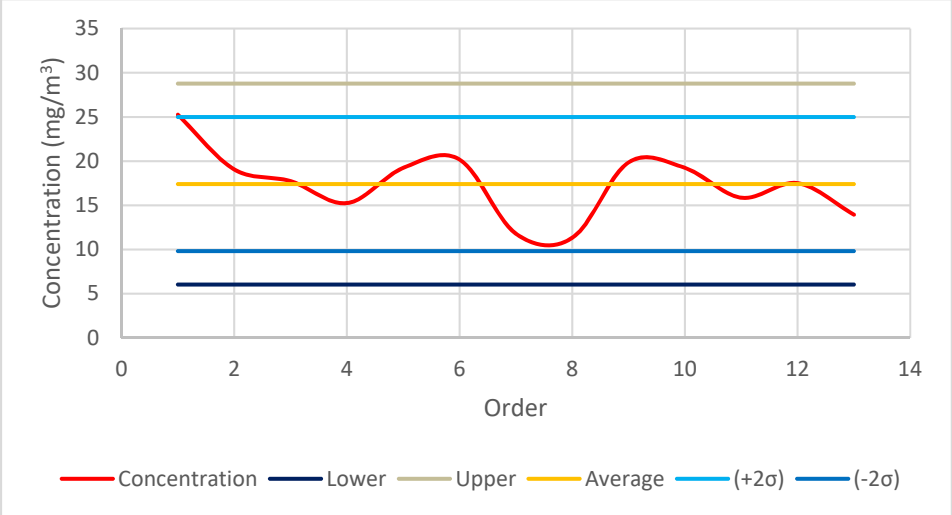

Figure **15** and

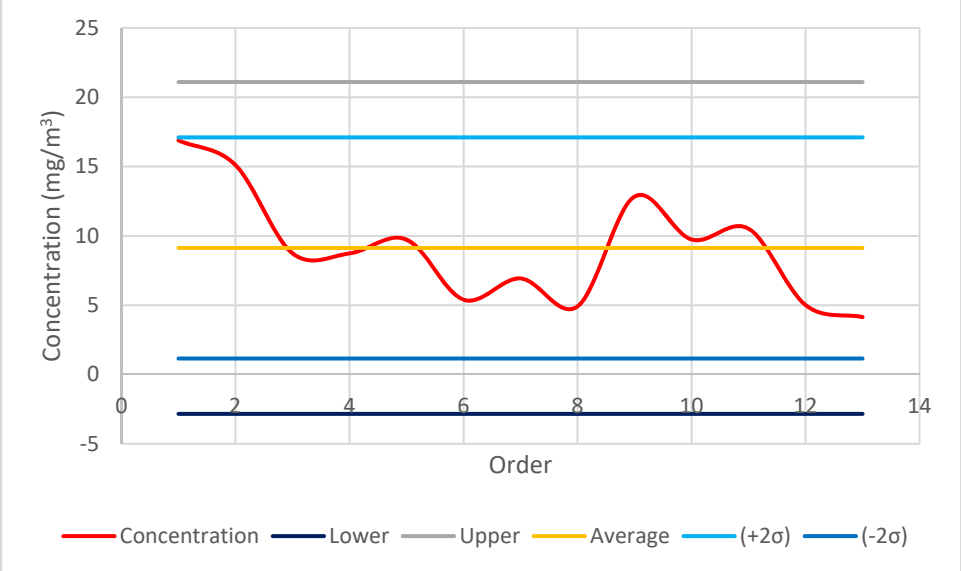

Figure 16 below. The control charts were made in order to visually inspect for outliers, which are data points which differs significantly from the other observations in a trial run. These were then tested for using the Dixon Outlier Test—no outliers were found in this test. Though statistics are useful for identifying outliers, the only reliable

justification for removing an outlier from a data set is if a known error occurred and is identified. For example, during this thesis fan burnout was a source of known error resulting in outliers.

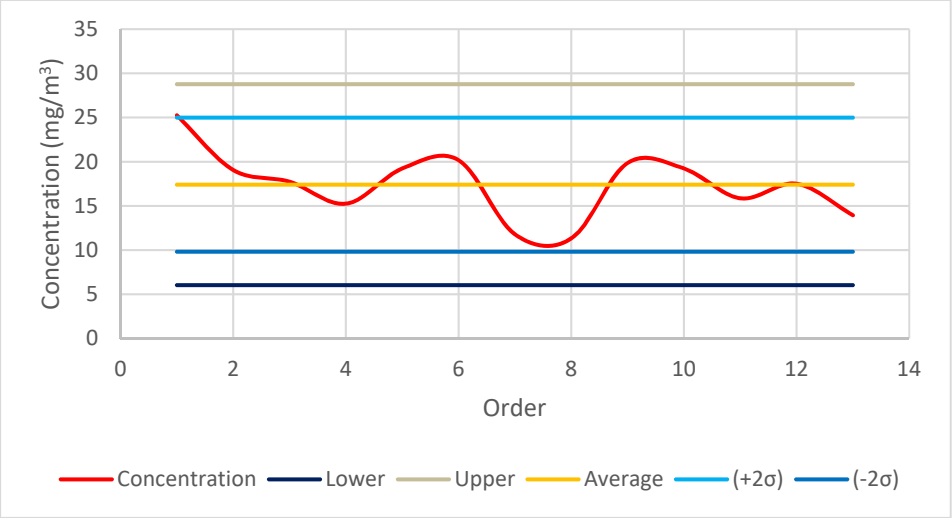

Figure 15. Control Chart for EOS Sampler Free Standing

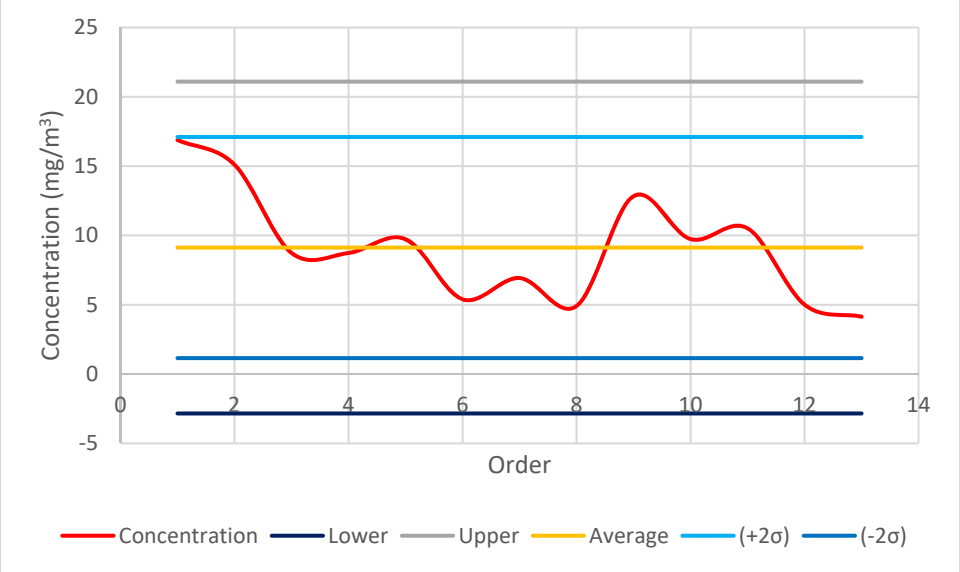

Figure 16. Control Chart for CFC Sampler Free Standing

Table 12 summarizes the descriptive statistics for this data. The CFC collected a mean±95% confidence interval of 9.0±2.6 mg/m^3, while the EOS collected 17.0±2.7 mg/m^3. Though the standard deviations are the same, the variance between each sampler is different, leaving a 2.7 mg/m^3 difference between the two different sampler variances. Additionally, the relative standard deviation (RSD) was higher for the CFC that the EOS, which indicates that the EOS performed more consistently. The sampling concentrations and their relative sampling ratios for the two samplers can also be seen in Figure 17.

Table 12. Descriptive Statistics for CFC vs EOS Sampler (mg/m^3)

Sampler	CFC	EOS
Mean	9.0	17.0
SE	1.202	1.060
SD	4.0	4.0
Variance	17.3	14.6
RSD	0.458	0.219
Variance from Inlet	2.7	

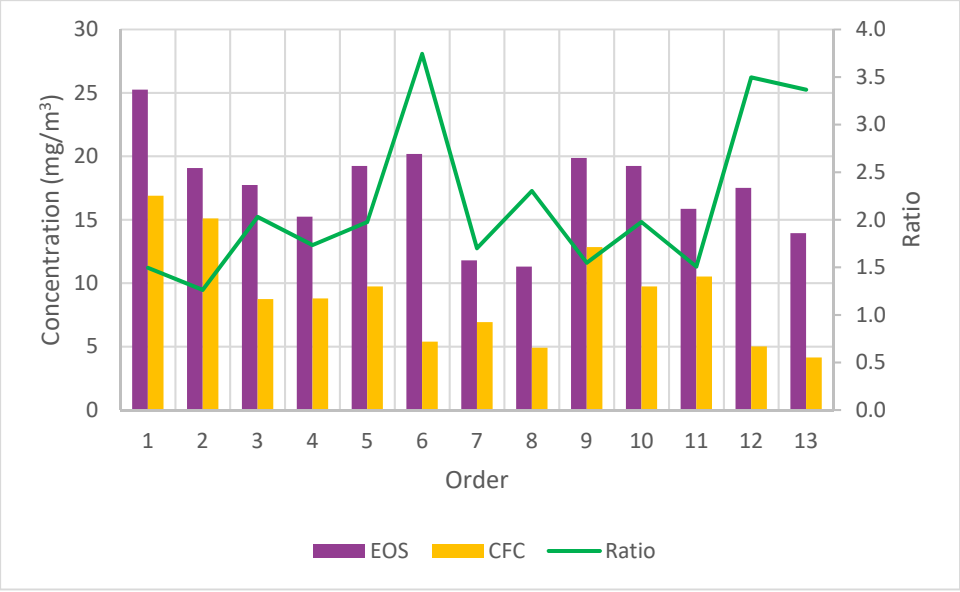

Figure 17. Concentration and Sampling Ratios of EOS and CFC Unmounted

After running the descriptive statistics, ANOVA and t-tests were chosen to further analyze the data. The ANOVA is appropriate for data sets where data follows a normal distribution, is independent, and variance within the groups are equal; the ANOVA is specifically useful for comparing the variances between data sets. The assumptions to perform ANOVA were tested via visual inspection and Shapiro-Wilk and Bartlett tests. The p-value for the Bartlett test was 0.776, indicating that the variances in the data sets were statistically equal. Shapiro-Wilk testing revealed a p-value for the CFC of 0.330 and a value of 0.664 for the EOS, indicating that both data sets are normally distributed. The box-and-whisker plot below demonstrates the variability outside of the upper and lower quartiles of data—represented by the "whiskers"—from the EOS and CFC samplers.

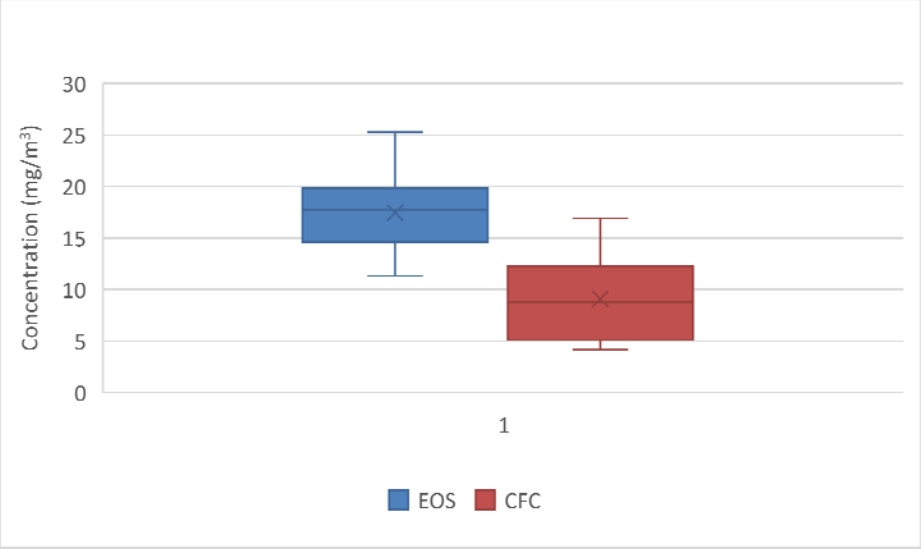

Figure 18. Box and Whisker Plot for EOS vs CFC

For all statistical testing α=0.05 was used. Since the first assumptions for an Analysis of Variance (ANOVA) were met, this test was performed—though the paired samples are technically not independent of each other. The result of the ANOVA was a p-value of 2.58E-05. This concurred with the paired t-test result (p-value: 0.001), that the samplers

did perform differently. Student t-tests are specifically used to compare sample means, which were useful for the data collected here, as the sample means with their 95% confidence intervals are representative of each sampler's performance. The p-value for variance within the sample pairs was 0.698, meaning that each paired sample was consistent with its mate. Since the samplers were placed in the same quadrant of MURPHEE with the same orientation, it is assumed that the variance between sampler performance resulted from the inlet itself, rather than positional effects which were minimized. If bias were contributed from these factors, the direction of this bias would not be easily discerned.

The next trial involved looking at the EOS mounted on top and on the bottom of the UAV while the rotors were not moving; in the top position, the EOS was facing upward instead of downward to allow for ease of mounting. Since the pilot study for this test did not indicate a difference between the EOS without being fixed to a body and when mounted, corresponding CFC samples were not taken—it was assumed that the CFC would also not be impacted by the UAV body since the sampler was in the same quadrant of the chamber as the initial performance test, whether in the top or bottom position. Figure 19 and Figure 20 below are the control charts for the stationary trials.

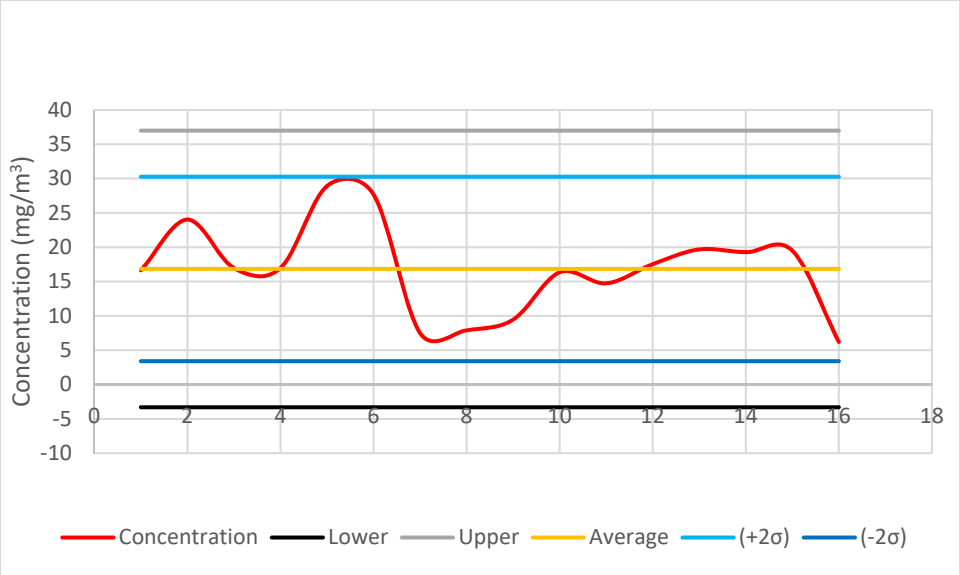

Figure 19. Control Chart for Stationary Sampling in the Top Orientation

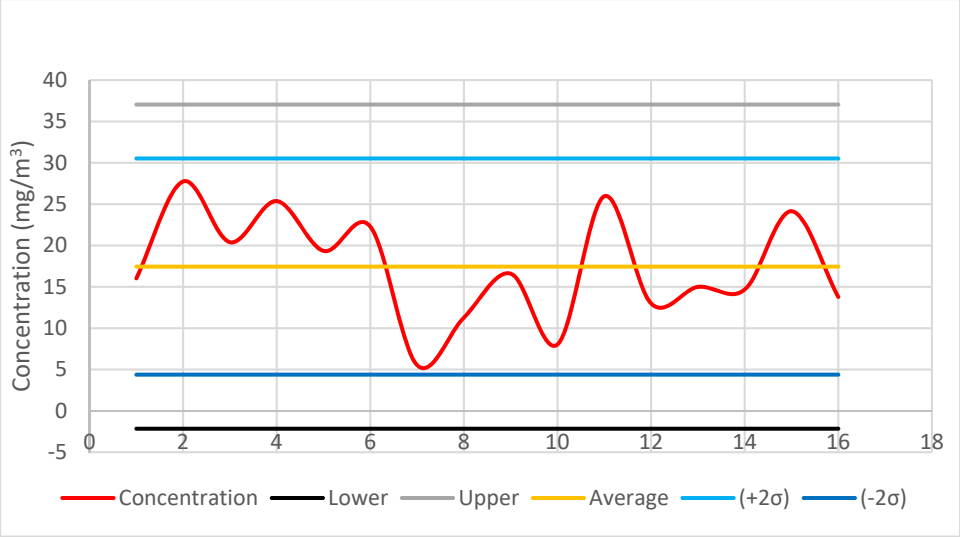

Figure 20. Control Chart for Stationary Sampling in the Bottom Orientation

The control charts for this test did not reveal any outliers, which Dixon Outlier testing confirmed. The EOS in the top position collected 16.8±3.6 mg/m^3, while the EOS on the bottom collected 17.4±3.5 mg/m^3. The standard deviations, RSDs, and variances are similar in this test indicating consistent and similar performance between the two sample

positions; however the variance for both orientations is almost three times higher than the variance when the EOS was not attached to the UAV. The difference in the variance from position of the inlet is approximately 3.0 mg/m^3. Sampling ratios for each paired trial are in Figure 21.

Table 13. Descriptive Statistics for EOS while Stationary (mg/m^3)

EOS Position	**Top**	**Bottom**
Mean	16.8	17.4
SE	1.678	1.633
SD	6.7	6.5
Variance	45.1	42.7
RSD	0.399	0.374
Variance from Inlet	3.0	

Figure 21. Concentration and Sampling Ratios of EOS Top and Bottom Positions while Stationary

A paired t-test and ANOVA were also run on these data. The results of these tests were a t-test p-value of 0.50 and an ANOVA p-value of 0.80, meaning that the sample means were not statistically different. Interestingly, though the variability was very

different from the first test, when tested using a t-test for unequal variances, the EOS was not statistically different from the EOS performance not affixed to a body. As before, the CFC and EOS were different. The results of this statistical test and those for other flight regimes are summarized in Table 18. The top orientation was not explored when comparing results to the original no-body trials, because the CFC and EOS were oriented downward as is done in traditional Industrial Hygiene samples. Since the null hypothesis could not be rejected for the EOS samples with no body and when attached to the UAV it can be inferred that the vehicle body did not have a significant impact on the sampler performance. However, the variance from the descriptive statistics is still an interesting observation, that deserves investigation with paired EOS and CFC samples in future studies.

Next, the same analytical procedures were repeated for the data collected during the hover regime. Via outlier testing, data points 3 and 4 from the bottom placement (as seen in

Figure **22**) were indicated for removal and were taken out prior to statistical analysis. These were likely outliers due to issues with the power source whose wiring broke from the solder connection to the fan—since it was unclear how early in each run the fan stopped working in both trials, the data were analyzed gravimetrically until grounds for removal was confirmed via statistics. The top placement control chart (Figure 23) revealed no outliers.

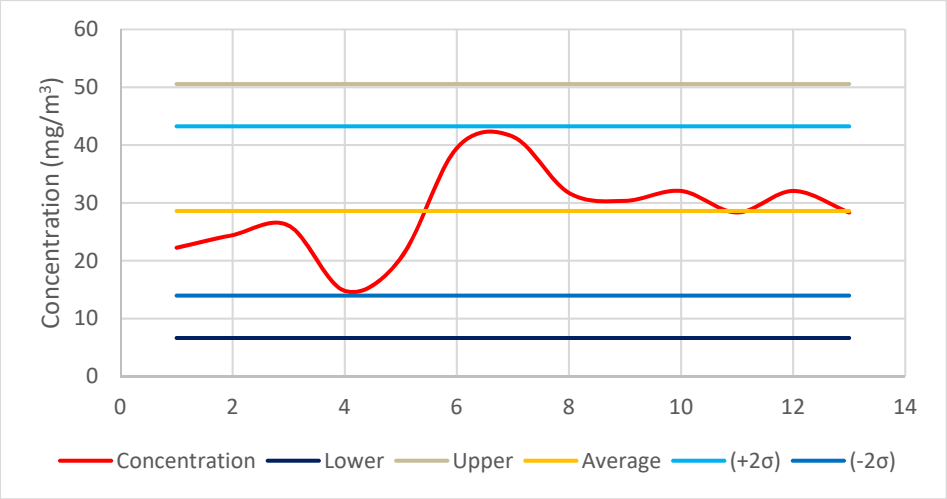

Figure 22. Control Chart for Bottom Placement in Hover

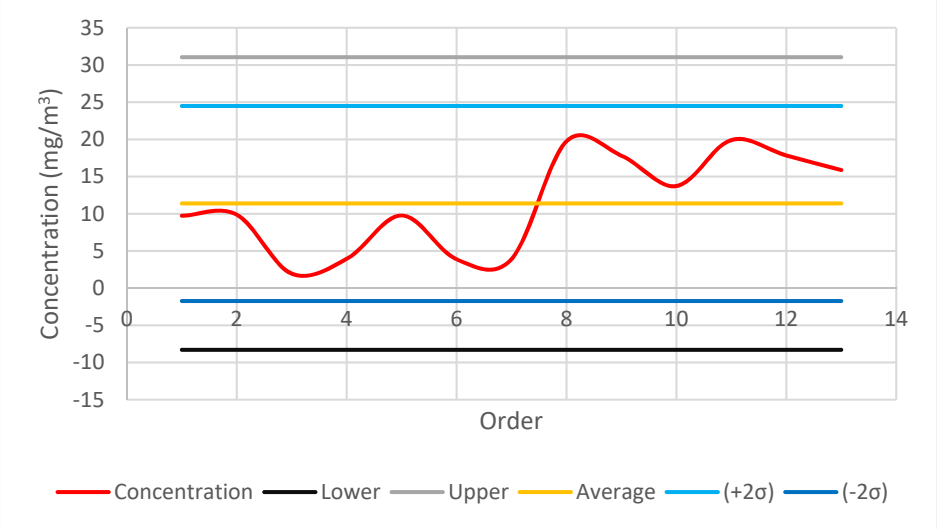

Figure 23. Control Chart for Top Placement in Hover

After taking the outliers out of the data set, the mean for the bottom placement was 28.3±5.3 mg/m^3, and the mean for the top placement was 11.4±4.0 mg/m^3. The rest of the descriptive statistics from the hover trial are in Table 14. Sampling ratios for each paired trial were also done on this data, these results and the sampled concentrations are in Figure 24. The sampling ratios were much higher in three of these trials, when compared

to the sampling ratios of the samplers in hover; this speaks to the variance that the rotors add to the sampling system.

Table 14. Descriptive Statistics for EOS in Hover (mg/m^3)

EOS Position	**Top**	**Bottom**
Mean	11.4	28.3
SE	1.818	2.392
SD	6.6	7.9
Variance	43.0	62.9
RSD	0.576	0.280
Variance from Inlet	19.9	

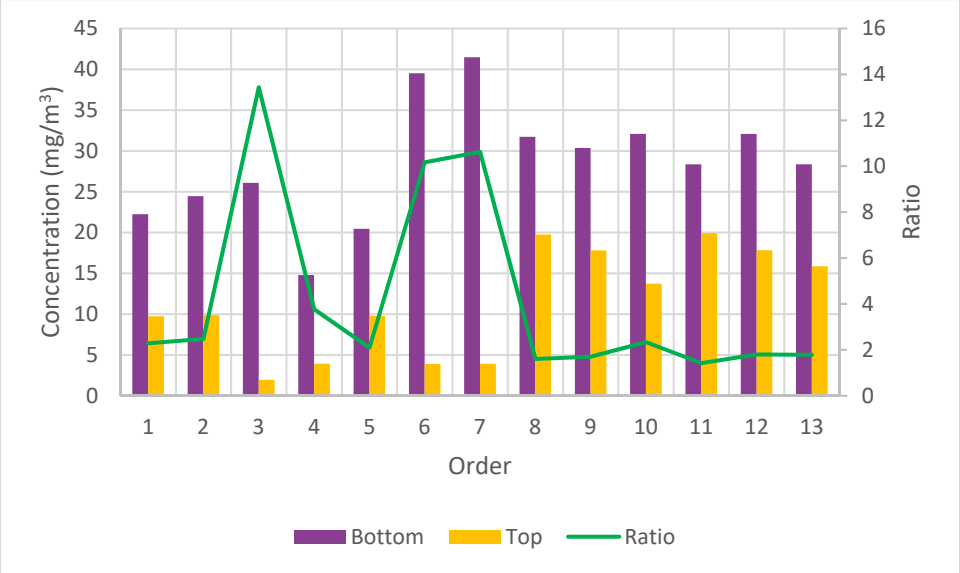

Figure 24. Concentration and Sampling Ratios of EOS Top and Bottom Positions while in Hover

During this test, the variances were even larger than the previous trial runs. Specifically, the difference between the variance for the different orientations was over six times as large as the stationary trials. The bottom was particularly different—having a larger variance, standard deviation, and mean—this could be attributed to ground effects, as the downward thrust of the rotors may cause more dust to be captured as it circulates

between the bottom of the UAS and the bottom of the chamber. However, the RSD for the bottom position was lower that the sampler in the top position, indicating that this might still be the better placement. The t-test p-value for top vs the bottom orientation was 0.001, so these data sets were statistically different. Since the variances do not meet the assumption to perform Standard ANOVA, it was not done in this case. A Welch's ANOVA yielded a p-value of 9.19E-06 and a Kruskal Wallis test performed on the dataset had a p-value of 1.20E-03, meaning that the data was significant—both agreeing with the t-test findings. Though sampling was attempted for the CFC in this flight regime (and later in forward flight), the collected samples all yielded non-detect results with the mass limit of detection (LOD) of 0.103 mg per filter. Though the CFC is commonly used to assess worker exposures, it has been previously observed that mass concentrations gathered by CFCs were underestimating exposures to large particles from the inhalable range to 100 microns—and therefore underestimating overall mass (Anthony et al., 2016). Though the sampler was not looking at larger particles (using Ultrafine Test Dust), the contributions of settling in the dynamic environment of the MURPHEE chamber likely had a significant impact on these results. This change in results can be seen in the relative mean and RSD difference in the sampler performance for both sampling positions in stationary vs in hover. Once the rotors were turned on, the sampler performance deviated based on position, but when in stationary the RSD and means were not statistically different based on position.

Originally, data collection was done with the 10° platform, as if the vehicle were in forward flight. The mean values from these trials are reported in Table 15. A student t-test was done comparing the 10° hover data (for top and bottom placement) to the hover

data with no angle (0°). For the top placement, the p-value was 0.030, meaning that the null hypothesis was rejected, and the data are different. Bottom placement yielded the same conclusion (p-value: 0.045). This suggests that the angle of the SUAS body relative to the ground does have an impact on the sampling results, but whether this remains true further off the ground or to what degree begs further analysis. This is important to keep in mind, because on days when outdoor sampling is attempted with variable winds the flight angle may be subject to change during the sampling event. Table 15 has the descriptive statistics for the uncorrected hover sampling. The means and variances were much larger in the uncorrected data set than for the corrected hover data; though the RSDs were lower—a potential positive indication for forward flight at slower speeds when possible.

Table 15. Descriptive Statistics for EOS in 10° Hover (mg/m^3)

EOS Position	**Top**	**Bottom**
Mean	21.3	38.3
SE	3.000	2.842
SD	7.3	7.5
Variance	54.0	56.5
RSD	0.345	0.196
Variance from Inlet	2.5	

Another data set was collected comparing the high pulse rate in hover to two other pulse rates. These data can be seen in Table 16. At 1200 pulses (low speed), takeoff and sustained hover is not likely. The differences between top and bottom sampler placement at varying speeds can be seen in Figure 25 and Figure 26.

Table 16. Mean Concentration for Variable Placements and Different Pulse Rates

Orientation	**High Pulse Rate**	**Medium Pulse Rate**	**Low Pulse Rate**
Top Placement	21.3±8.0 mg/m^3	15.0±6.0 mg/m^3	15.0±7.0 mg/m^3
Bottom Placement	38.3±8.0 mg/m^3	28.0±11.0 mg/m^3	39.0±0.3 mg/m^3

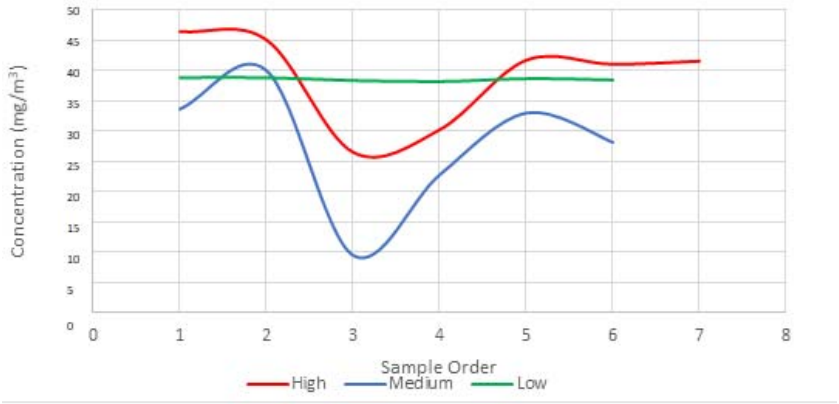

Figure 25. Concentration Collected at Varying Rotor Speeds in Bottom Placement

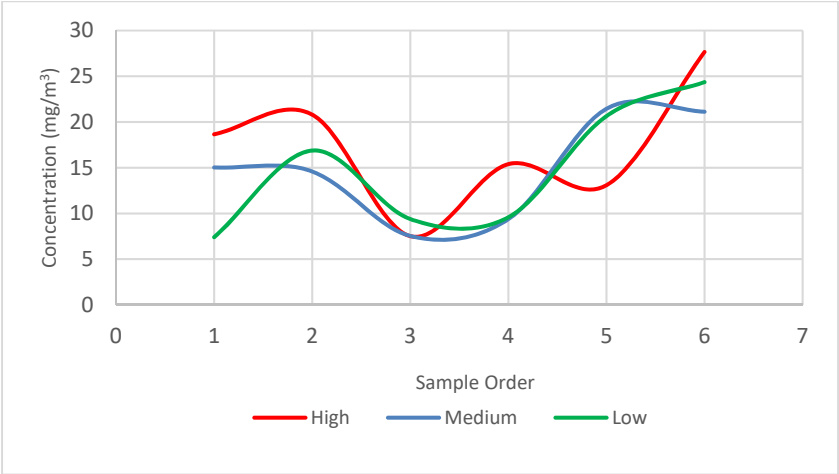

Figure 26. Concentration Collected at Varying Rotor Speeds in Top Placement

A t-test performed on the data set indicated no significant difference in means among bottom placement (p-value of 0.075) and the same in the means grouped by pulse rate for top placement (p-value of 0.350). These results indicate that the speed of the rotors is not as impactful as the EOS position relative to the rotors in sampler performance. High speed is most likely to sustain flight, and so this condition was used in hover and forward flight tests.

The final set of gravimetric data was collected during forward flight. The control charts for this flight regime revealed no outliers, save for two paired samples where the

sampler in the bottom position experienced sample loss post-collection. Though this sample was non-detect for concentration (with a mass LOD of 0.206 mg), its pair on the top—the true outlier—was functioning properly though its concentration was an order of magnitude higher than the other samples from the same position. The reason for this is unknown. The final seven samples for the top position were censored for inclusion in the data analysis and control chart. These were necessary as the sampler burned out at the beginning of the trials for that day, and the error was not observed until post-calibration at the end of the day. All censored data in Figure 27 and Figure 28 are depicted with red X's. The censored data were calculated using a log-probit method, discussed below.

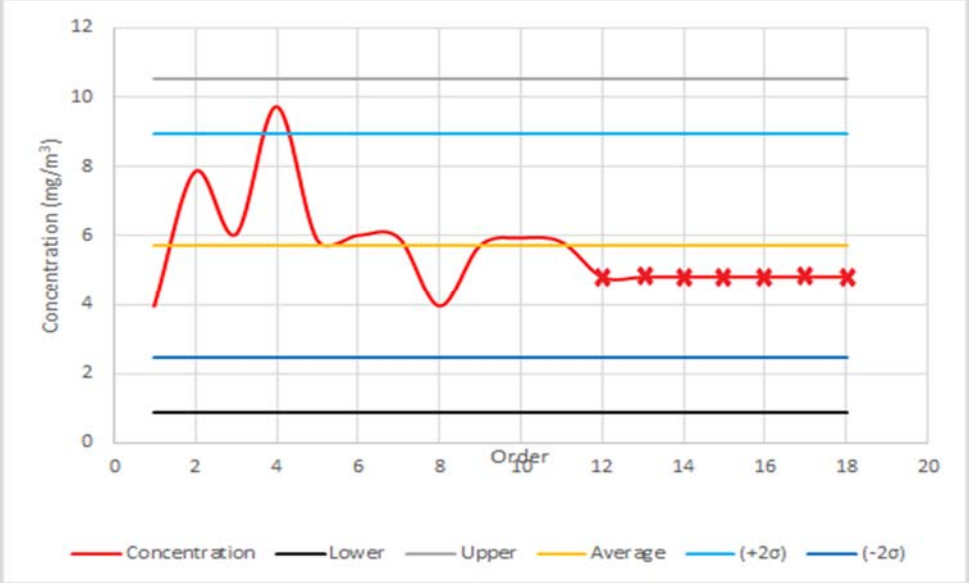

Figure 27. Control Chart for Top Position in Forward Flight

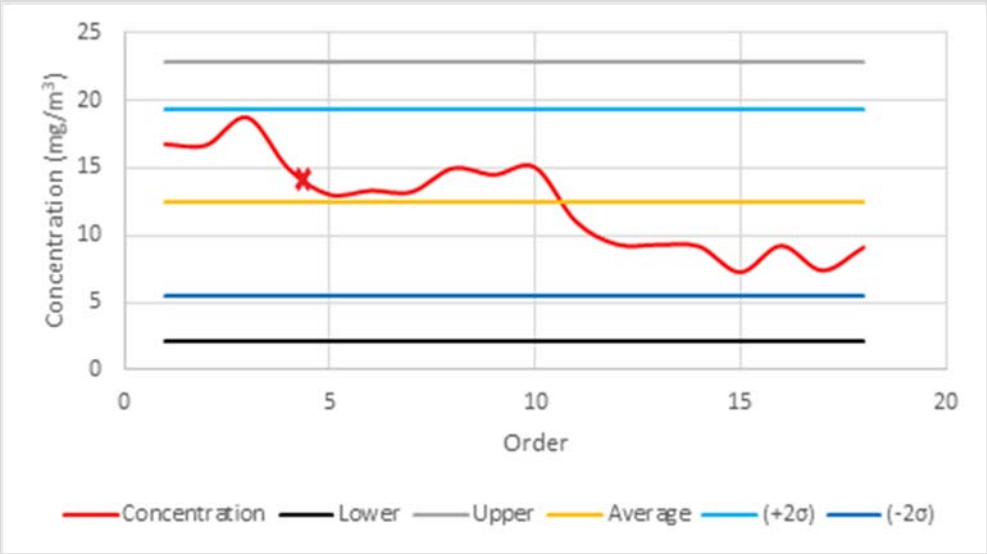

Figure 28. Control Chart for Bottom Position in Forward Flight

In the top sampler, the last seven samples were non-detect. In order to account for this censored data, the limit of detection (LOD) for the pilot study of samples was calculated using Equation 2. The resulting LOD was 4.8 mg/m^3. This value was substituted in for the non-detects in the top EOS position data.

Equation 13. $$\boldsymbol{LOD = 3 \times \sigma}$$

Using this information, the non-detect data was censored using a log-probit regression. This method was chosen as it generally has lower bias than other methods of censoring data (Hewett and Ganser, 2007). The log-probit regression was plotted using the Blom Plot Positioning equation (Equation 2).

Equation 14. $$\boldsymbol{Blom\ Pos = \frac{\left(m-\left(\frac{3}{8}\right)\right)}{\left(N+\left(\frac{1}{4}\right)\right)}}$$

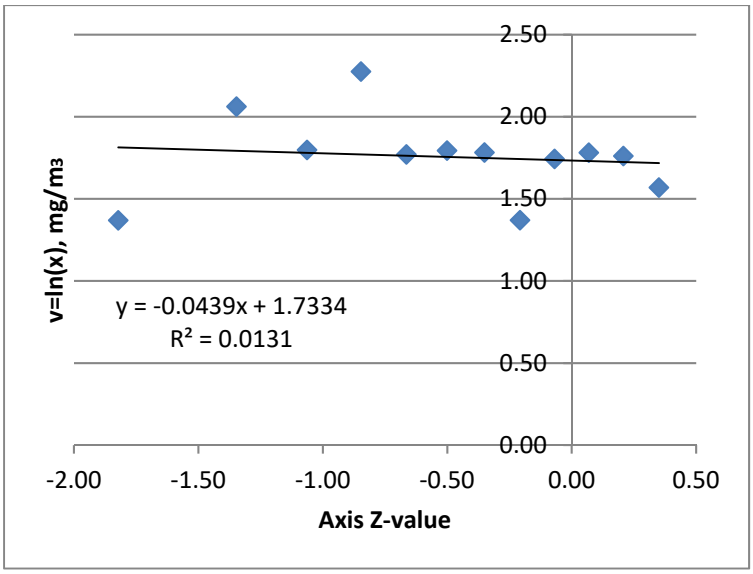

Figure 29. Plot Positioning for Top EOS Censored Data

After removing the outliers and correcting for the censored data, the descriptive statistics are as shown in Table 17. Using only the pilot study values (the first 11 data points), the Mean and SD for the Top position was 6.1±1.1 mg/ $m^3$and the bottom values were 12.4±1.7 mg/ m^3.

Table 17. Descriptive Statistics for EOS in Forward Flight (mg/m^3)

EOS Position	**Top**	**Bottom**
Mean	5.7	12.4
SE	0.328	0.815
SD	1.4	3.5
Variance	1.9	12.0
RSD	0.222	0.278
Variance from Inlet	10.1	

The censored data did lower the mean, and the t-test performed on the data revealed that there is a difference between the data sets (p-value of 0.001). Paired and unpaired t-tests were done on the data (the paired test was on the pilot study data); the results of both agreed. Shapiro-Wilk testing revealed that the data on the Top data was not normal. The

variances are also not equally distributed (Bartlett's test); so, ANOVA was not performed. In place of the ANOVA, a Kruskal Wallis test was performed instead. Here the p-value was 3.94, which agrees with the t-test results that the data were different.

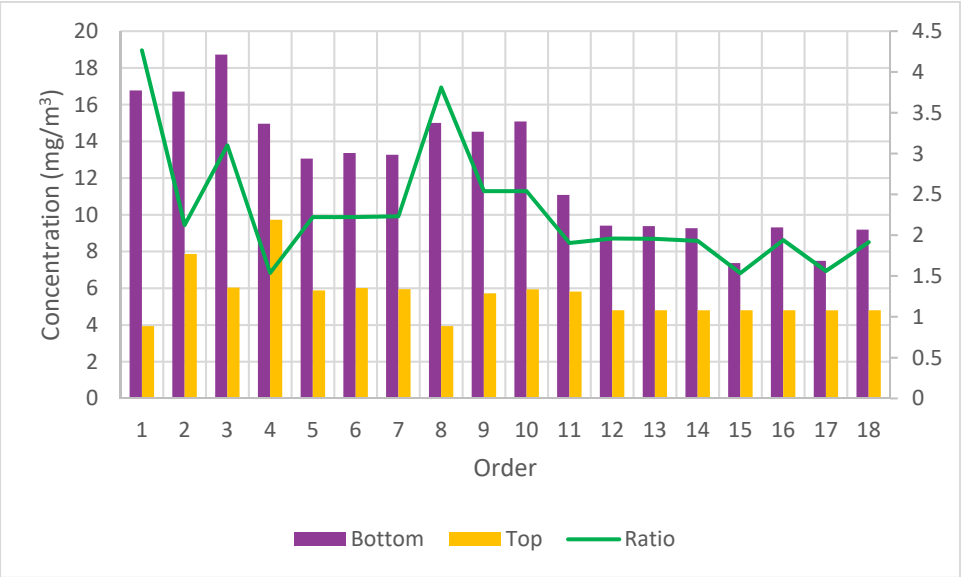

Figure 30. Concentration and Sampling Ratios of EOS Top and Bottom Positions while in Forward Flight

Based on the results in Figure 30, forward flight sampling ratios were on par with the stationary ratios and the highest ratios were five times lower than the highest ratio in hover. This is a positive indication for the sampler's relative performance being consistent across at least two flight regimes. Since the low flow sampling rate means that a sample is likely to be taken during forward flight, this consistency with stationary sampling supports the possibility of gathering usable data in forward flight.

Table 18 summarizes all the major statistical tests that were done during gravimetric analysis for the EOS included in the SUAS`1, in order to classify the

sampler. Overall, only 4 of 22 statistical tests run on the data were not significant, indicating that most tests run revealed data that were statistically different.

Table 18. Comparisons for Variable Flight Regimes, Samplers, and Orientations

Flight Regime	Sampler	Sampler Orientation	Statistical Test	P-value	Significant
Stationary	EOS	Top vs Bottom	ANOVA	0.800	No
Stationary	EOS	Top vs Bottom	Paired t-test	0.500	No
Stationary vs No Body	EOS	Bottom	Student t-test	1.000	No
Stationary vs No Body	EOS vs CFC	Bottom	Student t-test	0.001	Yes
Stationary vs No Body	EOS vs CFC	Bottom	ANOVA	2.58E-05	Yes
Hover	EOS	Top vs Bottom	Paired t-test	< 0.001	Yes
Hover vs Stationary	EOS	Top	Student t-test	0.045	Yes
Hover vs Stationary	EOS	Bottom	Student t-test	0.002	Yes
Hover vs No Body	EOS	Bottom	Student t-test	0.002	Yes
Hover vs No Body	EOS	Top	Student t-test	0.020	Yes
Hover vs No Body	EOS vs CFC	Bottom	Student t-test	< 0.001	Yes
Hover vs No Body	EOS vs CFC	Top	Student t-test	0.300	No
Forward Flight (FF)	EOS	Top vs Bottom	Paired t-test	< 0.001	Yes
FF	EOS	Top vs Bottom	Kruskal Wallis	3.94	Yes
FF vs Hover	EOS	Top	Student t-test	0.010	Yes
FF vs Hover	EOS	Bottom	Student t-test	< 0.001	Yes
FF vs Stationary	EOS	Top	Student t-test	< 0.001	Yes
FF vs Stationary	EOS	Bottom	Student t-test	0.015	Yes
FF vs No Body	EOS	Top	Student t-test	< 0.001	Yes
FF vs No Body	EOS	Bottom	Student t-test	0.006	Yes
FF vs No Body	EOS vs CFC	Top	Student t-test	0.020	Yes
FF vs No Body	EOS vs CFC	Bottom	Student t-test	0.049	Yes

To verify that the distribution of the particles collected was even across the filter surface, one of the samples was observed under SEM, as can be seen in Figure 31. The distribution did appear to be uniform, and the sample did confirm that the shape factor could be assumed to be one (spherical).

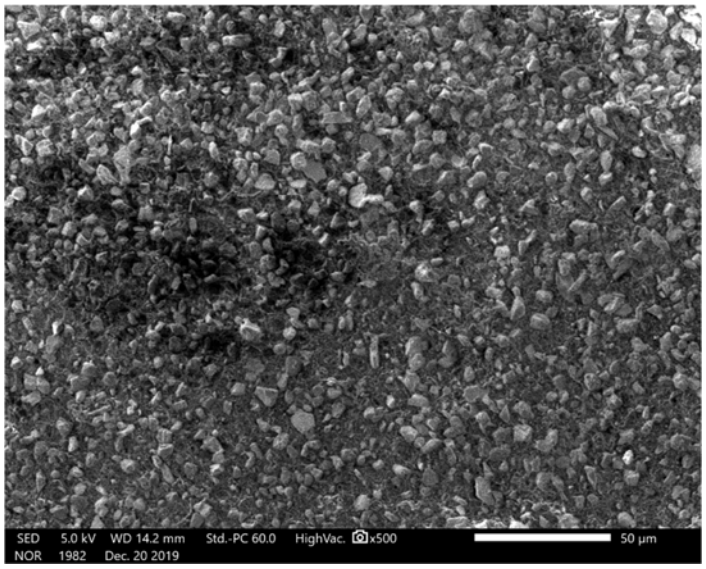

Figure 31. SEM View of Hover Test Bottom EOS #5 (FOV: 256x192 µm)

In addition to the other tests, the concentration was observed relative to the temperature, pressure, and humidity for the first study (EOS vs CFC) to determine if there were environmental impacts on the data collected. Environmental factors cannot be ruled out completely, as the MURPHEE was in an unairconditioned warehouse (though heated in the winter), so their potential bias was investigated here. Pressure was of interest as this factor is one that has the potential to impact the EOS fan performance. During the time when environmental data were collected, the temperature ranged from 60°F to 79°F, the humidity ranged from 60 to 70%, and the pressure centered around 30 inHg. The range of environmental data was limited for this uniform period of testing, and so the correlation coefficient was very low for each data set.

For the relationship between pressure and observed concentration, the calculated Pearson correlation coefficient was -0.185. This indicates a very low negative correlation between the observed atmospheric pressure and the sampled concentration. The fan itself

was rated inside a vacuum and did experience a drop in performance in real world conditions (rated 7.8 CFM vs 0.04 CFM), this was likely a combination of pressure change from the filter and higher atmospheric pressure than in the laboratory controlled conditions—see Appendix 3 for the manufacturer's fan pressure data. However, flux in atmospheric pressure was minimal throughout the month of testing. Additionally, the current being pulled in the fan's motor in real world conditions was an order of magnitude lower than the expected current (0.12 Amps vs 0.01 Amps); this may have also been an impact of pressure but does provide a rationale as to why the fan could not perform as a high-flow sampler as originally intended.

The Pearson correlation coefficient for humidity and concentration was -0.0908, again indicating very little correlation, in the negative direction. This was the lowest correlation, and a low impact on these test results can be assumed to be consistent because humidity is more likely to impact the agglomeration of particles in the environment (which in this case was relatively controlled via amount and type of aerosol and sampling time) and not impact the sampler performance itself. It is also of note that the humidity was moderate during the duration of testing, and previous research noted the greatest impact at the extreme ends of humidity (Zheng, 2001)

As with pressure, the Pearson correlation coefficient of this temperature to concentration relationship was near the same magnitude. Interestingly, the correlation was in the positive direction for temperature (0.182). This trend follows particle aerodynamic properties, as viscosity of gases is known to increase with temperature and properties like gravitational settling are negatively correlated with increasing viscosity (Hinds, 1999, p. 25). Though this is also not a strong correlation, real-time

measurements on this data were not retrieved and the temperature in the warehouse did fluctuate more widely than any of the other factors over the course of one day. As such, it is difficult to draw conclusions from this data set. As temperature changes, it is possible that the deposition mechanisms that impact collection efficiency would be affected. However, the particles investigated in this experiment were small, and temperature and pressure are more likely to impact gravitational settling than other collection efficiency factors, and gravitational settling has a greater bias to impact larger particles (Hinds, 1999, p. 192-195).

Results of OPC Data

In order to begin assessing the sampling bias of the EOS inlet, the MURPHEE was run at 60 Hz, with the rotors of the UAS spinning at the maximum pulse rate to simulate forward flight. Medium ISO Test Dust and the OPC were used to generate sampling distributions for EOS in top and bottom orientations, as well as for the background concentration (the rotors of the UAS turned off). The results of these tests yielded particle counts that were then converted to particle count concentrations. Converting the particle counts to mass concentrations was considered, but the most expedient assessment for particle size selectivity can be performed with OPC data in its native form. This also avoided adding large amounts of bias to the data—as OPC particle counts can severely over or underestimate the mass concentration depending on the shape factor and mass of the particles in question (Hinds, 1999, p. 370-376).

First, particle count concentrations were generated for the EOS sampler in the top and bottom orientation compared to the background concentrations in the chamber. The average concentration in the MURPHEE across all size ranges was 233.5±66.7 #/cm^3 and

the mean concentration for particles less than two microns was 231.3.1±66.2 #/cm^3. As seen in Figure 32 and Figure 33, the peak particle count concentrations occur at the lower particle sizes, specifically near one micron—further supporting the mean concentrations being dominated by the smaller particle sizes. Interestingly, the particle count concentrations see a dip in concentration at 0.7 µm for both orientations. Additionally, since Medium ISO Test Dust was used, there still should have been elevated counts at the higher end of the measured spectrum; however, it is possible that at the background flow rate and in a turbulent setting, the larger particles settled quickly and did not reach the door (where these tests were run—see Figure 6. The OPC used also provided a limitation to the experiment, as the only one available at the time of the experiment could only count particles up to 30 µm in size, so even if the experiment could be set up closer to the aerosol injection port, the half of the Medium ISO Test Dust distribution would still not be measured. Since the inlet behavior for the particle size of one micron was of the most interest, these conditions were deemed acceptable for initial characterization.

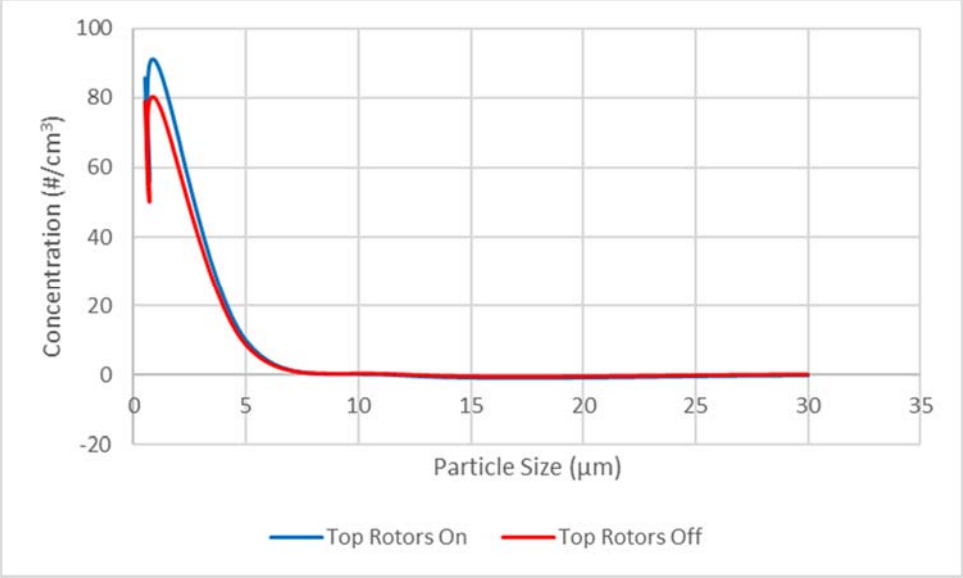

Figure 32. Particle Concentration Comparison UAS On vs Off Top Position.

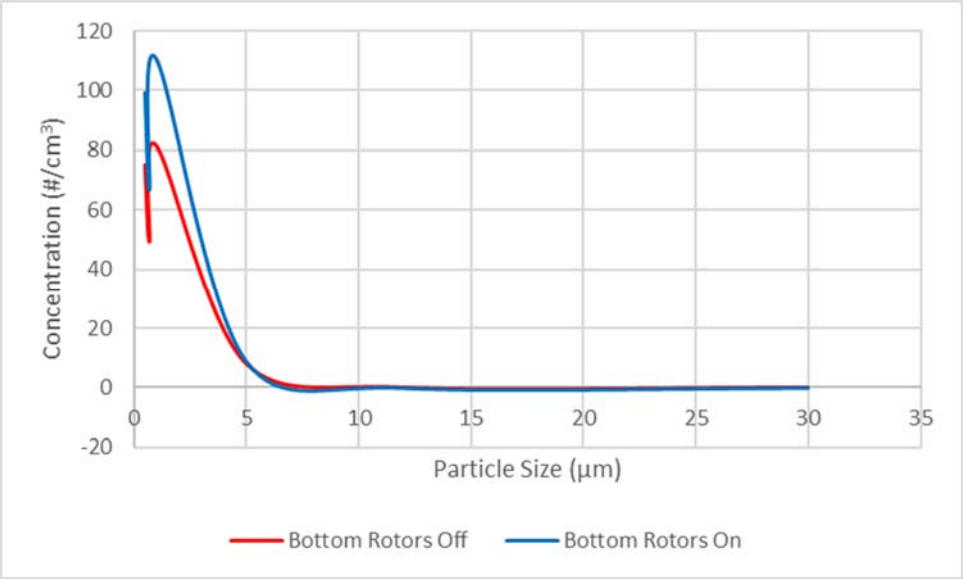

Figure 33. Particle Concentration Comparison UAS On vs Off Bottom Position

The particle concentration distributions above, and the cumulative percent distributions (Figure 34 and Figure 35) below, demonstrate the similarities between the generated distributions and expected aerosol distributions for Medium ISO Test Dust. Logically, in a particle count distribution, one would expect to see very few large particles, and even though some sizes should have registered the general trends are similar so the data that was collected is likely reliable for the lower size ranges.

Table 19. Cumulative Percent for Top and Bottom Positions with Rotors and Off

d_{AE} (µm)	Bottom Position		Top Position	
	Rotors On	Rotors Off	Rotors On	Rotors Off
0.5	35.65	36.19	36.61	37.47
0.7	59.66	59.97	60.51	61.28
1	99.38	99.22	99.06	99.01
5	99.99	99.23	99.99	99.99
12	99.99	99.23	100	100
30	100	100	100	100

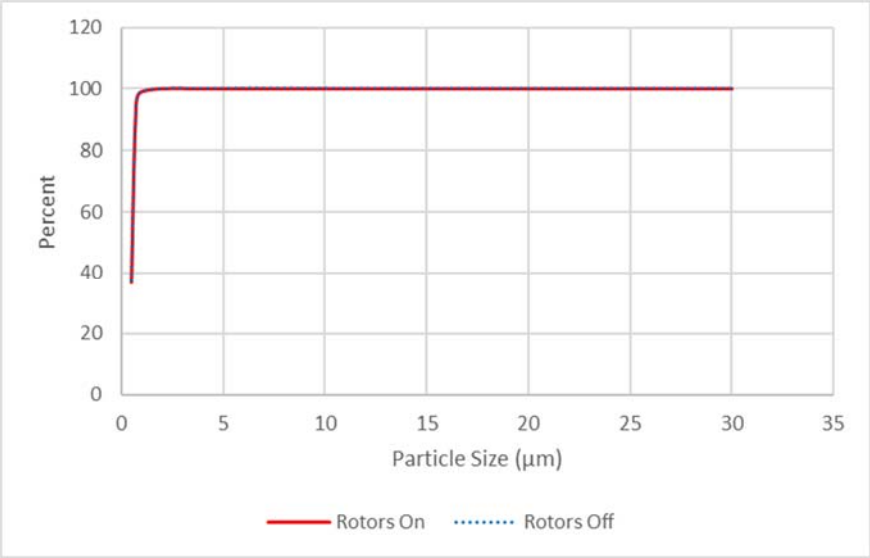

Figure 34. Cumulative Percent Distribution for Top Positioning

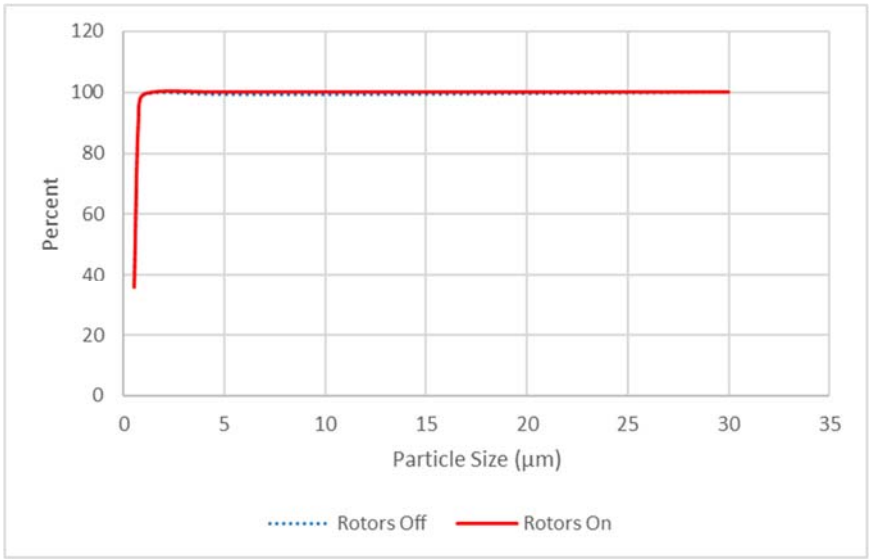

Figure 35. Cumulative Percent Distribution for Bottom Positioning

As was visually observed in the earlier figures, Table 20 and Figure 36 confirm that the EOS was oversampling across all particle sizes. As with the gravimetric analysis, the bottom sampling position was heavily skewed to the right for all size ranges except for the five micron bin when compared to what was modeled in the design of the inlet. Absolute errors were below 15 for particles of one micron and under in the top position,

so when compared to the modeling only this position is the most attractive for conducting sampling. The low particle counts in the larger bins, coupled with the low sampling efficiencies greater than 30 µm in the top position, is not a positive indication for reliable sampling for larger particles. The lowest projected efficiency was 24% for the 30 µm bin, though even if this were achieved, a reliable sample for bioaerosol identification—not quantification—may also not be possible, even though only one spore/cm^3 is technically necessary for PCR identification, a higher number of spores is better as many of the spores collected on the filter may be lost during the PCR preparation process (Chew et al., 2006; Oggioni et al., 2002).

Table 20. Aspiration Efficiency in Top vs Bottom Positioning Compared to Model

	Top Position			Bottom Position		
microns	Percent of Actual	Projected Efficiency	Absolute Error	Percent of Actual	Projected Efficiency	Absolute Error
0.5	114	100	14	132	100	32
0.7	113	100	13	136	100	36
1	111	100	11	136	100	36
5	135	91	43	107	91	16
12	170	65	105	108	65	43
30	2.46	24	21.54	163	24	139

Figure 36 and Figure 37 show the calculated percent difference of the sampled background concentrations and what the OPC measured at the EOS in the top and bottom positions. The percent differences were calculated via Equation 15.

$$\% \boldsymbol{Difference} = \frac{|\boldsymbol{actual - experimental}|}{\frac{\boldsymbol{actual + experimental}}{\boldsymbol{2}}} \times \boldsymbol{100}$$ Since the percent difference is calculated with an absolute value, the below figures do not necessarily indicate the direction of the sampling bias, only the magnitude. The relative aspiration efficiencies from Table 20, indicate that the sampling bias is positive for all of the size bins except for

the 30 µm bin in the top position. This relative under-sampling at the 30 µm bin in the top position may be due to losses occurring in the sampling tubing used to connect the inlet to the OPC, as particles above 5 µm in diameter are most likely to be impacted by this, especially in turbulent sampling conditions. Accounting for the approximately 2 ft of connection tubing and the slight curvatures in the tubing (<90° bend overall), the estimated losses were less than 20% for particles 1-2 µm in diameter and near 75% for particles at 30 µm (Liu and Luey, 2009).

Equation 15. $$\% \boldsymbol{Difference} = \frac{|actual - experimental|}{\frac{actual + experimental}{2}} \times \mathbf{100}$$

When the percent difference was calculated from what was collected with the rotors on and the background levels, the top and bottom sampling positions both start off with an oversampling bias of about 35% difference for fine particles, of 0.5 to 2 µm. The difference between sampling positions remains consistent until around 3 µm and 12 µm, where the percent difference is equal for both samplers. While the percent difference increased until this value, over 12 µm the percent differences diverged—with the top position's difference from the background decreasing and the bottom position increasing. The trends for the lower particle sizes can be more clearly seen in Figure 37, where the data from the top and bottom positions were combined to create the 95% confidence interval. This chart emphasizes the fact that the sampling conducted at the larger particle sizes is highly variable, and likely not reliable.

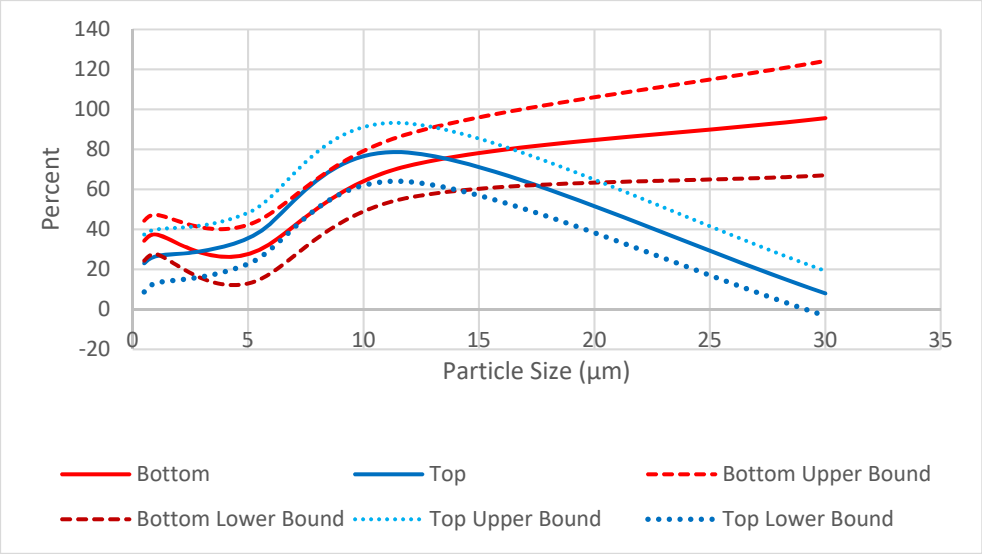

Figure 36. Percent Difference Between SUAS with Rotors On vs Rotors Off for EOS with 95% CI

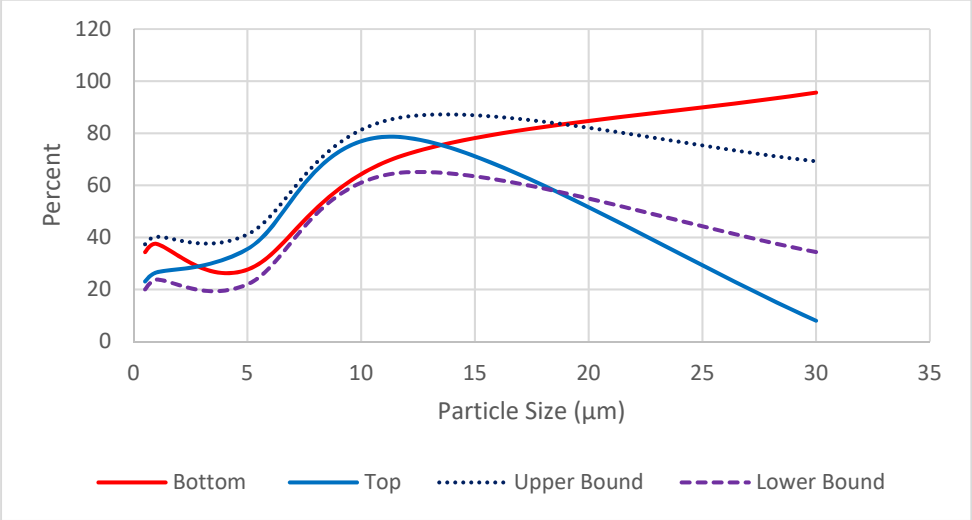

Figure 37. Percent Difference Between SUAS with Rotors On vs Rotors Off for EOS with Bounding

Ultimately, comparison tests conducted in MURPHEE revealed a positive sampling bias for the EOS. This is especially prevalent at the larger particle size ranges (over 12 µm), though the reliability of this data in general is questionable and use of the EOS for

particles above this size is not recommended. This trend of decreased sampler performance for large particles in increased sampling velocity conditions is also supported in literature, as the high inertia of large particles make it less likely that they can follow the flow stream near the sample inlet. Though turbulent conditions are often ideal for these larger inertia driven particles, the rotors create mixing conditions at the inlet and this inertia likely pushed the larger particles outward and downward, away from the inlets mounted on the center of the UAV (Chavez, 2017; Wilcox, 1956).

Since the EOS was specifically designed with biological spores around the size of those produced by anthrax (about one µm in diameter), the 35% overestimate or lower is a helpful benchmark for detection purposes. Accurately determining concentration with this nascent technology, is not likely if the factors leading to the right tailed bias are not accurately discerned and eliminated in future research. However, the fact that the concentration is not underestimated, makes this technology ideal for aerosol detection. Though the top position had a lower absolute error when compared to the model, and had lower percent differences from the background data near the one micron diameter size, this data alone is not enough to definitively determine that the top position is optimal over the bottom position—as ground effects likely had a role in the behavior of the sampling in the bottom position. The nature of ground effects, causes air to be "recirculated" underneath the aircraft, creating a cushion of sorts which is generally thought to increase multirotor SUAS performance (Light, 1993; Eberhart, 2017). Though beneficial for flight, this could be a contributor to the significant oversampling trend for the bottom position throughout these experiments. Ground effects are highly suspect here, because SUAS turbulence produced negative sampling bias in earlier orientation

investigations (Chavez, 2017). In the summary table (**Error! Reference source not found.**) on page **Error! Bookmark not defined.**, the likelihood of not meeting the TPMs described in Chapter III is given. The EOS Sampling Bias achieving ±25% was deemed "Possible", this is because the original TPM was very conservative for bioaerosol sampling and the suspected impact of ground effects on the bottom sampling position are predicted to be very high. This is especially relevant, as bottom placement generally produced the most accurate results in previous research.

Results from Additional Performance Measurement Metrics

All the performance metrics from this study are summarized in Table 21. The rest of this section covers the performance measures not related to the sampler's aspiration efficiency.

Table 21. TPMs for Preliminary Design Review

System Element	Parameter	Target TPM Value	Current TPM Value	Likelihood of Not Meeting Target
UAV Frame, Battery, Propulsion	Weight	20 lbs	6.48 lbs	Very Unlikely
	Endurance	30 min	19 min	Very Likely
Operator	Time for start-up and system interface	30 min	50 min	Possible
Payload—EOS Bioaerosol Sampler	Sound Level Measurement	60 dBA	44.9 dBA	Unlikely
	Sampling Bias (<5 µm)	±25%	+35%	Possible

One such measure investigated was the impact of power demand on sampling performance. This is important because the sampler mounted on an active SUAS will

have less power available to it the longer the system is operational. To evaluate the true impacts of power demand on the sampler, the trials will need to be done with one or more 12V batteries as would be used in an operational SUAS, with motors and other system components online as well. Here the power available was artificially altered by decreasing the Voltage available through the adjustable DC power source. Tests did not occur below 11V, as this is sometimes used as the turnback voltage in initial performance testing for SUAS and because the current draw through the system at 11V was already 0.01 Amps. The results shown in Table 22 are from an early test, where the seal between the filter platform and the fan was not ensured, so the average LPM drawn for these runs was lower than when a tight seal was verified (at 12V with a proper seal the flow rate increased to 1.072 LPM with 0.02 Amps drawn).

Table 22. Impacts of Varying Voltage and Current of Flow Rate

Order	Volts	Amps	Amp read	Avg LPM
3	12	0.3	0.02	1.071
4	12	0.16	0.02	1.066
5	12	0.12	0.02	1.068
1	11.5	0.3	0.02	0.832
2	11.5	0.16	0.02	0.829
8	11.5	0.12	0.02	0.821
7	11	0.3	0.01	0.672
6	11	0.16	0.01	0.694
9	11	0.12	0.01	0.696

Regardless of maximum current available, the current pulled through the system did not exceed 0.02 Amps, so voltage available was the operating factor in determining fan flow rate. As seen in Figure 38, the sample order had little impact on the flow rate, but the flow rate did decrease as less power was available to the sampler. In this figure, the red

line represents the 12V maximum power available, the violet is 11.5V, and the green line is the minimum 11V tested.

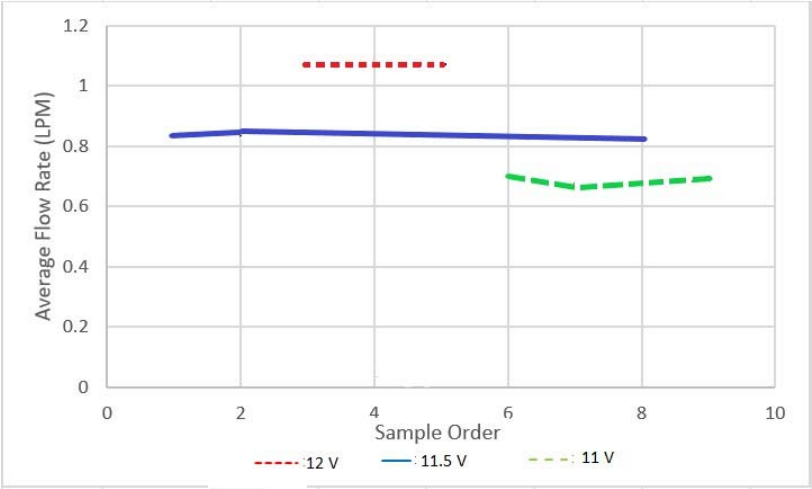

Figure 38. Sample Order vs Flow Rate and Varying Voltages

The cassette for the EOS sampler was printed with a 47-mm inlet (open faced) and a 75-mm diameter base for attaching the fan to the cassette. The initial height of the sampler was 25-mm, slightly taller than the standard height of one stage of a sampling filter. The weight of the prototype EOS cassette was 60 g (0.13 lbs). The total weight of the system was evaluated via taking an average of six measurements for the sampler itself and the UAV and estimating the weight of additional payload necessary for making such a vehicle flight worthy (based on real world rapid design process outputs for a hexrotor SUAS for radiological detection in urban environments). The results yielded 112.0 g (0.25 lbs) for the sampler (with filter) and 1205.5 g (2.66 lbs) for UAV (including motors, props, and ESC's). Weight and current breakdowns for each component are listed in

Table 23

		Mass on Vehicle		Power on Vehicle			
Component	Quantity	Mass ea (g)	**Mass Total (g)**	Voltage Ea (V)	**Voltage Total (V)**	Current Ea (A)	**Total Current (A)**
Air Vehicle Frame	1	1205.5	1205.5				
Propeller	4	inc	inc				
Speed controller	4	inc	inc		12		20
Motor	4	inc	inc		12		20
Auto-pilot	1	39	39	5	5	1.5	1.5
Battery	2	515	1030				
GPS	1	200	200	5	5	1	1
On-board Logic	1	39.86	39.86	5	5	0.1	0.1
Modem	1	14.5	14.5	5	5	0.8	0.8
Modem signal tx	1	15	15				
Video Transmitter	1	18	18	12	12	0.14	0.14
VTX Antenna	1	11.5	11.5				
RC Receiver	1	16.8	16.8	5	5	0.1	0.1
LIDAR	1	160	160	5	5	0.5	0.5
Camera	1	12	12	5	5	0.15	0.15
DC Step-down	3	21	63				
Power Distro	1	TBD	TBD				
EOS Bioaerosol Sampler	1	112	112		12	0.02	0.02
		Total A/V Weight	2,937.16	g	Total Power	63.2	watts
		Total A/V Weight	**6.48**	**lbs**			

.

The battery was assumed to be a 4S battery with a weight of 515 g, and this value was used in conjunction with the measurements taken to estimate the endurance of the system. The estimated endurance yielded 19.31 min (19 min 19 sec) of flight time. The

equations used to arrive at this estimate are detailed in Appendix 1. These equations yield an optimistic flight time, as real-world factors are minimized—however it serves as a good benchmark of design, as endurance needs to be maximized the frame and battery choices will likely need to change for real world use.

Table 23. Weight and Power Estimates for SUAS Components

		Mass on Vehicle		Power on Vehicle			
Component	Quantity	Mass ea (g)	**Mass Total (g)**	Voltage Ea (V)	**Voltage Total (V)**	Current Ea (A)	**Total Current (A)**
Air Vehicle Frame	1	1205.5	1205.5				
Propeller	4	inc	inc				
Speed controller	4	inc	inc		12		20
Motor	4	inc	inc		12		20
Auto-pilot	1	39	39	5	5	1.5	1.5
Battery	2	515	1030				
GPS	1	200	200	5	5	1	1
On-board Logic	1	39.86	39.86	5	5	0.1	0.1
Modem	1	14.5	14.5	5	5	0.8	0.8
Modem signal tx	1	15	15				
Video Transmitter	1	18	18	12	12	0.14	0.14
VTX Antenna	1	11.5	11.5				
RC Receiver	1	16.8	16.8	5	5	0.1	0.1
LIDAR	1	160	160	5	5	0.5	0.5
Camera	1	12	12	5	5	0.15	0.15
DC Step-down	3	21	63				
Power Distro	1	TBD	TBD				
EOS Bioaerosol Sampler	1	112	112		12	0.02	0.02
		Total A/V Weight	2,937.16	g	Total Power	63.2	watts
		Total A/V Weight	**6.48**	**lbs**			

The sound level measurements taken yielded a sound level measurement of 44.9 dBA at three feet from the source. This was above the manufacturer's projected sound level of 42 dBA—perhaps because the centrifugal fan spins faster when the flow rate is

lower. At the source the fan was measured to be 60 dBA, this is a worst-case scenario measurement and still would not breach into hazardous noise. For comparison, intermittent office noise in the measurement space measured an average of 36.7 dBA. This means that even though the primary use of the system is integration with SUAS, the sampler could be used to monitor bioaerosols in alternative environments—such as near a patient in a medical ward—without disturbing human operators. 60 dBA is approximately the sound level of a normal conversation, and the technical performance measure was set on this basis (Risojević et al., 2018). While integrated into the SUAS sound levels would be higher, but the operator is not likely to stay near the system during operational periods anyway.

Investigative Questions Answered

Specific Aim 1: The first aim of the research was to complete the development of a bioaerosol sampling inlet capable of SUAS integration. The technical performance measures for the defined system components were used to set goals for the next design phase and follow-on research. Modeling was used to select 5 micron cellulose nitrate membrane filters and a 47mm inlet size for best projected performance in variable sampling conditions.

Specific Aim 2: Assess design to minimize aspiration bias and increase other performance factors. Key considerations include the effects of wind speed, turbulence, orientation, and sampler flow rate on particle aspiration. Future modification recommendations will be made. Gravimetric analysis was used here to evaluate the

performance of the sampler relative to a CFC, it's performance in various flight regimes, and in two different positions.

Specific Aim 3: Determine the size selectivity bias for the UAS airframe and aerosol sampler in forward flight. Particle size sampling bias characterization was produced for forward flight in a calm air environment. This was addressed using an OPC and sampling while the rotors were on and off, to compare how much of the background was being sampled.

Summary

This chapter revisited some of the assumptions made in the design process and addressed the assumptions encountered during the testing of the EOS's performance. The chapter reported gravimetric analysis results for the EOS vs the CFC, and for the top positioning vs the bottom positioning of the samplers. OPC data were used to evaluate the aspiration efficiency of the developed inlet, and a variety of other metrics were measured in order to determine if the designed sampler could feasibly be integrated into SUAS in the future.

VI. Conclusions and Recommendations

Chapter Overview

This chapter includes the major conclusions gathered from this research, recommendations for future research, and ultimately why this research was significant. Conclusions discussed include an assessment of the relative efficacy of the EOS vs CFC, the EOS in variable positions, and an evaluation of the TPMs as they stand at this point in the design process. Recommendations for future research aim at eliminating the

limitations and narrowing the number of assumptions made in this research and highlighting the likely next steps to move forward in the system design process.

Conclusions of Research

The results of the weight and endurance TPMs are relatively clear. Meeting endurance goals may be possible, as similar airframes have been flown for that length of time—however, would likely require switching to a different frame. Further analysis would be required to determine which configuration would optimize this metric. Keeping weight below the targeted value should be feasible, even if a change in multirotor-frame is necessary to meet endurance goals (heavier hex-rotor or octo-rotor frames usually perform better in this respect). The operator metric of time for interface is one that can only be evaluated in the final design phase—as the user becomes more familiar with the operating system, the time for start-up will decrease, as was demonstrated in radiological SUAS testing that successfully met this time goal. The SLM metric was limited in this design phase to the noise produced by the EOS itself, and results from this test would likely exceed the set goal limit if the entire operational SUAS were considered. However, due to distance from operator to the SUAS this performance measure may be safely dropped for future consideration. Knowing that the EOS itself is not a hazardous noise source is useful information for future adaptations of the sampler.

The final TPM investigated was the sampling efficiency of the EOS. Analysis of these results determined that the EOS was oversampling across all particle sizes measured. The absolute error from the modeled aspiration efficiency to what was measured for the target particle diameters was lowest when the EOS was in the top

position. The sampling results also revealed that the EOS was unreliable for particles larger than 12 µm. This is important because 12 µm is what was determined to be the optimal size of shed skin cells to harbor "hitchhiking" bacteria or fungal spores that may impact human health. Ultimately there was a maximum 35% overestimate for all particles under 12 µm in diameter. Since these trials were done in an environment where ground effects may have skewed the results to the right, this should be considered a conservative performance evaluation with future trials to determine its validity.

The performance of the EOS and the CFC was significantly different, with the EOS collecting almost twice as high a concentration as the CFC; however, the CFC did have a larger variance and RSD. Since the CFC has been well characterized, it would have been ideal for the performance to be similar, but the lower RSD and the ability of the EOS to still collect samples regardless of flight regime lend the design merit. It is also of merit, that the CFC is known for sometimes under-sampling at the large particle ranges which might negatively skew the mass-based concentrations collected. Throughout all the other trials, the bottom sampling position yielded higher mass-concentrations than the EOS placed in the top position. This may have been due to ground effects, as the sampler closer to the rotors was hypothesized to create more variable and lower sampling concentrations. The RSDs of the sampler in the bottom position were lower for all flight regimes except for while stationary and in forward flight—where the RSDs were approximately equal though RSD was still lower for the bottom position while stationary. This may be due to the rotors creating well-mixed conditions, compared to the bottom. The SUAS body itself did not impact the sampling results. Also, of note, is that the placement of the sampler (on top vs on the bottom) did not impact the EOS's

performance while the rotors were off. The only other statistical test where the null hypothesis of sample difference was failed to be rejected was the EOS's performance in hover vs the CFC's performance while free-standing. Overall, the findings suggest that the top sampling position yields more consistent results, and while the sampler overestimated concentrations across the particle size range tested, while in hover the sampler did perform similarly to the well-characterized free-standing CFC.

Environmental factors such as temperature, humidity, and pressure did not yield any significant findings (with Pearson correlation coefficients less than 0.19), meaning that they are suspected to have minimal impact on the results gathered over the course of this research. Due to limitations imposed by the chamber size, the flight regimes of vertical rise and descent were not investigated. For a complete picture of how a sampler would be impacted by these conditions, a larger chamber—where actual flight is possible—would be necessary. The small width of the chamber also posed a limitation on the data collected, as ground effects were very prevalent. Possible solutions to remedy the influence of ground effects on the sampled concentration are posed in Recommendations for Future Research.

Significance of Research

This research aimed to develop a cost effective and efficient means of collecting bioaerosol samples from a multirotor SUAS platform. This is important because bioaerosols can be attributed to several health effects—such as pollen triggering allergies, or bio-aerosolized anthrax being used to target citizens as part of terrorist attacks. Currently, 29 CFR 1910.1030 covers workers who are exposed to bloodborne pathogens,

which particularly applies to laboratories and clinical settings where human tissues are manipulated, and other workers are covered from microbial harm via the general duty clause. Outside of this, very few regulations exist to evaluate the hazards potentially presented by bioaerosols in our native environments—whether endemic or introduced by malicious parties.

This research directly impacts the environmental, health and safety industries in and outside of the DoD and will empower health risk agencies to perform longitudinal studies that will assist in identifying background levels of endemic bioaerosols in remote, difficult, or hazardous areas. This research adds to the existing body of research surrounding bioaerosol sampling and sets a precedent for continued innovations in developing a cost-effective bioaerosol sampling platform for universal use.

Recommendations for Future Research

Advanced bench testing is the first priority; more analysis of size selectivity and inlet efficiency can be done, as well as observing effects on live biological particles and developing their analysis methods (most filter sampling kills biologicals). Selectivity and efficiency tests may also be performed during integration phase/field testing. During integration, performance of system and sampler must be analyzed together (e.g. system power demand, endurance, cost, etc.). A more thorough investigation of environmental factors—especially temperature and pressure—is warranted. Though bias was determined to be minimal from these factors as experiments took place in the space of one month (October), in extreme high or low temperatures or pressure environments, the bias may be greater. System power demand may place limitations on sampler performance in

current configuration– all testing was done in a continuously supplied 12V DC environment, battery operated SUAS will have less power available over operation time.

Ground effects from the small chamber size were a significant contributor to bias in these experiments. In order to alleviate this in further experiments, several avenues may be considered. Figure 39 demonstrates a potential set-up for future research that might minimize the impacts of ground effects on the results. The simplest form of this design would involve cables attached through the center of the SUAS via custom printed breadboards. The lower cable in this set-up would be required to withstand great amounts of tension (depicted by the red arrows in the figure), as it would be negating the force of lift produced by the rotors (shown in blue). Though the top cable would mostly act to keep the SUAS in place at the center of the chamber, it too may have to contribute to some downward force to negate the significant lift from the rotors in hover.

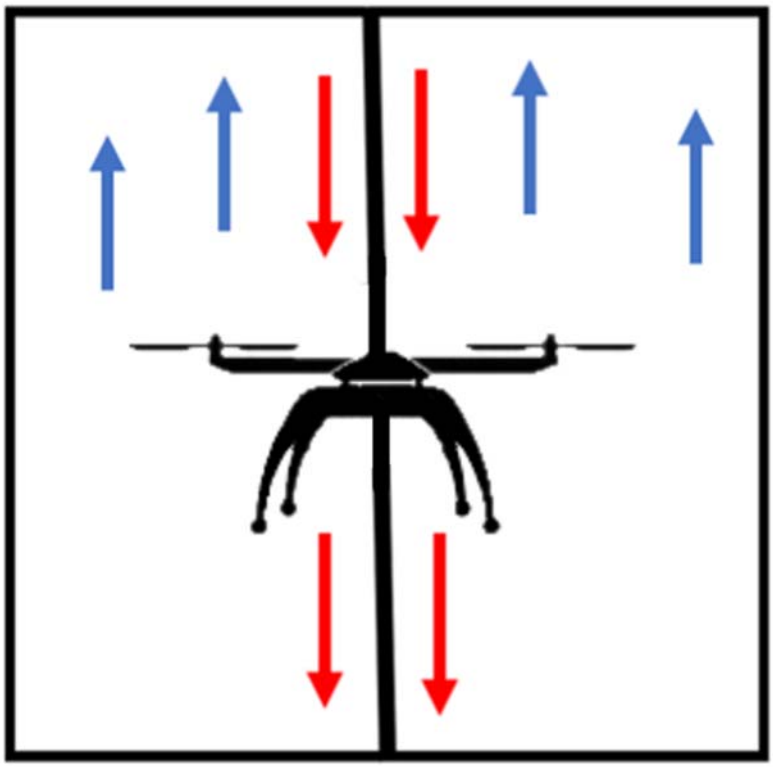

Figure 39. Free Body Cross-Section of MURPHEE for Future Research

Also worth exploring with a design team, is the possibility of building a cage to suspend the SUAS perpendicular to the bottom of the chamber. Since the length is significantly larger than the width of the chamber, this would minimize ground effects even further—though some backwash from the rotors would likely be present on the sides of the narrow chamber. This concept is similar to one used in a larger wind tunnel in Russell's study for NASA, though in that research it was an arm mount designed to demonstrate different yaw angles and flow dynamics for aerosol sampling were not a consideration (Russell et al., 2016). Ultimately, the only way to eliminate ground effects as a factor in sampling, would be to obtain a flight capable SUAS and operate it in a large exposure chamber, or even outside (assuming samples drawn would not introduce new contaminants to the environment).

Another area for potential research moving forward is investigating the possibility of fan technology improvements to convert the EOS into a high flow sampler. Being able to accomplish both high and low flow sampling with the same inlet design increases mission set to include personal and environmental sampling in a broad variety of operating conditions.

Summary

Throughout the course of this research, it was found that the top sampling position of the EOS on the SUAS yielded more consistent results. While the sampler overestimated concentrations for the entire particle size range tested, the sampler aspiration efficiency reached a peak of efficiency 35% for all the particle sizes below <12 µm. Within the particle size bin of interest, 1-2 µm, it performed even better in the top sampling position, with an efficiency of 20%. In hover the sampler did perform similarly to the well-characterized free-standing CFC, but for all other cases the CFC was significantly different in performance.

Appendix 1. SUAS Endurance Calculations

Component	Equations				Equations		
mass w/o motor, battery[kg]		1.9					
gravity[m/sec^2]		9.86		Total mass[kg]	C2+C13*C12+C17*C18/1000	2.93	
air density[kg/m^3]		1.2					
prop diameter[in]		11		P_prop_reqd[W]	(SQRT(G3*C3/(2*C4*C17*0.25*PI()*C6^2)))^3*2*C4*0.25*PI()*C6^2/C7	63.2499	
prop diameter[m]	C5*25.4/1000	0.2794					
prop efficiency		0.8		I_motor_reqd[A]	G5/(C11*C8)	5.342053	
motor efficiency		0.8					
number battery cells		4		I_total[A]	G7*C17+C19	22.36821	
rated battery capacity[Ah]		5					
battery voltage[volts	C9*3.7	14.8		t_endurance[min]	60*C16/G9	19.31312	Max endu
battery mass [kg]		0.515					
nbatteries		2					
battery efficiency		0.9					
f_usable		0.8					
total usable batt cap	C13*C10*C14*C15	7.2					
nmotor		4					
motor mass[g]		0					
aux_current[A]		1					

Appendix 2. DOE Guidance for Radiological SUAS

Customer Needs

Detecting and locating the existence of CBRNE material in an urban environment

Tactically deployable and operable

Capable of semi-autonomous operation with human-in-the-loop control

1. Tactical Deployability & Responsiveness

- **Size, weight, & number of people required**
- **Time to set-up, launch, enter hazard area**

2. Urban Suitability

- **Navigation in urban environment**

3. Data Exploitability

- **SNR & source geo-location**

4. Data Timeliness

- **Time for data to be presented to operator**

Appendix 3. 12V DC Fugetek Fan Manufacturer's Data

DC BLOWER

75x75x30mm(2.95"x2.95"x1.18")

General Specification:

- Frame:Plastic 94V-0
- Impeller:Plastic 94V-0
- Lead wire:UL Type
  (+):Red (-):Black
- Operation Temperature:-10℃~ 70℃

Motor Protection:

- Impedance Protected
- Reverse Polarity Protected

Specifications(Normal) S=Sleeve bearing B=One ball bearing D=Two ball bearing

Model No.	Bearing System	Rated Voltage (VDC)	Speed Type	Rated Current (A)	Rated Speed (RPM)	Air Flow (CFM)	Air Pressure (mmAg)	Noise Level (dBA)	Weight (g)
HT□C07530	S/D	12	H	0.30	3500	12.02	16.81	42.0	85
			M	0.16	3000	9.40	9.30	38.0	
			L	0.12	2500	7.81	5.96	33.0	
		24	H	0.16	3500	12.02	16.81	42.0	
			M	0.12	3000	9.40	9.30	38.0	
			L	0.10	2500	7.81	5.96	33.0	

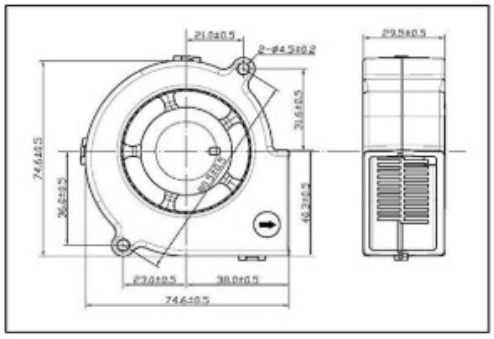

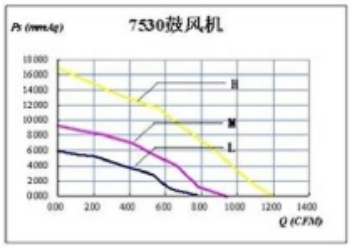

◎ All reading are typical values at rated voltage.
◎ Specifications are subjected to change without prior notice.

Retrieved from: https://www.amazon.com/Fugetek-Brushless-HT-07530D12-75x75x30mm-Computer/dp/B00B2ARV22

Bibliography

ACGIH (2019). 'Fans', in Industrial Ventilation: A Manual of Recommended Practice for Design. 30th edn. Cincinnati, OH: *Signature Publications*. ch. 7, pp. 4-5.

Anthony, R., Sleeth, D., & Volckens, J. (2016). Sampling Efficiency of Modified 37-mm Sampling Cassettes Using Computational Fluid Dynamics. *Journal of Occupational and Environmental Hygiene*, 13(2), 148–158. https://doi.org/10.1080/15459624.2015.1091961.Sampling

Aurell, J., Mitchell, W., Chirayath, V., Jonsson, J., Tabor, D., & Gullett, B. (2017). Field Determination of Multipollutant, Open Area Combustion Source Emission Factors with a Hexacopter Unmanned Aerial Vehicle. *Atmospheric Environment*, *166*(11), 433–440. https://doi.org/10.1016/j.atmosenv.2017.07.046.Field

Austin, R. (2010). 'Aerodynamics and Airframe Configurations', in Unmanned Aircraft Systems: UAVS Design, Development and Deployment. 1st edn. West Sussex, United Kingdom: John Wiley & Sons, Inc., pp. 30.

Bates, T. S., Quinn, P. K., Johnson, J. E., Corless, A., Brechtel, F. J., Stalin, S. E., Meinig, C., & Burkhart, J. F. (2013). Measurements of atmospheric aerosol vertical distributions above Svalbard, Norway, using unmanned aerial systems (UAS). *Atmospheric Measurement Techniques.* 6, 2115-2120. https://doi.org/10.5194/amt-6-2115-2013.

Beaulieu, H. J. *et al.* (1980). A comparison of aerosol sampling techniques: "open" versus "closed-face" filter cassettes. *American Industrial Hygiene Association Journal*. 41(10), 758-765. https://doi.org/10.1080/15298668091425608

Brinsfield, K., & Brothers, R. (2018). "BioWatch: Lessons Learned and the Path Forward". Retrieved May 5, 2019, from https://www.dhs.gov/news/2014/06/10/written-testimony-oha-acting-assistant-secretary-and-st-under-secretary-house.

Carrera, M., Zandomeni, R. O., Fitzgibbon, J. E., & Sagripanti, J. L. (2007). Difference between the spore sizes of *Bacillus anthracis* and other Bacillus species. *Journal of Applied Microbiology,* 102:2, 303-312. https://doi.org/10.1111/j.1365-2672.2006.03111.x

Carroll, W. F., & Foster, B. L. (2011). *Prudent Practices in the Laboratory: Handling and Management of Chemical Hazards*. (The National Research Council, Ed.). Washington DC: The National Academies Press.

Crazzolara, C., Ebner, M., Platis, A., Miranda, T., Bange, J., & Junginger, A. (2019). A new multicopter-based unmanned aerial system for pollen and spores collection in the atmospheric boundary layer. *Atmospheric Measurement Techniques*, 12, 1581–1598. https://doi.org/https://doi.org/10.5194/amt-12-1581-2019

Chavez, I. D. (2017). *Optimal Configurations for Aerosol Monitoring with Multi-Rotor Small Unmanned Aerial Systems* (Masters thesis). Retrieved from Defense Technical Information Center. (Accession No. AD1051571).

Chew, G. L., Wilson, J., Rabito, F. A., Grimsley, F., Iqbal, S., Reponen, T., … Morley, R. L. (2006). Mold and Endotoxin Levels in the Aftermath of Hurricane Katrina : A Pilot Project of Homes in New Orleans Undergoing Renovation, *Environmental Health Perspectives.* 114(12), 1883–1889. https://doi.org/10.1289/ehp.9258

Chu, J. (2018). Researchers are using virtual-reality to train drones. *MIT News*. Accessed: 12 Feb 19.

Chung, K.K., & Ogden, T.L. (1986). Some Entry Efficiencies of Disk-like Samplers Facing the Wind. *Aerosol Science and Technology*, 5(1), 81-91. https://doi.org/10.1080/02786828608959078

Cook, D., Sleeth, D., Matthew, S., Larson, T., & Larson, R. (2015). A Comparison of the Closed-Face Cassette at Different Orientations While Measuring Total Particles. *Journal of Occupational and Environmental Hygiene*, 12(3), 199–204. https://doi.org/10.1080/15459624.2014.968248

Davies, R.R., and Noble, W.C. (1962). Dispersal of bacteria on desquamated skin. *Lancet*, 2, 1459.

Dehghan, S., Golbabaei, F., Mousavi, T., Mohammadi, H., Kohneshahri, M. H., & Bakhtiari, R. (2020). Production of Nanofibers Containing Magnesium Oxide Nanoparticles for the Purpose of Bioaerosol Removal. *Pollution*, 6(1), 185–196. https://doi.org/10.22059/poll.2019.278394.604

Després, V., Huffman, J. A., Burrows, S. M., Hoose, C., Safatov, A., Buryak, G.,et al. (2012). Primary biological aerosol particles in the atmosphere: a review. *Tellus B,* 64, 2-40. doi:10.3402/tellusb.v64i0.15598

Eberhart, G. M. (2017). *Modeling of Ground Effect Benefits for Multi-Rotor Small Unmanned Aerial Systems at Hover* (Masters thesis). Retrieved from Ohio LINK Electronic Theses & Dissertations Center. (Accession No. ohiou1502802483367365)

Edmonds, J., Lindquist, H. D. A., Sabol, J., Martinez, K., Shadomy, S., Cymet, T., & Emanuel, P. (2016). Multigeneration Cross-Contamination of Mail with *Bacillus anthracis* Spores. *PLOS ONE* 11(4): e0152225. https://doi.org/10.1371/journal.pone.0152225

Enderby, J. C. (2012). *Comparative Analysis of Two Biological Warfare Air Samplers Using Live Surrogate Agents* (Masters thesis). Retrieved from Defense Technical Information Center. (Accession No. A559613).

Eninger, R. M., & Johnson, R. L. (2015). Unmanned aerial systems in occupational hygiene—learning from allied disciplines. *Annals of Occupational Hygiene*: 59, 949-58.

Fitch, J. P., Raber, E., & Imbro, D. R. (2003). Technology Challenges in Responding to Biological or Chemical Attacks in the Civilian Sector. *Science,* 302(5649), 1350-1354. https://doi.org/10.1126/science.1085922.

Fletcher, R.A, & Bright, D.S, (2000). Shape Factors of ISO 12103-A3 (Medium Test Dust), *Filtration + Separation*, 37(9), 48-56. ISSN 0015-1882, https://doi.org/10.1016/S0015-1882(00)80200-1.

Fornace, K.M., Drakeley, C. J., William, T., Espino, F., & Cox, J., (2014). Mapping infectious disease landscapes: unmanned aerial vehicles and epidemiology, *Trends in Parasitology*, 30(11), 514-519. https://doi.org/10.1016/j.pt.2014.09.001.

Harper, M., & Muller, B. S. (2002). An evaluation of total and inhalable samplers for the collection of wood dust in three wood products industries. *Journal of Environmental Monitoring*, 4(5), 648–656. https://doi.org/10.1039/B202857N

Hewett, P., & Ganser, G. H. (2007). A Comparison of Several Methods for Analyzing Censored Data. *The Annals of Occupational Hygiene,* 51(7), 611-632. https://doi.org/10.1093/annhyg/mem045

Hinds, W. C. (1999) 'Sampling of Measurement and Concentration', in Aerosol Technology: Properties, Behavior, and Measurement of Airborne Particles. 2nd edn. New York, NY: John Wiley & Sons, Inc., pp. 206–230.

Hurley, K.V., Wharton, L., Wheeler, M.J. (2019). Car cabin filters as sampling devices to study bioaerosols using eDNA and microbiological methods. *Aerobiologia*. 35**,** 215–225. doi:10.1007/s10453-018-09554-y

Jacobson, A. R., and Morris, S. C., "The Primary Air Pollutants—Viable Particles, Their Occurrence, Sources, and Effects," in Stern, A. C. (Ed.), *Air Pollution*, 3d ed., Academic Press, New York, 1976.

Jimenez-sanchez, C., Hanlon, R., Aho, K. A., Powers, C., Morris, C. E., Iii, D. G. S., & Pearce, D. A. (2018). Diversity and Ice Nucleation Activity of Microorganisms Collected With a Small Unmanned Aircraft System (sUAS) in France and the United States. *Frontiers in Microbiology*, 9, 1–12. https://doi.org/10.3389/fmicb.2018.01667

John, W., & Kreisberg, N. (1999). Calibration and Testing of Samplers with Dry, Polydisperse Latex. *Aerosol Science and Technology*, 31(2-3), 221-225. doi:10.1080/027868299304264

Juozaitis, A., Willeke, K., Grinshpun, S. A., & Donnelly, J. (1994). Impaction onto a Glass Slide or Agar versus Impingement into a Liquid for the Collection and Recovery of Airborne Microorganisms. *Applied Environmental Microbiology*, *60*(3), 861–870.

Kind, R. J., & Tobin, M. G. (1989). Flow in a Centrifugal Fan of the Squirrel Cage Type. *The American Society of Mechanical Engineers*, (89-GT-52).

Lazna, T. (2018). The Visualization of Threats Using the Augmented Reality and a Remotely Controlled Robot. *IFAC-PapersOnLine*, *51*(6), 444–449. http://doi.org/10.1016/j.ifacol.2018.07.113

Leber, J. (2014, October). Doctors Without Borders Is Experimenting With Delivery Drones To Battle An Epidemic. *Fast Company*. Retrieved from https://www.fastcompany.com/3037013/doctors-without-borders-is-experimenting-with-delivery-drones-to-battle-an-epidemic

Lee, Ji-Hyun, & Jo, Wan-Kuen (2005). Exposure to aiborne fungi and bacteria while commuting in passenger cars and public buses. *Atmospheric Environment.* 39. 7342-7350. http://doi.org/10.1016/j.atmosenv.2005.09.013

Light, J. S. (1993) Tip Vortex Geometry of a Hovering Helicopter Rotor in Ground Effect, *Journal of the American Helicopter Society*, 38(2), 34–42.

Liu, D.-L., & Luey, K. T. (2009). *Airborne Particulate Sampling in Environmental Control Systems*, (TR-20098550-10). El Segundo, CA.

Matsumoto, K. & Yunoki, T. & Nakamura, K. (2004). Effect of Fiber Diameter, Porosity and Basis Weight on Pore Size and Pore Size Distribution of Stainless Steel Nonwoven Fiber Filter. *Kagaku Kogaku Ronbunshu*. 30. 79-86. http://doi.org/10.1252/kakoronbunshu.30.79.

NIOSH. (2012). Components for Evaluation of Direct-Reading Monitors for Gases and Vapors. (Publication No. 2012–16). Dept of Health and Human Services, Center for Disease Control and Prevention.

Oggioni, M. R., Meacci, F., Carattoli, A., Ciervo, A., Orru, G., Cassone, A., & Pozzi, G. (2002). Protocol for Real-Time PCR Identification of Anthrax Spores from Nasal Swabs after Broth Enrichment. Journal of Clinical Microbiology, 40(11), 3956–3963. https://doi.org/10.1128/JCM.40.11.3956

O'Hanlon, M. (2018). *Forecasting Change in Military Technology, 2020-2040*. Washington DC. Center of Foreign Policy at Brookings.

Paik, S., & Vincent, J. H. (2002). Aspiration efficiencies of disc-shaped blunt nozzles facing the wind, for coarse particles and high velocity ratios, *Journal of Aerosol Science*. *33*, 1509–1523.

Paik, S. Y., & Vincent, J. H. (2018). The Orientation-averaged Aspiration Efficiency of IOM-like Personal Aerosol Samplers Mounted on Bluff Bodies, *The Annals of Occupational Hygiene*. *48*(1), 3–11. https://doi.org/10.1093/annhyg/meg088

Pöllänen, R., Toivonen, H., Peräjärvi, K., Karhunen, T., Smolander, P., Ilander, T., Rintala, K., Katajainen, T., Niemelä, J., Juusela, M., & Palos, T. (2009). Performance of an air sampler and a gamma-ray detector in a small unmanned aerial vehicle, *Journal of Radioanalytical and Nuclear Chemistry.* 282-433. https://doi.org/10.1007/s10967-009-0284-3

Powers, C. W., Hanlon, R., Grothe, H., Ii, A. J. P., Marr, L. C., & Iii, D. G. S. (2018). Coordinated Sampling of Microorganisms Over Freshwater and Saltwater Environments Using an Unmanned Surface Vehicle (USV) and a Small Unmanned Aircraft System (sUAS). *Frontiers in Microbiology*, 9(August), 1–12. https://doi.org/10.3389/fmicb.2018.01668

Qian, J., Hospodsky, D., Yamamoto, N., Nazaroff, W., & Peccia, J. (2012). Size-resolved emission rates of airborne bacteria and fungi in an occupied classroom. *Indoor Air*, *22*, 339–351. https://doi.org/10.1111/j.1600-0668.2012.00769.x

Reponen, T. *et al.* (2011) 'Biological Particle Sampling', in Kulkarni, P., Baron, P. A., and Willeke, K. (eds) *Aerosol Measurement: Principles, Techniques, and Applications*. 3rd edn. John Wiley & Sons, Inc., pp. 549–570.

Risojević, V., Rozman, R., Pilipović, R., Češnovar, R., & Bulić, P. (2018). Accurate Indoor Sound Level Measurement on a Low-Power and Low-Cost Wireless Sensor Node. *Sensors (Basel, Switzerland)*, *18*(7), 2351. doi:10.3390/s18072351

Roedler, G. J., & Jones, C. (2005). Technical Measurement. *INCOSE-TP-2003-020-01*, (December), 1–65.

Russell, C., Field, M., Willink, G., Field, M., & Glasner, B. (2016). Wind Tunnel and Hover Performance Test Results for Multicopter UAS Vehicles (Publication No. ARC-E-DAA-TN31096). National Aeronautics and Space Administration.

Schmale III, D.G., Dingus, B.R. and Reinholtz, C. (2008), Development and application of an autonomous unmanned aerial vehicle for precise aerobiological sampling above agricultural fields. *J. Field Robotics*, 25: 133-147. doi:10.1002/rob.20232

Smith, B., Beman, M., Gravano, D. and Chen, Y. "Development and validation of a microbe detecting UAV payload," *2015 Workshop on Research, Education and Development of Unmanned Aerial Systems (RED-UAS)*, Cancun, 2015, pp. 258-264. doi: 10.1109/RED-UAS.2015.7441015

Soo, J.-C., Monaghan, K., Lee, T., Kashon, M., & Harper, M. (2016). Air sampling filtration media: Colleciton efficiency for respirable size-selective sampling. *Aerosol Science and Technology*, *50*(1), 76–87.

Sproles, N. (2000), Coming to grips with measures of effectiveness. *Syst. Engin*., 3: 50-58. doi:10.1002/(SICI)1520-6858(2000)3:1<50::AID-SYS4>3.0.CO;2-U

Titus, E., Slagley, J., & Eninger, R. (2019). *Establishing a Scientific Basis for the 90% Solution: Test Chamber Characterization.* (Poster). Presented at Chemical and Biological Defense Science and Technology Conference. 20 Nov 2019.

Vincent, J. H. (2007). Aerosol Sampling: Science, Standards, Instrumentation and Applications. West Sussex, England: John Wiley & Sons Ltd

Wilcox, J. D. (1956). Isokinetic Flow and Sampling. *Journal of the Air Pollution Control Association*, *5*(4), 226–245. https://doi.org/10.1080/00966665.1956.10467715

Yoon, S., Lee, H. C., & Pulliam, T. H. (2016). Computational Analysis of Multi-Rotor Flows. *American Institute of Aeronautics and Astronautics*, 1–11.

Yuanping He, Zhaolin Gu, Weizhen Lu, Liyuan Zhang, Tomoaki Okuda, Kentaro Fujioka, Hui Luo, Chuck Wah Yu, (2019). Atmospheric humidity and particle charging state on agglomeration of aerosol particles, *Atmospheric Environment*, 197, pp 141-149. https://doi.org/10.1016/j.atmosenv.2018.10.035.

Zaripov, S., & Koch, W. (2014). Numerical Study of the RespiCon Sampler Performance in the Calm Air Numerical Study of the RespiCon Sampler Performance, *Aerosol Science and Technology*, 48:1, 74-80, DOI: 10.1080/02786826.2013.859653

Zheng, W., Reponen, T., Grinshpun, S., Górny, R., Willeke, K. (2001). Effect of sampling time and air humidity on the bioefficiency of filter samplers for bioaerosol collection, *Journal of Aerosol Science*, 32(5) pp. 661-674. https://doi.org/10.1016/S0021-8502(00)00108-7.

Vita

First Lieutenant Stephanie A. Ohms is from Lake Winnebago, Missouri. In 2016 she graduated from the United States Air Force Academy, with a Bachelor of Science in Biology and was commissioned as an officer in the Air Force Biomedical Sciences Corps. She was assigned to Minot Air Force Base, North Dakota as a Bioenvironmental Engineer where she served as the Occupational Health Program Officer in Charge, ensuring the health and safety of the 5th Bomb Wing and the 91st Missile Wing. In addition to this duty, Lieutenant Ohms served as an alternate Radiation Safety Officer from 2017 to 2018. In 2018 Lieutenant Ohms was selected to attend the Air Force Institute of Technology at Wright Patterson Air Force Base, Dayton, Ohio as part of the Health Professions Educational Requirements Board (HPERB) to earn her master's degree in Industrial Hygiene. After graduation she will work at the United States Air Force School of Aerospace Medicine.

REPORT DOCUMENTATION PAGE

Form Approved
OMB No. 074-0188

1. REPORT DATE *(DD-MM-YYYY)*	2. REPORT TYPE	3. DATES COVERED *(From – To)*
26-03-2020	Master's Thesis	August 2018 – March 2020

TITLE AND SUBTITLE

Development and Characterization of a Filter-based Bioaerosol Sampler Capable of Integration into Small Unmanned Aerial Systems

5a. CONTRACT NUMBER

5b. GRANT NUMBER

5c. PROGRAM ELEMENT NUMBER

6. AUTHOR(S)

Ohms, Stephanie A., 1st Lieutenant, USAF

5d. PROJECT NUMBER

5e. TASK NUMBER

5f. WORK UNIT NUMBER

7. PERFORMING ORGANIZATION NAMES(S) AND ADDRESS(S)
Air Force Institute of Technology
Graduate School of Engineering and Management (AFIT/ENV)
2950 Hobson Way, Building 640
WPAFB OH 45433-8865

8. PERFORMING ORGANIZATION REPORT NUMBER

AFIT-ENV-MS-20-M-230

9. SPONSORING/MONITORING AGENCY NAME(S) AND ADDRESS(ES)
Darrin Ott, PhD
711 HPW/RHM, 2510 5th Street
Wright-Patterson AFB, OH 45433-7913
(937) 713-7921

10. SPONSOR/MONITOR'S ACRONYM(S)

AFRL/RHIQ (example)

11. SPONSOR/MONITOR'S REPORT NUMBER(S)

12. DISTRIBUTION/AVAILABILITY STATEMENT
DISTRUBTION STATEMENT A. APPROVED FOR PUBLIC RELEASE; DISTRIBUTION UNLIMITED.

13. SUPPLEMENTARY NOTES
This material is declared a work of the U.S. Government and is not subject to copyright protection in the United States.

14. ABSTRACT

In developing functional SUAS, performance characteristics that indicate system capability should be developed prior to initiating initial system design. Key performance parameters should be developed involving all system elements (including vehicle body, operator, ground station, sensor, and algorithm or processing module). A bioaerosol sampler designed specifically for use in SUAS was characterized based on designated performance measures to determine overall effectiveness compared to traditional bioaerosol samplers. For a system with a goal of accurately identifying and quantifying areas of airborne biological contamination or surveying background levels for longitudinal studies, performance parameters such as weight of the vehicle with payload and sampler specific parameters were quantitatively evaluated. These sampler-specific parameters include operational noise levels, power demand compared to performance, and particle size sampling fraction. These were evaluated in a series of lab-based tests to determine if the developed model of bioaerosol sampler could be deployed for use in military environments. Overall, it was found that the developed EOS inlet oversampled for the background concentrations, though this may be due to ground effects on the system—as the bottom placement for the sampler performed worse than expected based on previous research in comparison to the sampler closer to the rotors.

15. SUBJECT TERMS
Bioaerosol, Filtration, SUAS, Aspiration Efficiency

16. SECURITY CLASSIFICATION OF:			17. LIMITATION OF ABSTRACT	18. NUMBER OF PAGES	19a. NAME OF RESPONSIBLE PERSON
a. REPORT	b. ABSTRACT	c. THIS PAGE			Dr. Jeremy Slagley, AFIT/ENV
U	U	U	UU	106	19b. TELEPHONE NUMBER (937) 255-6565, ext 4632 (jeremy.slagley@afit.edu)

Standard Form 298 (Rev. 8-98)
Prescribed by ANSI Std. Z39-18